MORPHOLOGY AND SEDIMENTOLOGY OF A SUBMARINE CANYON SYSTEM ON THE LOWER TRENCH SLOPE OF THE PERU-CHILE FOREARC

A THESIS SUBMITTED TO THE GRADUATE DIVISION OF THE UNIVERSITY OF HAWAII IN PARTIAL FULFILLMENT OF THE REQUIREMENTS FOR THE DEGREE OF

MASTER OF SCIENCE

IN GEOLOGY AND GEOPHYSICS

DECEMBER 1989

By

Douglas Donald Bergersen

Thesis Committee:

William T. Coulbourn, Chairman

Ralph Moberly

Jane Tribble

We certify that we have read this thesis and that, in our opinion, it is satisfactory in scope and quality as a thesis for the degree of Master of Science in Geology and Geophysics.

THESIS COMMITTEE

William J. Coulbourn

Chairman

ACKNOWLEDGEMENTS

The path towards completing this thesis has been marked by many bifurcations, some of which proved to be shortcuts, some of which impeded my progress, but all of which were educational. At this time I would like to thank those individuals who made this manuscript possible.

I thank the crew and shipboard personnel of the R/V *Moana Wave* for their aid in collecting this data set. I thank Alexander Shor, Jane Tribble, and Ralph Moberly for their insightful comments and criticisms concerning the content of this thesis. Finally, a special thanks goes to my advisor, William Coulbourn, for his patience, understanding, suggestions, and friendship during the course of this work.

ABSTRACT

Continental margins are the sites for a number of downslope sediment transport processes including sediment gravity flows, slumping, debris flows, and turbidity currents. Typically, these margins are traversed by submarine canyons which act as conduits for the transportion of shelf sediment to deeper water environments. A detailed SeaMARC II side-scan and bottom sampling survey conducted aboard the University of Hawaii research vessel *Moana Wave* across the Peru-Chile forearc mapped a submarine canyon system from near the slope break off southern Peru to its termination in the trench off northern Chile. This project investigates the relationship of sedimentation to tectonics by focusing on: 1) the degree to which canyon trends follow structural controls as opposed to regional slope, 2) the characteristics of sediment within and adjacent to canyons, and 3) the efficiency of a canyon system in bypassing coarse sediment across the trench slope environment. For this particular portion of the forearc, canyon trends appear to be influenced more by such structural controls as faulting and block rotation than by slope failure caused by overloading. Given this observation, canyon trends can then be used to construct a tentative tectonic history of the margin back to the proposed time of inception. Core sites, selected from Global Positioning System (GPS) and Transit satellite navigated side-scan images and 3.5 kHz profiles, are precisely located with respect to such channel morphologic units as thalwegs and levees. General canyon facies descriptions can be made from the grain-size, mineralogical, and carbonate data analyzed from core tops adjacent to the channels and across the lower trench slope. Grain-size data suggest that this canyon system acts as an efficient conduit for passing coarse sediment across the Arequipa forearc basin and the lower trench slope; very little sand is dispersed outside the channel banks. Trends in mineral ratios and carbonate content with respect to distance from the canyon are less distinct. With the collection of similar data sets from other active canyon systems, the

sedimentological patterns presented here may be further refined to develop a facies model for modern canyons.

TABLE OF CONTENTS

LIST OF TABLES

LIST OF ILLUSTRATIONS

Plates

CHAPTER 1

INTRODUCTION

Deciphering the tectonic history of a continental margin and understanding how its changing structure affects sediment dispersal patterns is a tantilizing problem in marine geology. The established methods of interpreting seismic lines, 3.5 kHz profiles, gravity, magnetics, and sediment property data have produced at least a general tectonic history for all the margins of the world. With the advent of side-scan imagery and detailed swath map bathymetry, further refinement of and elaboration upon the history of selected margins became possible. One geomorphic feature common to all margins and easily surveyable with side-scan imaging techniques is submarine canyon systems. These canyon systems in turn are useful for deciphering the tectonic and sedimentary history of a margin.

A 1987 cruise aboard the University of Hawaii research vessel *Moana Wave*, across the inner trench slope of the Peru-Chile margin was designed to: 1) map and sample a canyon system from near its head at the shelf slope break to its mouth in the trench; 2) examine the near-surface sedimentology of canyons and channels and their associated morphologic units such as thalweg, levee, overbank, and basin deposits; 3) assess the effectiveness of a canyon system in transporting coarse sediment across the inner trench slope; and 4) establish the merit of using canyons to identify structures and tectonic forces. Core sites were chosen during the cruise by the location of features in side-scan images; Global Positioning System (GPS) and Transit satellites provided navigation for the side-scan images. This selection process allowed the collection of a very detailed and precisely located data set. The purpose of this thesis is to: 1) map an active submarine canyon system as it traverses the inner trench slope, 2) examine structural and tectonic controls influencing canyon morphology and canyon trends, and 3) identify

physical or textural properties which might be useful for distinguishing channel, levee, and overbank deposits from adjacent slope deposits.

History and Background

Submarine canyons are common along all active and passive margins. Their origin has been attributed to such mechanisms as stream downcutting during low sea level stands (Spencer, 1903; Shepard, 1933; Stetson, 1936; Veatch and Smith, 1939; Knebel and others, 1979), tsunamis (Bucher, 1940), underground water circulation (Johnson, 1939), faulting (Gates and Gibson, 1956), turbidity flows (Daly, 1936; Whitaker, 1974), or combinations of these (Shepard and Dill, 1966). Continued expansion of canyons may occur by sliding, slumping, sand spillover, bioerosion, sand flow, sand creep, turbidity currents and debris flows (Stubblefield and others, 1982; May and others, 1983; Stanley and others, 1986; Kastens and Shor, 1986; Damuth and others, 1988). Schumm and Phillips (1986) ascribe ground-water sapping as responsible for subaerial canyon expansion along the coast of Canterbury, New Zealand.

Given that canyons act primarily as conduits for passing sediment across the continental slope, defining their facies is a problem; a thick sequence of sediments within the canyon isn't expected. Instead, the deposits of an active canyon may include a veneer of coarse sediment blanketing boulders in the thalweg, stratified finer-grained deposits forming levees adjacent to the canyon, and still finer-grained distal overbank deposits, which presumably grade into the "normal" slope deposits. One of the goals of this thesis is to identify sediment properties which characterize the deposits of an active canyon.

Most information on canyon facies has been inferred from studies of ancient submarine fan deposits now exposed on land (Mutti, 1974; Ricci Lucchi and Valmori, 1980; Shanmugan and Moiola, 1988). Understanding of submarine fan morphology in

actualistic settings has benefited from a number of studies using side-scan sonar techniques (Garrison and others, 1982; Damuth and Flood, 1983; Bouma and others, 1985; Maldonado and others, 1985; Flood and Damuth, 1987). Channel meandering across the middle fan, cutoff and abandoned meanders, levees, and overbank deposits occur on the Mississippi Fan, the Amazon Fan, and the Valencia Fan. Analysis of sinuous distributary channels on the Amazon Fan (Flood and Damuth, 1987) showed that the relationships between meander wavelength and both channel width and radius of meander curvature of submarine fan channels are similar to those observed for large subaerial rivers; in the submarine setting, however, channel width, depth, and cross-sectional area decrease down a fan channel. Submarine canyons, on the other hand, generally widen and sometimes deepen towards their mouth. Coarse sediments largely bypass the upper and middle fan via channels and are deposited on the lower fan (Damuth and Flood, 1983; Normark and others, 1986). Current debate on fan deposition models centers around the mechanism by which channels are filled, specifically on the Mississippi Fan. Shor and Kastens (preprint) favor a "sudden-infilling model" whereby channels are filled nearly instantaneously by slump or debris flow events. Bouma and others (1986) propose a "gradual-infilling model" whereby small-volume transport events in the form of low-density turbidity currents or river-flood derived, hemipelagic suspensions occurring during a post-glacial transgression cause channel infilling. A high-frequency, low-volume turbidite model is also favored by Damuth and others (1988) for the aggradation of levee complexes on the Amazon Fan.

Submarine fans represent the depocenter for sediment transported through canyons; hence, relating factors significant for fan development to those responsible for canyon development is somewhat tenuous. For example, the dynamics of turbidity flows fluctuate in response to changes in slope, becoming more erosional with increasing gradients. The gradient within a fan channel is in general less than the gradient within

a canyon. Presumably, a change in turbidity flow dynamics occurs in the vicinity of the canyon mouth, whereby the current switches from being primarily an erosional agent to a depositional agent. Submarine canyon facies, therefore, should ideally be mapped from active systems because: 1) only the most recent tectonism has affected the distribution of the sediments, 2) the sediments have undergone minimal diagenetic alteration subsequent to their time of deposition, and 3) with increasing age of the deposit, information concerning its depositional environment is lost. Unfortunately, the paucity of samples from active canyon settings precludes a clear understanding of their facies; canyon facies patterns are presently being inferred from the study of ancient examples preserved on land. Although canyons act primarily as sediment conduits, some studies have been successful in describing how channel-fill units relate to the area's tectonic history (e.g. von der Borch and others, 1985; Morris and Busby-Spera, 1988). An inherent problem with these fill-units is that they represent abandoned features which quite possibly underwent depositional processes different from more active canyon segments. Often these units have been subjected to at least one period of tectonic deformation, affecting their lateral and vertical continuity, and disrupting such features as levee and overbank deposits. Another problem is scale; canyons commonly have lateral dimensions of a few kilometers, making outcrop exposures of limited value because they show only a small portion of the entire system. Hence, sediment bypassing, tectonic deformation, and limited outcrop exposure make identification and classification of canyon facies from ancient canyon deposits a difficult proposition.

Submersible dives, side-scan imaging, and bathymetric swath mapping provide detailed morphological observations of modern submarine canyons. Most information regarding erosional agents and their effects on canyon morphology comes from passive margin settings (Belderson and Kenyon, 1976; Malahoff and others, 1980; McGregor and others, 1982; Farr and others, 1983; Alonso and others, 1985) and to a lesser extent from

transform margin settings (Barnard, 1978). Observations of modern canyons in subduction settings are sparse. Farre and others (1983) propose one model for the development of canyons on passive continental margins which distinguishes a youthful phase from a mature phase by the position of the canyon head with respect to the shelfbreak. Upon breaching the shelfbreak, a canyon passes from its youthful phase where growth is dominated by retrogressive slope failure, and enters into a mature phase where erosion comes primarily from coarse sediment being washed down from the shelf. The degree to which their model applies to active continental margins is undetermined. Some questions still need to be examined including the role that geologic structure plays in the headward development of canyons, the relative importance of the shelfbreak in such a dynamic environment for defining the maturity of a canyon system, and the accuracy of applying passive-margin canyon processes to active-margin canyons.

Geophysical surveys across forearcs, usually with a primary objective other than the study of the detailed morphology and sedimentology of a canyon system, have provided the most information about canyon size, shape, and drainage basin extent in active-margin settings (Aubouin and others, 1982; Smoot, 1983). Side-scan surveys across the Bonin forearc by SeaMARC II (Taylor, pers. comm.) and the Peru margin (Bartlett, 1987; Hussong and others, 1988) have provided some insights on how tectonics affect canyons, but the absence of accompanying sediment samples precluded an understanding of the facies associated with these systems. Thus, due in part to the the limited coverage and resolution afforded by seismic data collected at sea and the near absence of detailed bottom sampling, only general maps of submarine canyons and their deposits have been compiled for most active margins (e.g. von Huene, 1972; Bouma and Nilsen, 1978; Carlson and Karl, 1984; Taylor and Smoot, 1984; Bartlett, 1987).

During the summer of 1987, the Hawaii Institute of Geophysics conducted a cruise (MW87-09) to survey the Peru-Chile forearc and trench between 17^{o} 30' S and 20^{o} 15' S

latitude. The area discussed in this thesis includes the lower trench slope between approximately 18^{o} 25' S and 19^{o} 20' S (Figure 1). The discussion centers around a submarine canyon that breaches the structural high and traverses the lower trench slope. Based on pre-existing bathymetric data (Coulbourn, 1977) and the general trend of the canyon, the canyon source is apparently the Rio Moquequa, near the town of Ilo, Peru (Figure 1). Therefore, I refer to the mapped canyon as Moquequa Submarine Canyon (MSC). To understand the morphology, mineralogy, and sediment textures associated with MSC, an understanding of the tectonics affecting the Arica Bight geology, both onshore and offshore, is necessary.

Figure 1. Side-scan coverage in the vicinity of the Arica Bight offshore southern Peru and northern Chile. Shaded pattern denotes the area discussed in this thesis. The Moquequa River is the proposed subaerial connection to the canyon discussed herein. Contour interval is 200 m.

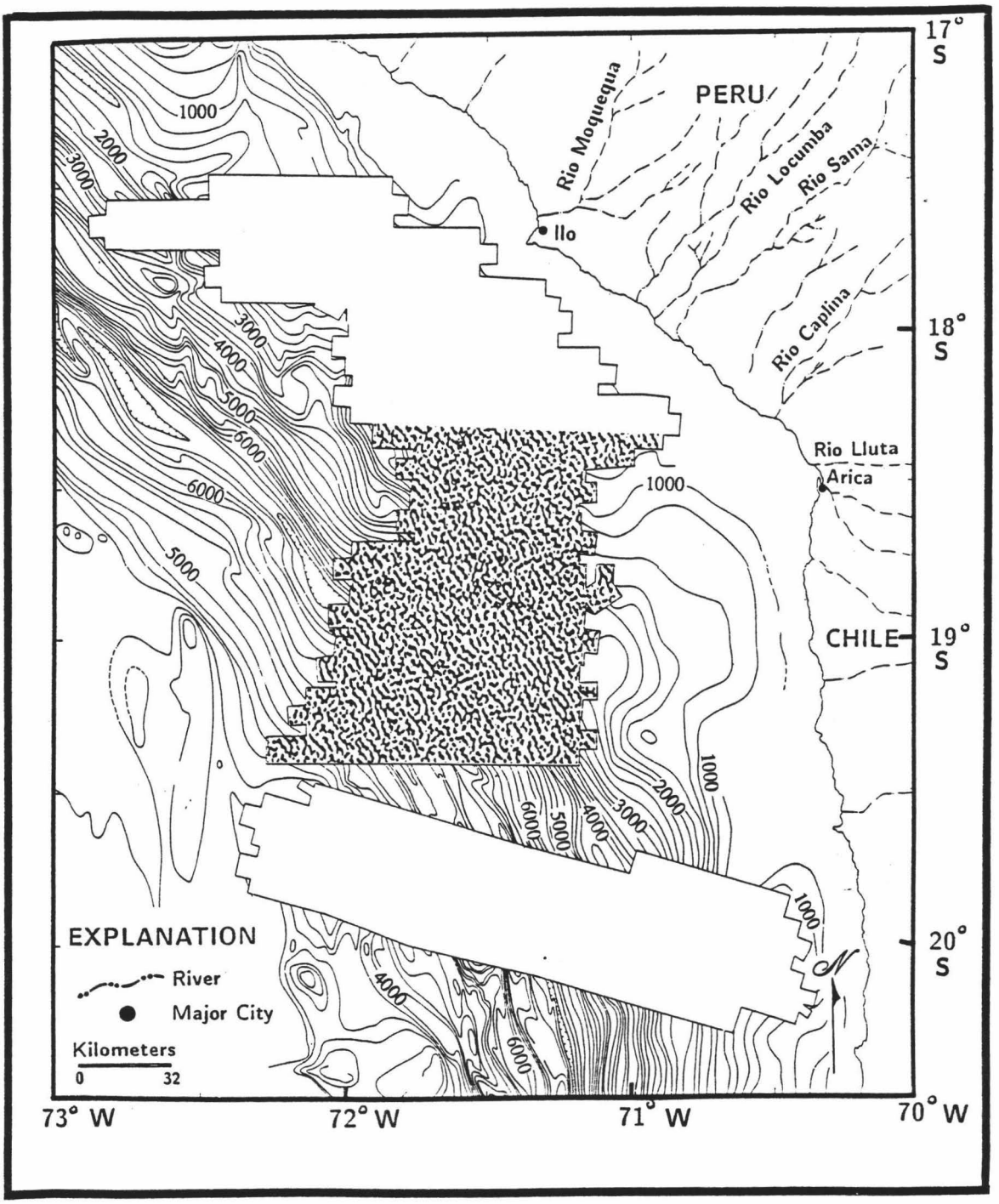
17° S
18° S
19° S
20° S
73° W
72° W
71° W
70° W
PERU
CHILE
Rio Moquequa
Rio Locumba
Rio Sama
Rio Caplina
Rio Lluta
Ilo
Arica
1000
2000
3000
4000
5000
6000
EXPLANATION
River
Major City
Kilometers
0
32
N

CHAPTER 2

TECTONIC FRAMEWORK

The major tectonic features in the survey area are shown in Figure 2. The Peru-Chile trench marks the junction where the Nazca plate is subducted beneath the South American plate. The Nazca plate moves eastward at a rate of 6 cm/yr relative to the mantle, whereas the South American plate moves westward at 3 cm/yr (Minster and Jordan, 1978). This margin can be classified as overstepped (Moore, 1983), where the upper plate (South American plate) moves toward the trench. Underthrusting of the Pacific plate is believed to have begun no later than Late Triassic or Early Jurassic (James, 1971). Break-up of the Farallon plate into the Gorda, Cocos, and Nazca plates occurred approximately 26 Ma (Handschumacher, 1976). In the Arica Bight area, the zone of convergence is convex eastward. The Peru-Chile margin is segmented along strike according to the dip of the Benioff zone: areas with essentially no inclination are differentiated from areas where the zone dips at an angle of approximately 30^{o} (James, 1971). Areas above flat, relatively shallow subducted slabs tend to lack recent volcanism and tend to have mostly compressional neotectonics. Segments of steeply dipping Benioff zones along this margin, such as under the Arica Bight, correspond to areas exhibiting well-developed Pliocene and Quaternary volcanism and dominantly extensional recent tectonics (Megard and Philip, 1976; James, 1981; Jordan and others, 1983).

The Central Andean volcanic arc dominates the onshore geology of southern Peru and northern Chile. The Central Andean orogen is composed of three principal provinces (Figure 3): the Western Cordillera (Cordillera Occidental) composed of the calc-alkaline volcanic arc; the Eastern Cordillera (Cordillera Oriental) consisting of deformed Paleozoic marine sedimentary rocks that have been intruded by magmas of Mesozoic and Cenozoic age; and the Altiplano, a vast intermontane plateau separating

Figure 2. Major offshore tectonic features of the Arica Bight. Normal faults dissect the Nazca Plate prior to its subduction beneath the South American Plate. Three major basins trap sediment transported from the subaerial portion of the forearc; Moquequa Canyon crosses the Arequipa Basin on its path to the trench. Modified after Coulbourn (1980).

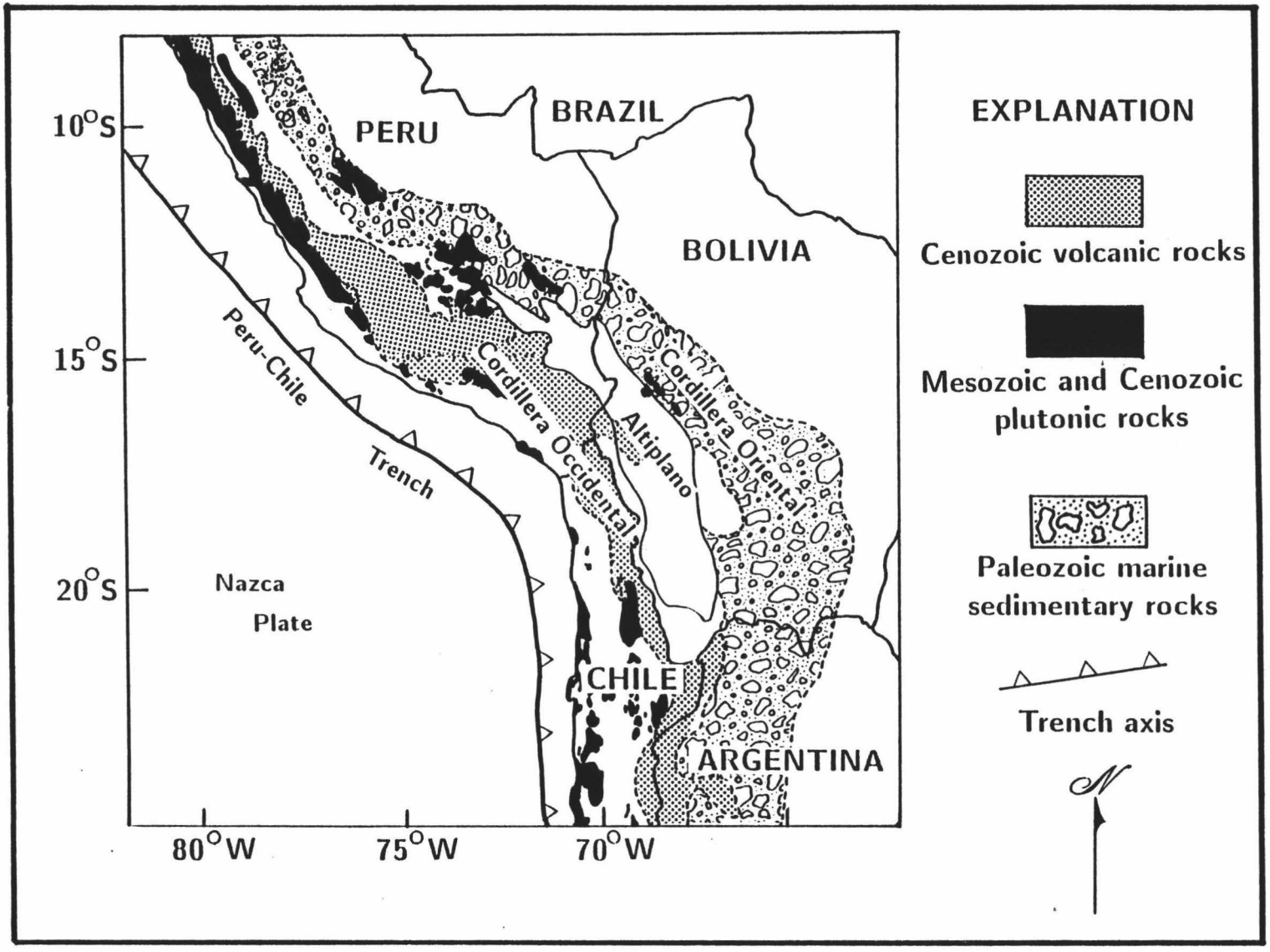
10°S
15°S
20°S
80°W
75°W
70°W
PERU
BRAZIL
BOLIVIA
CHILE
ARGENTINA
Peru-Chile
Trench
Nazca
Plate
Cordillera Occidental
Altiplano
Cordillera Oriental
EXPLANATION
Cenozoic volcanic rocks
Mesozoic and Cenozoic plutonic rocks
Paleozoic marine sedimentary rocks
Trench axis
N

Figure 3. Three principle provinces of the central Andean orogen. Modified after James, 1981, and Tosdal and others, 1984.

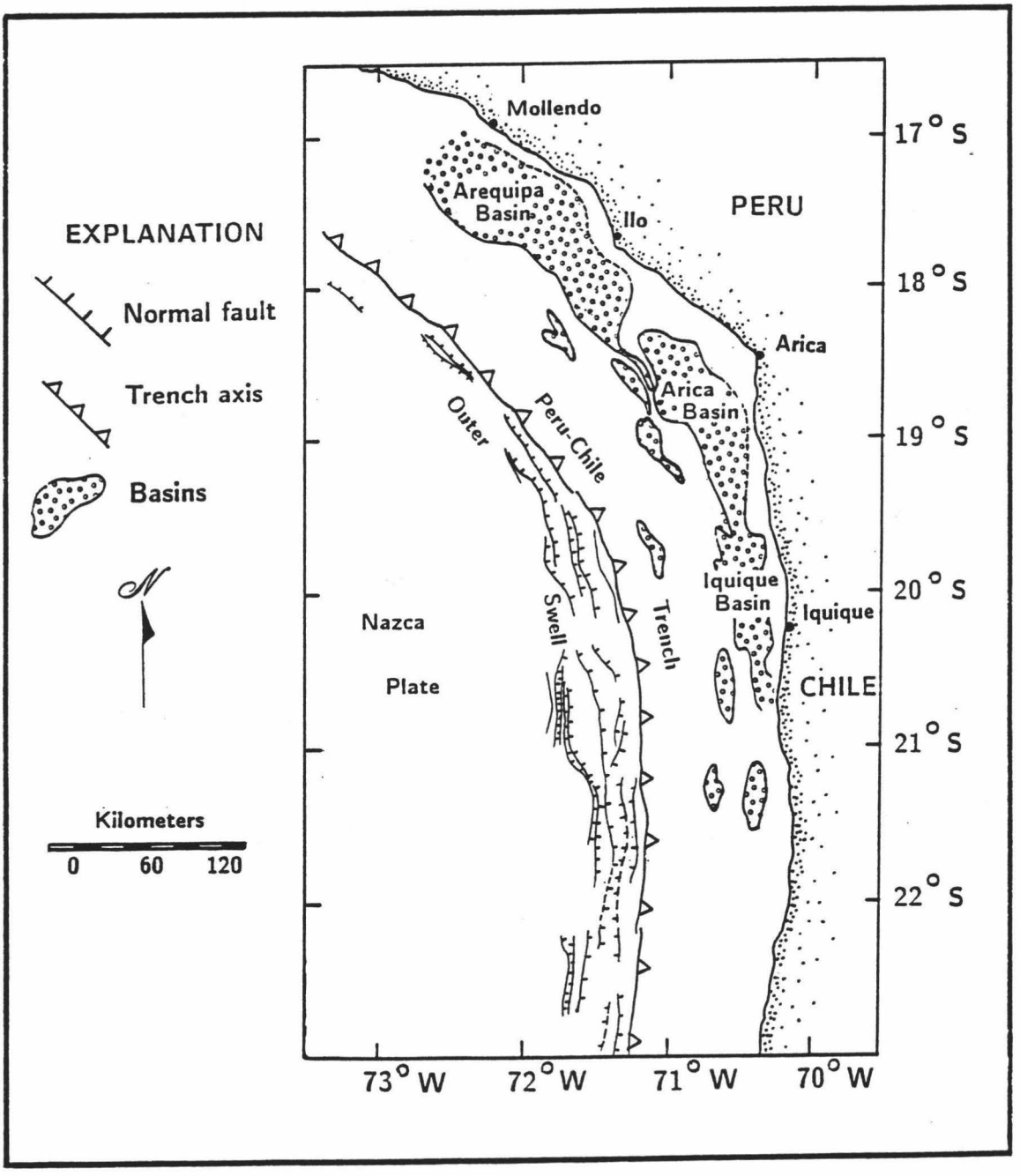
EXPLANATION
Normal fault
Trench axis
Basins
N
Kilometers
0
60
120
Mollendo
Arequipa Basin
Ilo
PERU
Arica
Arica Basin
Outer
Peru-Chile
Trench
Swell
Nazca
Plate
Iquique Basin
Iquique
CHILE
17° S
18° S
19° S
20° S
21° S
22° S
73° W
72° W
71° W
70° W

the Western and Eastern Cordilleras (James, 1971; James, 1981). In the Cordillera Occidental region of southern Peru, a succession of Mesozoic and Cenozoic magmatic arcs have developed on a basement of Precambrian metamorphic rocks (Shackleton and others, 1979). In the latest Oligocene (25 to 26 Ma), felsic pyroclastic eruptions began and continued episodically throughout the Miocene, coinciding with the episodic uplift of the Cordillera Occidental's western slope; andesitic volcanism resumed in the latest Miocene or early Pliocene and has continued to the present (Tosdal and others, 1981). The Cordillera Occidental can be further subdivided into three, morphostructural units trending parallel to the coast: 1) a seaward unit called the Cordillera de la Costa, 2) a broadly longitudinal, asymmetrical depression called the Llanuras Costaneras, and 3) the main Cordillera Occidental. A summary of the Cenozoic landform and tectonic evolution of southernmost Peru is given by Tosdal and others (1984, and references therein). They describe a cessation of the Late Cretaceous-Paleogene magmatic-arc activity by the Eocene and an ensuing period of erosion which gradually reduced the arc to a subdued topography. Subsidence of the coastal area permitted the development of a coastal plain by the latest Oligocene. During the latest Oligocene and earliest Miocene, the region experienced more rapid uplift with the eruption of rhyodacitic ignimbrites and, farther inland, andesitic to dacitic pyroclastic flows. Further uplift closely followed and led to the initiation of multiple pediment formation. Active pedimentation ceased in the late Miocene (post-8.9 Ma) or earliest Pliocene. In early to middle Pliocene, sea level fell to a position at or below its present position, allowing the rivers to incise deep canyons into the Cordillera de la Costa. During the late Pliocene and Pleistocene the Cordillera de la Costa underwent several cycles of vertical movement, each marked by marine transgression and regression and terrace formation (Tosdal and others, 1984).

Three major basins occupy the forearc of the Arica Bight area between 18^{o} S and 22^{o} S (Figure 2). This study focuses on the Moquequa canyon system after it leaves the

northernmost of these basins, the Arequipa Basin. First described by Johnson and others (1975), the Arequipa basin is bounded to the southwest by an undulating structural high interpreted to be of imbricate thrust origin (Coulbourn and Moberly, 1977). Coulbourn and Moberly (1977) hypothesized the landward dipping reflectors within the basin resulted from vertical movements of the structural high and an eastward migration of the axis of maximum sedimentation. Earliest descriptions of the sediments covering this margin (Zen, 1959) match those along other active margins (Damuth, 1980; McMillen and others, 1982; Coulbourn and others, 1982); the sediment is composed of olive-gray, diatomaceous, hemipelagic silts and clays. Zen (1959) pointed out the lack of a simple correlation between grain size and distance from shore, suggesting some form of bypassing from shallow to deep-water regions. Coulbourn (1977) emphasized the dominant control plate tectonics has on sedimentary facies and gravity has on the redistribution of sediment. On a broad scale, he made quantitative distinctions between sediments accumulating on the Nazca plate, sediments depositing on the continental slope, and sediments displaced from the slope. One of the objectives of this thesis is to distinguish sediment facies on a much finer scale: statistically distinguishing sediments from the canyon thalweg, levee, and overbank environments from sediments accumulating on the slope.

CHAPTER 3

METHODS

Seafloor imaging and bathymetry

The SeaMARC II seafloor mapping system was used to collect side-scan images and bathymetry for the area of the Peru-Chile margin outlined in Figure 1. SeaMARC II is a long-range, side-scan sonar system which produces geometrically correct acoustic images of the seafloor (Hussong and Fryer, 1983). In addition, the system can calculate bathymetry for the ensonified swath of the seafloor by measuring the direction to a seafloor reflector (in R,H space; Figure 4) and converting to position and depth (X,Z space). A thorough description of the SeaMARC II system is given by Blackinton and others (1983).

The SeaMARC II side-scan images are composed of 1024 pixels on each side of the swath; thus for a 10-km swath each pixel represents the echo strength from a band at a constant width of 5 m (Hussong and Fryer, 1983). Pattern recognition on the seafloor is a function of the signal beam-width, range, ping-repetition rate, and ship's speed. Typically, such linear features as channels or faults are recognizable if they have dimensions of a few to several tens of meters, whereas such 3-dimensional features as small mounds or sediment ponds must have dimensions on the order of 100 or more meters before displaying a recognizable shape. Reprocessing techniques applied to the raw data to enhance features include along-track gain correction, angle-varying gain correction to compensate for the array beam pattern, pixel relocation for bottom-tracking errors, and contrast mapping (Appendix A describes in more detail the reprocessing techniques applied to the side-scan data). Due to the loss of detail in reducing an original 2 m by 1.5 m mosaic of images to page size, the side-scan mosaic encompassing the Moquequa Submarine Canyon system is shown as plates in Appendix B. Selected portions of the mosaic are displayed as figures and are discussed within the

Figure 4. Schematic of the SeaMARC II tow sled. Data is collected in R, Θ space and converted to X,Z space for bathymetric mapping (after Hussong and Fryer, 1983).

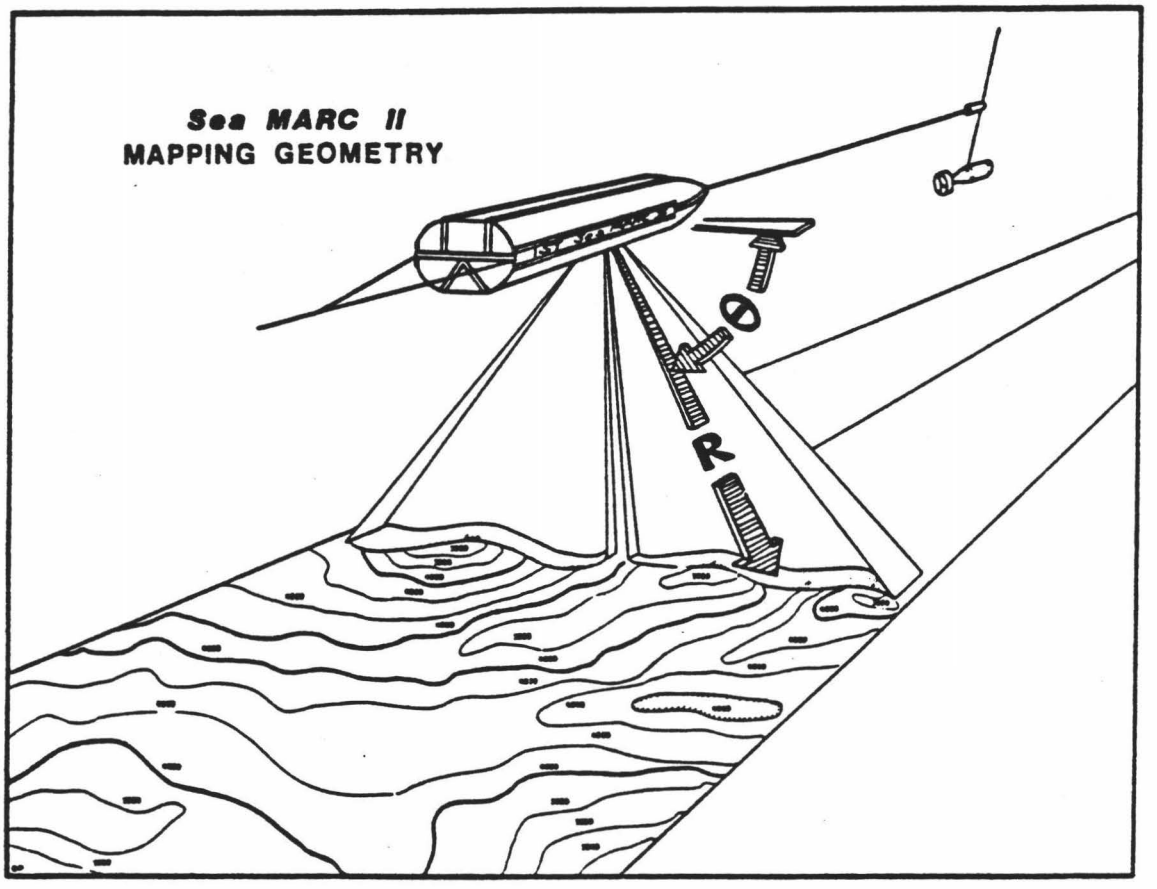
Sea MARC II
MAPPING GEOMETRY
θ
R

text. Contoured bathymetry maps were created using a combination of SeaMARC II bathymetry, side-scan data, and 3.5 kHz bathymetry.

Sediment Properties

Twenty-nine cores located in and around the Moquequa canyon system were analyzed for grain size, mineralogy, carbonate content, and microconstituents. Nineteen of these cores were collected on MW87-09; the remaining cores were collected during 1974 and 1972 cruises of the *R/V Kana Keoki*. Within this area, core sites were not randomly distributed, but rather they were targeted to sample specific geomorphic features. Shear strength was measured on all MW87-09 core tops and bottoms, and at selected intervals deemed interesting by the shipboard scientists. All cores collected on MW87-09 were split and described immediately after their acquisition (Table 1). Core descriptions follow the conventions used in the Deep Sea Drilling Project and Ocean Drilling Project shipboard procedures. Sediment color was assigned according to the Munsell color code.

$CaCO_3$ content was measured by the carbonate-bomb technique of Muller and Gastner (1971). The carbonate bomb consists of a pressure gauge attached to a clear acrylic container. Approximately 1 gram of dry sample was placed within the container, to which five grams of concentrated hydrochloric acid was added and the resulting pressure measured. Calibration of the bomb prior to the initial measurements produced the pressures shown in Table 2. The relationship between the weight of carbonate sediment and the mean pressure released (Figure 5) was analyzed by linear regression, resulting in the following equation:

$$\text{Amount carbonate (g)} = \mathbf{P} \times 0.048265$$

where **P** represents the measured pressure. This equation was used to calculate all subsequent carbonate abundances (Table 3).

TABLE 1.

Location, Water Depth, and Length of Cores Collected During MW8709, Peru-Chile Margin

FFC = free fall core
PC = piston core
RD = rock dredge
PD = pipe dredge

Station	Core	Latitude (S)	Longitude (W)	Depth (m)	Length (cm)	
1	FFC1	18°15.3'	71°58.0'	2390	67	Light olive gray (5Y 5/2) hemipelagic mud with scattered black spots overlying grayish olive (10y 4/2) mud
	FFC2	18°14.1'	71°55.3'	2465	66	Olive gray (5Y 3/2) hemipelagic mud, slightly bioturbated and mottled
	FFC3	18°12.5'	71°50.6'	1657	43	Olive gray (5Y 3/2) hemipelagic mud interbedded with coarse sand
	FFC4	18°11.9'	71°46.9'	1615	78	Olive gray (5Y 3/2) hemipelagic mud with scattered sand lenses
2	PC1	17°59.9'	71°48.1'	980	87	Olive gray sand (5Y 3/2), resettled from suspension, overlying fining upward sequences of dark olive gray (5Y 3/2) medium sand and moderate olive gray (5Y 4/2) mud
3	PC2	17°59.3'	71°47.5'	955	No sample	
	PC3	18°00.4'	71°47.2'	960	Bag of sample	
4	PC4	17°59.5'	71°42.1'	1060	193	Olive gray (5Y 3/2) hemipelagic mud
5	FFC5	18°03.'3	71°26.3'	1070	36	Olive gray (5Y 3/2) hemipelagic mud grading into light olive gray (5Y 5/2) mud
	FFC6	18°04.0'	71°27.5'	1150	Lost	
	FFC7	18°03.4'	71°28.2'	1045	14	Olive gray (5Y 3/2) sandy mud
	FFC8	18°04.0'	71°29.2'	1055	Lost	
	FFC9	18°03.4'	71°31.2'	1160	104	Olive gray (5Y 3/2) hemipelagic mud with coarse silt layers
	FFC10	18°03.4'	71°32.6'	1180	Lost	

TABLE 1.

(Continued) Location, Water Depth, and Length of Cores Collected During MW8709, Peru-Chile Margin

Station	Core	Latitude (S)	Longitude (W)	Depth (m)	Length (cm)	
6	FFC11	17°41.1'	72°22.9'	2045	Lost	
	FFC12	17°41.1'	72°30.0'	2695	71	Olive gray (5Y 3/2) hemipelagic mud with dark olive gray (5Y 4/2) mottling
	FFC13	17°41.2'	72°34.6'	3265	96	Light olive gray (5Y 5/2) hemipelagic mud with dark gray (N2) burrows
7	FFC14	17°41.0'	72°22.7'	2045	72	Grayish olive (10Y 4/2) mud with moderate olive gray (5Y 4/2) laminae beginning at 30 cm
	FFC15	17°40.9'	72°16.8'	1625	Lost	
	FFC16	17°40.9'	72°16.0'	1635	16	Olive gray (5Y 3/2) hemipelagic mud
8	RD1	17°51.2'	72°00.1'	1840	2 kg soft sed.	
9	RD2	18°01.8'	71°54.5'	2040	400 kg	
10	RD3	17°59.3'	71°49.5'	1045		
		17°58.6'	71°49.2'	1015	100 kg	
11	FFC17	17°50.0'	71°44.8'	805	50	Dark grayish olive (10y 3/2) hemipelagic mud overlying light grayish olive (10y 5/2) mud containing a moderate olive brown (5y 4/4) burrow
	FFC18	17°50.0'	71°42.7'	770	55	Sandy olive black (5y 2/1) mud overlying grayish olive (5y 10/2) hemipelagic mud with sandy laminae
	FFC19	17°50.0'	71°40.9'	750	49	Olive gray (5y 3/2) muddy sand overlying mottled grayish olive (10y 4/2) mud with sandy olive gray (5Y 3/2) laminae
	FFC20	17°50.0'	71°39.6'	725	64	Olive gray (5Y 3/2) muddy sand with sand-rich laminae
12	PD1	18°19.6'	71°34.5'	2000	30 kg	
		18°17.5'	71°35.2'	1600		
13	PD2	18°19.9'	71°35.6'	1925	3 kg rock	
		18°18.5'	71°34.8'	1725	40 kg mud	

TABLE 1.

(Continued) Location, Water Depth, and Length of Cores Collected During MW8709, Peru-Chile Margin

Station	Core	Latitude (S)	Longitude (W)	Depth (m)	Length (cm)	
14	FFC21	18°14.9'	71°26.6'	1320	96	Top 4 cm, olive brown (5Y 4/3) clay, disturbed in splitting; grayish-olive clay (10Y 4/2) with sandy laminae and olive brown (5Y 4/3) burrows
	FFC22	18°14.9'	71°23.6'	1250	36	Grayish olive (10Y 4/2) mud with black spots
	FFC23	18°14.9'	71°21.0'	1195	63	Olive brown (5Y 4/3) slightly sandy mud grading into grayish olive (10Y 4/2) clay
	FFC24	18°14.9'	71°19.2'	1130	44	Disturbed olive brown (5Y 3/4) mud overlying grayish olive (10y 4/2) mud
15	FFC25	18°00.5'	71°23.0'	940	32	Olive brown (5Y 3/4) sandy mud with a strong H2S odor
	FFC26	17°59.6'	71°22.9'	920	63	Homogeneous, olive gray (5Y 3/2) hemipelagic mud; top 40 cm is fluid compared to lower 20 cm
	FFC27	17°57.5'	71°23.1'	850	58	Olive brown (5Y 3/4) unconsolidated mud overlying grayish olive (10Y 4/2) mud with burrows of olive brown (5Y 3/4) mud and pods of olive gray (5Y 3/2) fine sand
	FFC28	17°56.7'	71°23.2'	825	68	Olive brown (5Y 3/4) bioturbated mud; burrows filled with grayish blue green (5BG 5/2) mud
24	FFC44	18°14.1'	71°03.8'	645	45	Olive gray (5Y 5/2) sandy mud
	FFC45	18°14.2'	71°06.1'	660	35	Olive gray (5Y 3/2) unconsolidated muddy sand with a few semi-consoloidated clay clasts overlying grayish olive (10Y 4/2) sandy mud
	FFC46	18°14.3'	71°07.7'	605	9	Olive gray (5Y 3/2) muddy sand
	FFC47	18°14.2'	71°08.6'	550	Lost	
25	FFC48	18°12.0'	71°16.1'	1078	39	Moderate olive gray (5Y 4/2) hemipelagic mud
	FFC49	18°10.0'	71°16.5'	1045	37	Soupy, olive brown (5Y 3/4) silty clay overlying moderate olive brown (5Y 4/4) clay with sandy laminae
	FFC50	18°08.3'	71°16.5'	1052	87	Olive brown (5Y 3/4) to moderate olive gray (5Y 4/2) mud with scattered laminae of sand

TABLE 1.

(Continued) Location, Water Depth, and Length of Cores Collected During MW8709, Peru-Chile Margin

Station	Core	Latitude (S)	Longitude (W)	Depth (m)	Length (cm)	
		LOWER TRENCH SLOPE				
16	FFC29	18°53.3'	71°30.4'	3300	Lost	
	FFC30	18°53.3'	71°27.7'	3730	85	Mottled light olive gray (5Y 5/2) to grayish olive(10Y4/2) mud with white specks
	FFC31	18°53.3'	71°26.3'	2880	101	Light olive brown (5Y 5/5) mud overlying regularly laminated light olive gray (5Y 5/2) hemipelagic mud
	FFC32	18°53.2'	71°23.9'	2750	95	Dusky yellow green (5GY 5/2) hemipelagic mud with a small degree of bioturbation
17	FFC33	18°48.8'	71°33.2'	3545	5	Olive gray (5Y 3/2) medium sand
	FFC34	18°48.9'	71°30.1'	3430	83	Moderate olive brown (5Y 4/4) to moderate olive gray (5Y 4/2) hemipelagic mud with numerous cross-laminated, fine- to medium-grained, olive gray (5Y 3/2) sand (fairly clean) laminae; mottling is prevalent in the lower half of the core and an olive black (5Y 2/1) layer at 41 cm emits an H2S odor
	FFC35	18°48.9'	71°28.8'	3210	87	Heavily mottled and laminated moderate olive gray (5Y 4/2) to moderate olive brown (5Y 4/4) hemipelagic mud; intermittant silt layers mark the base of fining upward sequences
18	PC5	18°44.1'	71°28.0'	3290	No sample	
	PC6	18°44.1'	71°28.0'	3290	127	Cycles of olive gray (5y 4/2) and grayish olive (10y 4/2) to light olive (10y 5/2) mud laminae
19	PC7	18°43.8'	71°33.6'	3265	109	Light grayish olive (10Y 5/2) mud with scattered pods of olive gray (5Y 3/2) fine-sand
20	FFC36	18°34.0'	71°39.5'	2535	73	Slightly mottled grayish olive (10Y 4/2) hemipelagic mud
	FFC37	18°33.9'	71°36.3'	2405	87	Light olive brown (5Y 5/6) mud overlying mottled light olive gray (5Y 5/2) mud
	FFC38	18°34.4'	71°34.2'	2670	82	Mottled dark grayish olive (10Y 3/2) sandy mud

TABLE 1.

(Continued) Location, Water Depth, and Length of Cores Collected During MW8709, Peru-Chile Margin

Station	Core	Latitude (S)	Longitude (W)	Depth (m)	Length (cm)	
	FFC39	18°34.5'	71°31.5'	2625	Lost	
21	FFC40	18°29.4'	71°39.3'	2540	93	Olive brown (5Y 3/4) mud grading into light grayish olive (10Y 5/2) mottled mud
	FFC41	18°29.5'	71°37.8'	2505	92	Moderate olive brown (5Y 4/4) mud with scattered olive brown (5Y 2/4) mottling grading into moderate grayish olive (10Y 5/2) mud; sand laminae visible at the base of the core
22	FFC42	18°48.4'	71°54.0'	4980	91	Heavily mottled grayish olive (10y 4/2) to greenish gray (5G 6/1) mud with laminae of varying colors
	FFC43	18°48.5'	71°51.5'	4810	93	Dusky yellow (5Y 6/4) mud overlying pale olive (10Y 6/2) to grayish olive (10Y 4/2) bioturbated hemipelagic mud
23	PC8	18°49.5'	71°40.6'	3925	109	Core top upset during cutting; olive gray (5Y 3/2) mud laminated with lighter-colored mud near the core bottom

TABLE 2

Values Used in the Carbonate Bomb Calibration. Weights of Powdered Calcite and the Pressures Released when Treated with HCl

Wt. $CaCO_3$ (grams)	Run #1 (psi)	Run #2 (psi)	Run #3 (psi)	Run #4 (psi)	Run #5 (psi)	Average (psi)
0.1	2.1	2.1	2.3	2.2	2.1	2.16
0.2	4.2	4.4	4.4	4.3	4.4	4.34
0.3	6.3	6.2	6.3	6.3	6.2	6.26
0.4	8.2	8.1	8.6	8.1	8.4	8.28
0.5	10.1	10.1	10.3	10.3	10.2	10.20
0.6	12.2	12.3	12.4	12.4	12.4	12.34
0.7	14.3	14.1	14.1	14.2	14.1	14.16
0.8	16.5	16.5	16.5	16.4	16.6	16.50
0.9	18.9	18.5	18.5	18.6	18.5	18.60
1.0	20.9	20.8	21.6	21.2	21.1	21.12

Figure 5. Average pressures in pounds per square inch from five calibration tests of the carbonate bomb. Least squares linear regression produced the inset formula used for calculating carbonate content.

CARBONATE BOMB CALIBRATION

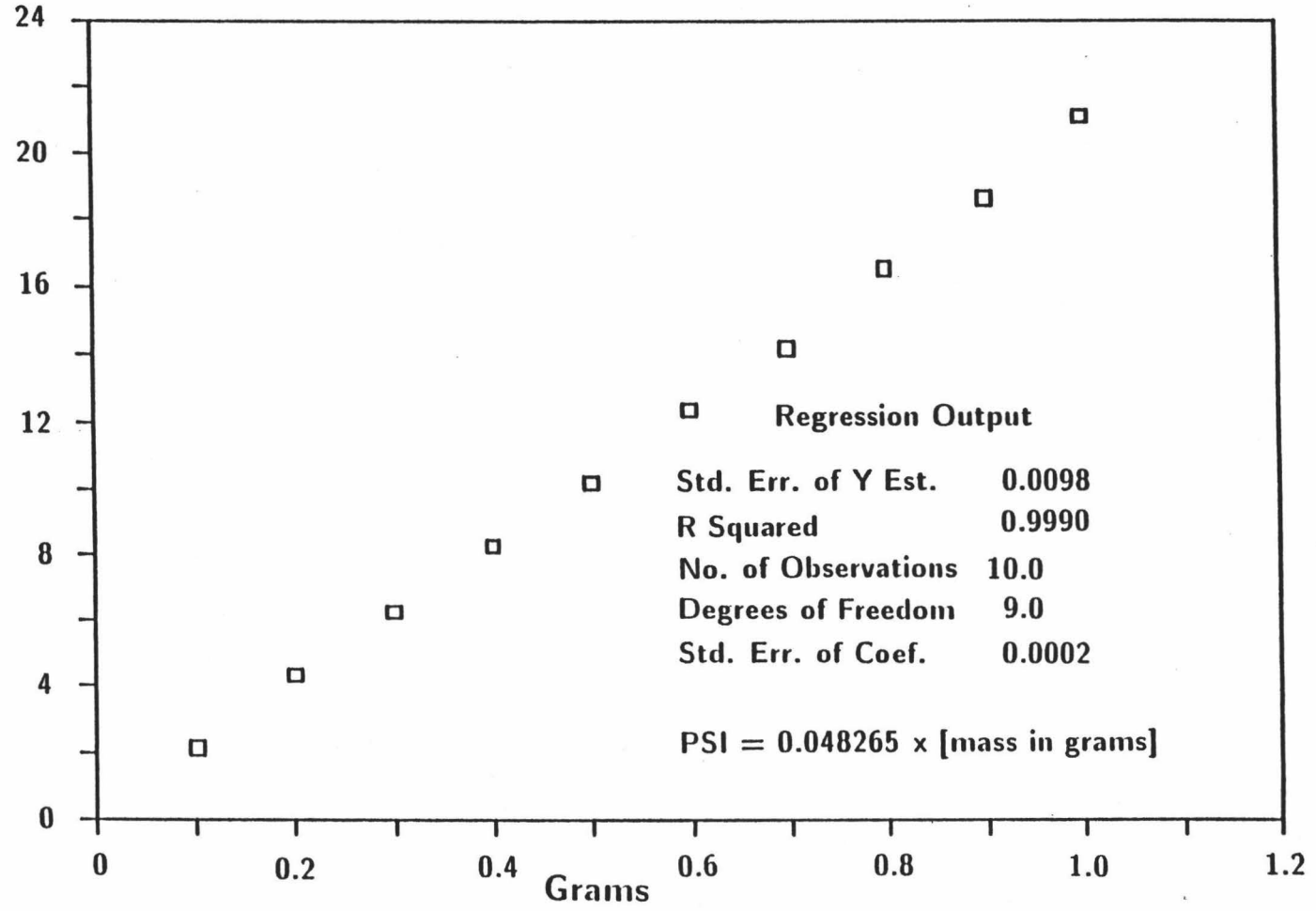

TABLE 3

Carbonate content in core tops collected from the Peru-Chile margin.

Core	Sample Weight (gm)	Pressure Released (psi)	Carbonate Abundance (%)	Thalweg Distance (km)
KFFC26	1.00	1.6	7.72	60.1
KFFC27	1.00	0.8	3.86	40.1
FFC32	1.02	1.0	4.73	27.6
KPC10	1.00	0.8	3.86	25.5
FFC31	1.00	0.5	2.41	23.0
FFC30	1.01	0.5	2.39	20.0
KPC16	1.00	1.5	7.24	17.2
FFC43	1.00	1.1	5.31	16.5
FFC42	0.30	0.5	8.04	13.6
KFFC30	1.02	1.0	4.73	10.4
FFC35	1.01	0.9	4.30	8.4
PC6	1.01	0.7	3.35	6.8
PC8	1.01	1.3	6.21	6.0
FFC37	1.01	0.6	2.87	6.0
FFC36	1.00	0.6	2.90	4.9
FFC34	1.00	0.5	2.41	4.8
KFFC31	1.02	0.3	1.42	4.0
FFC9	1.01	1.0	4.78	3.2
FFC40	1.01	1.0	4.78	2.5
PC7	1.02	0.7	3.31	2.2
FFC38	1.02	0.7	3.31	2.0
FFC41	1.00	1.2	5.79	1.7
FFC5	1.00	3.0	14.48	1.6
KPC9	1.00	0.8	3.86	1.0
FFC7	1.00	0.7	3.38	1.0
FFC33	1.18	3.3	13.50	0.8
KFFC32	1.02	0.5	2.37	0.8
KPC11	1.00	1.0	4.83	0.6
KFFC34	1.01	0.3	1.43	0.4

Grain size was measured by sieving and pipetting, following the methodology of Folk (1974) and Lewis (1984). Appendix C gives a detailed description of sample preparation and pipetting procedures. To summarize these procedures, about 10 grams from each core top was dried and weighed. This sample was then treated with 10 ml hydrogen peroxide and 10 ml distilled water, dried, and then reweighed to obtain the organic content. The final treatment prior to pipetting was disaggregation with a stock solution of sodium hexametaphosphate (Calgon) and distilled water. After disaggregation, the sample was sieved through a 200 mesh screen (64 micron) into a 1000 ml graduated cylinder, separating the sand fraction from the silt and clay fraction. The sand fraction was dried and weighed to determine the coarse fraction.

An additional 20 ml of dispersant was added to the cylinder prior to pipetting. The cylinder was then stirred and allowed to settle 24 hours to check for clay flocculation. Size intervals from 4-phi to 9-phi were extracted, dried, and weighed. Weight percents for each interval were computed by the program PIPE.FOR (Appendix C) and are shown in Table 4. Mean grain size for each sample was computed by the method of moments (Griffiths, 1967; Table 4).

Bulk mineralogy was determined through the analysis of X-ray diffractograms. Powdered samples were mounted unoriented and X-rayed from 2^{o} to 70^{o} 2Θ under CuK-α radiation. Mineral peaks were identified qualitatively (Brindley and Brown, 1980). Five minerals groups (quartz, feldspar, calcite, clinoptilolite, and total clay) were analyzed semi-quantitatively according to the procedures followed by Mann and Mueller (1979). Relative intensities were scaled according to mineral type and converted to relative percentages and ratios (Table 5).

A torvane was used to measure the approximate undrained shear strength. The torvane permits rapid determination of a large number of shear strength values in samples with different orientations of failure planes. The instrument has a stress range

TABLE 4

Grain Size Distribution in Core Tops Collected from the Moquequa Submarine Canyon System, Peru-Chile Margin

Sample	Organics (%)	Sand (%)	4.5 (%)	5.0 (%)	5.5 (%)	6.0 (%)	7.0 (%)	8.0 (%)	9.0 (%)	Clay (%)	Mean (phi)
FFC5	.181	5.263	9.075	10.436	7.712	7.714	14.972	12.251	7.259	25.137	6.82
FFC7	.458	80.382	1.908	1.145	1.909	.763	2.672	1.145	0.763	8.855	4.28
FFC9	2.972	5.297	3.875	7.753	10.335	10.336	19.380	12.273	4.522	23.257	6.82
FFC30	1.471	.401	.669	1.337	8.689	6.017	20.054	12.032	18.716	30.614	7.73
FFC31	1.295	.576	1.439	3.597	6.475	9.353	14.387	18.704	13.670	30.504	7.61
FFC32	1.241	.372	.620	3.722	8.065	6.824	17.991	21.092	13.646	26.427	7.54
FFC33	.266	49.135	2.664	3.992	4.662	4.660	6.658	5.326	4.660	17.977	5.48
FFC34	4.865	2.523	5.406	5.404	12.613	27.026	10.812	18.919	9.009	3.423	6.27
FFC35	0.000	8.118	3.076	10.454	11.683	12.300	7.995	7.995	10.454	27.925	6.87
FFC36	3.628	2.902	6.045	3.024	5.442	4.836	18.137	25.394	1.209	29.383	7.32
FFC37	0.452	.753	3.013	7.529	10.542	4.518	22.591	21.837	11.295	17.470	7.09
FFC38	0.547	16.963	2.052	3.419	12.997	6.156	17.100	12.995	4.789	22.982	6.61
FFC40	2.112	.452	3.769	3.772	5.279	6.033	21.116	3.018	4.522	49.927	7.87
FFC41	1.644	1.038	2.595	6.055	7.353	7.784	19.464	18.166	3.028	32.873	7.39
FFC42	.917	2.599	.766	11.467	9.939	10.703	17.583	8.411	14.524	23.091	7.04
FFC43	.627	1.003	6.267	5.638	6.266	10.026	14.410	18.797	15.037	21.929	7.22
PC6	2.900	11.602	5.675	8.827	10.089	8.827	16.394	10.088	3.153	22.445	6.51
PC7	2.811	1.205	1.007	2.003	2.011	12.049	18.070	15.060	9.039	36.745	7.73
PC8	4.798	5.397	2.249	6.746	10.496	13.493	17.240	4.498	1.498	33.585	7.03
KPC9	.598	3.984	.995	7.969	7.968	7.968	20.916	16.934	10.954	21.714	7.09
KPC10	.385	46.667	12.821	3.846	5.128	5.128	6.412	5.769	2.563	11.281	5.11
KPC11	.000	4.643	6.633	4.147	9.121	13.268	17.413	19.070	8.294	17.411	6.80
KPC16	.000	1.037	3.112	6.225	3.112	7.261	17.635	8.296	18.674	34.648	7.67
KFFC26	.000	1.258	2.095	4.195	8.387	10.480	17.820	17.820	11.530	26.415	7.35
KFFC27	.214	.429	2.147	3.219	2.147	8.583	15.021	24.677	11.804	31.759	7.71
KFFC28	.000	.568	2.839	.005	4.259	7.104	14.202	26.995	9.938	34.090	7.80
KFFC3O	.497	4.801	7.451	9.935	9.931	8.278	14.073	14.073	8.278	22.683	6.81
KFFC31	1.092	6.332	14.193	16.377	15.282	15.284	12.008	8.735	9.826	0.871	5.69
KFFC32	1.121	7.623	12.331	3.364	10.088	3.364	14.572	16.818	14.575	16.144	6.77
KFFC34	2.000	3.333	1.113	3.332	10.001	8.888	21.112	17.776	4.444	28.001	7.24

TABLE 5

Percent Abundances of 5 Mineral Groups Identified by X-ray Diffraction in Core Tops Collected from the Peru-Chile Margin

Core	Quartz Abund.	Feld. Abund.	Calc. Abund.	Clay Abund.	Clinop. Abund.	F/Q Ratio	Ca/Q Ratio	Clay/Q Ratio	Clin/Q Ratio	Ca/F Ratio	Clay/F Ratio	Clay/QF Ratio
KFFC26	25	23	0	51	0	0.9	0.0	2.0	0.0	0.0	2.1	1.0
KFFC27	19	17	0	62	0	0.8	0.0	3.1	0.0	0.0	3.6	1.7
FFC32	23	18	0	57	0	0.7	0.0	2.3	0.0	0.0	3.0	1.3
KPC10	17	32	10	39	0	1.8	0.6	2.2	0.0	0.3	1.2	0.7
FFC31	23	17	0	58	0	0.7	0.0	2.4	0.0	0.0	3.3	1.4
FFC30	23	17	0	56	2	0.7	0.0	2.3	0.1	0.0	3.1	1.3
KPC16	21	15	0	61	2	0.7	0.0	2.8	0.1	0.0	4.0	1.6
FFC43	21	19	0	56	2	0.8	0.0	2.5	0.1	0.0	2.9	1.3
FFC42	21	18	0	58	1	0.9	0.0	2.7	0.0	0.0	3.0	1.4
KFFC30	19	38	10	30	1	1.9	0.5	1.5	0.0	0.2	0.7	0.5
FFC35	22	22	9	45	0	0.9	0.4	1.9	0.0	0.4	2.0	1.0
PC6	27	22	0	48	1	0.8	0.0	1.7	0.0	0.0	2.1	0.9
PC8	16	18	0	65	0	1.0	0.0	3.9	0.0	0.0	3.6	1.8
FFC37	21	19	0	56	2	0.9	0.0	2.6	0.1	0.0	2.8	1.3
FFC36	20	22	0	54	2	1.0	0.0	2.6	0.1	0.0	2.4	1.2
FFC34	17	41	2	36	1	2.3	0.1	2.0	0.0	0.0	0.8	0.6
KFFC31	17	46	0	34	1	2.5	0.0	1.9	0.0	0.0	0.7	0.5
FFC9	13	42	8	33	1	3.0	0.6	2.4	0.0	0.2	0.8	0.6
FFC40	23	17	0	59	0	0.7	0.0	2.5	0.0	0.0	3.4	1.4
PC7	20	18	0	58	2	0.9	0.0	2.8	0.1	0.0	3.1	1.4
FFC38	24	23	0	52	0	0.9	0.0	2.1	0.0	0.0	2.1	1.0
FFC41	13	61	0	25	0	4.6	0.0	1.8	0.0	0.0	0.4	0.3
FFC5	18	27	12	41	0	1.4	0.6	2.2	0.0	0.4	1.5	0.9
FFC7	8	90	0	0	0	10.0	0.1	0.0	0.0	0.0	0.0	0.0
KPC9	18	23	3	50	3	1.2	0.2	2.6	0.1	0.1	2.1	1.2
FFC33	7	81	0	10	0	11.0	0.0	1.4	0.0	0.0	0.1	0.1
KFFC32	20	22	3	48	5	1.0	0.1	2.3	0.2	0.1	2.2	1.1
KPC11	21	21	3	50	2	1.0	0.1	2.3	0.1	0.1	2.3	1.1
KFFC34	21	24	2	51	0	1.1	0.1	2.3	0.0	0.1	2.0	1.1

of 0 to 2.5 kg/cm^2. The blades on the vane were inserted into the center of the spit core until the plate was flush with the sediment surface. The dial head was then rotated until the blades slipped, giving the amount of torque applied to the sediment at failure. All shear strengths were averaged over a 1 m core interval (Table 6).

Smear slides were prepared using PRO-TEXX mounting medium. Percentage estimates were made for quartz, feldspar, mica, clay and zeolites, pyrite and other opaques, glauconite, volcanic glass, undifferentiated carbonate, diatoms, radiolaria, foraminifera, coccoliths, sponge spicules, and an unspecified category labeled "others."

TABLE 6

Shear Strengths for Cores Collected During MW8709, Peru-Chile Margin. Shear Strength Averaged Over a 1 Meter Interval.

Core	Shear Strength (kg/cm2)
FFC32	0.80
FFC31	0.68
FFC30	0.93
FFC43	0.68
FFC42	0.73
FFC35	0.35
PC6	0.70
PC8	0.25
FFC37	0.60
FFC36	1.15
FFC34	0.43
FFC9	0.85
FFC40	1.17
FFC38	0.88
PC7	1.15
FFC41	1.03
FFC5	1.80
FFC33	0.00
FFC7	0.75

CHAPTER 4

SIDE-SCAN INTERPRETATION

The main channel composing the Moquequa Submarine Canyon system follows a sinuous, north-south trend across the Arequipa Basin, apparently heading at the Rio Moquequa in southern Peru (Figure 6a). Within the basin, this channel exhibits sinuosities up to 2.0 and relief of approximately 200 to 300 m. The meander-like bends in the channel are a product of large slumps formed by cut-bank erosion along the walls. Tributary channels of lesser relief, averaging 100 m, coelesce with MSC from the northeast near the structural high. One channel in the southeast portion of Figure 6a has formed a small fan behind the structural high (note the deflection of contours in a downslope direction near free-fall cores FFC44, FFC45, FFC46, and FFC47). Sediment waves of less than 100 m relief are a pervasive feature in the Arequipa Basin east of MSC's main channel.

After traversing the Arequipa Basin, the morphology of Moquequa Submarine Canyon changes dramatically upon breaching the structural high bounding the basin (Figure 6, a and b; top border of Figure 7). Across the lower trench slope, MSC becomes more entrenched and less sinuous than its tributaries that cross the Arequipa Basin. The breach in the high trends northwest-southeast, parallel to the Peruvian coastline (top border of Figure 7 and Figure 8a, A) and exhibits over 500 m of relief (Figure 6b). Although this trend could be purely an accident of erosion, it seems more likely to result from a regional fabric or a fault. Listric, normal faults dissect the margin, causing block rotation and landward tilting of reflectors (Figure 9). MSC appears to cross the structural high along one of these fault planes. The offset in canyon relief, 600 m on the western bank and 860 m on the eastern bank, probably results from the downward rotation of the block on the seaward side of the fault. This thinning and wearing away of the margin by mechanical entrainment of the descending oceanic plate

Figure 6. SeaMARC II bathymetry for the Arequipa Basin (a) and for the lower trench slope (b). Core locations discussed in thesis are shown as dots and dredges are shown as triangles. The K prefix denotes cores collected during the KK74 or KK72 cruise in this area; all other cores collected during MW87-09. Depths listed are multiples of 100.

FFC = Free-fall core
PC = Piston core
D = Rock dredge
PD = Pipe dredge

● = Core lost
○ = Core recovered

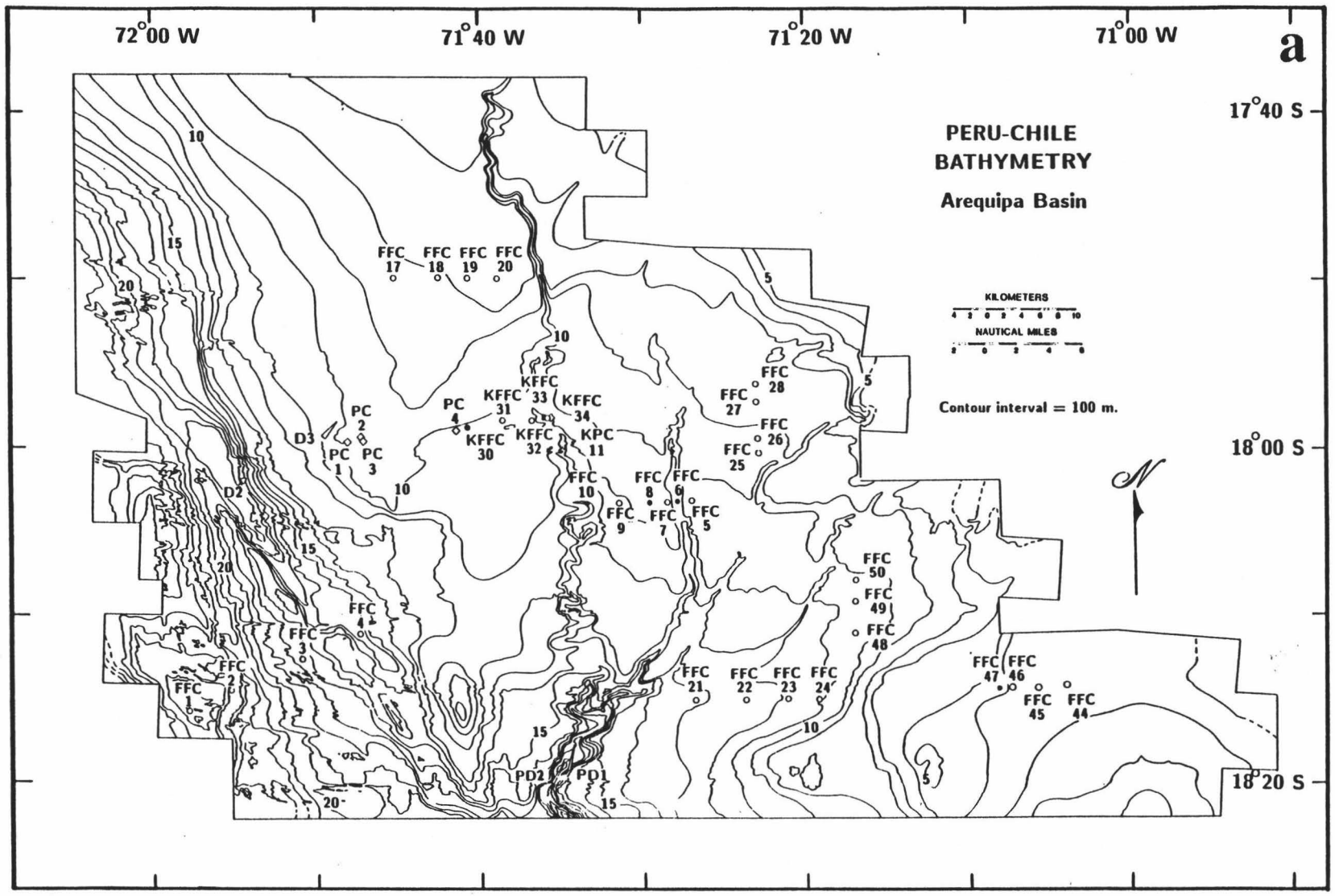
72°00 W
71°40 W
71°20 W
71°00 W
a
17°40 S
18°00 S
18°20 S
PERU-CHILE
BATHYMETRY
Arequipa Basin
KILOMETERS
NAUTICAL MILES
Contour interval = 100 m.
N
FFC 17
FFC 18
FFC 19
FFC 20
FFC 1
FFC 2
FFC 3
FFC 4
PC 1
PC 2
PC 3
PC 4
D2
D3
KFFC 30
KFFC 31
KFFC 32
KFFC 33
KFFC 34
KPC 11
FFC 5
FFC 6
FFC 7
FFC 8
FFC 9
FFC 10
FFC 21
FFC 22
FFC 23
FFC 24
FFC 25
FFC 26
FFC 27
FFC 28
FFC 44
FFC 45
FFC 46
FFC 47
FFC 48
FFC 49
FFC 50
PD1
PD2

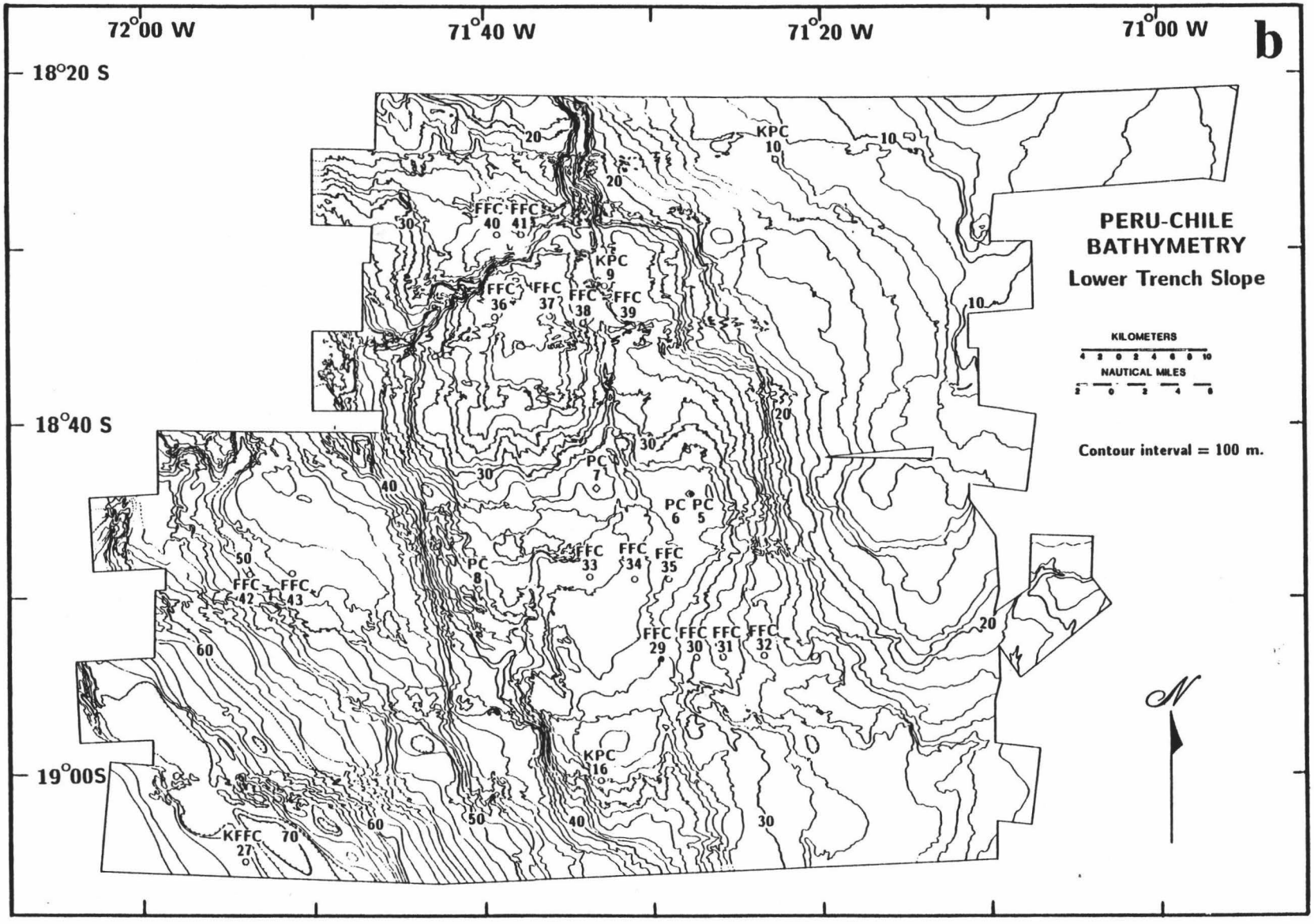
b
72°00 W
71°40 W
71°20 W
71°00 W
18°20 S
18°40 S
19°00S
PERU-CHILE
BATHYMETRY
Lower Trench Slope
KILOMETERS
NAUTICAL MILES
Contour interval = 100 m.
N
KPC 10
FFC 40
FFC 41
KPC 9
FFC 36
FFC 37
FFC 38
FFC 39
PC 7
PC 6
PC 5
PC 8
FFC 33
FFC 34
FFC 35
FFC 42
FFC 43
FFC 29
FFC 30
FFC 31
FFC 32
KPC 16
KFFC 27

Figure 7. Interpretation enhancing the regional physiography visible in the side-scan images collected across the lower trench slope (see Appendix B). Shading is based on a light source from the northeast. Scarps are generally drawn as lines, sedimentary bedforms as dot patterns, and tributaries as alternating dots and lines. Also shown are the locations of the single-channel seismic and 3.5 kHz profiles discussed in subsequent figures.

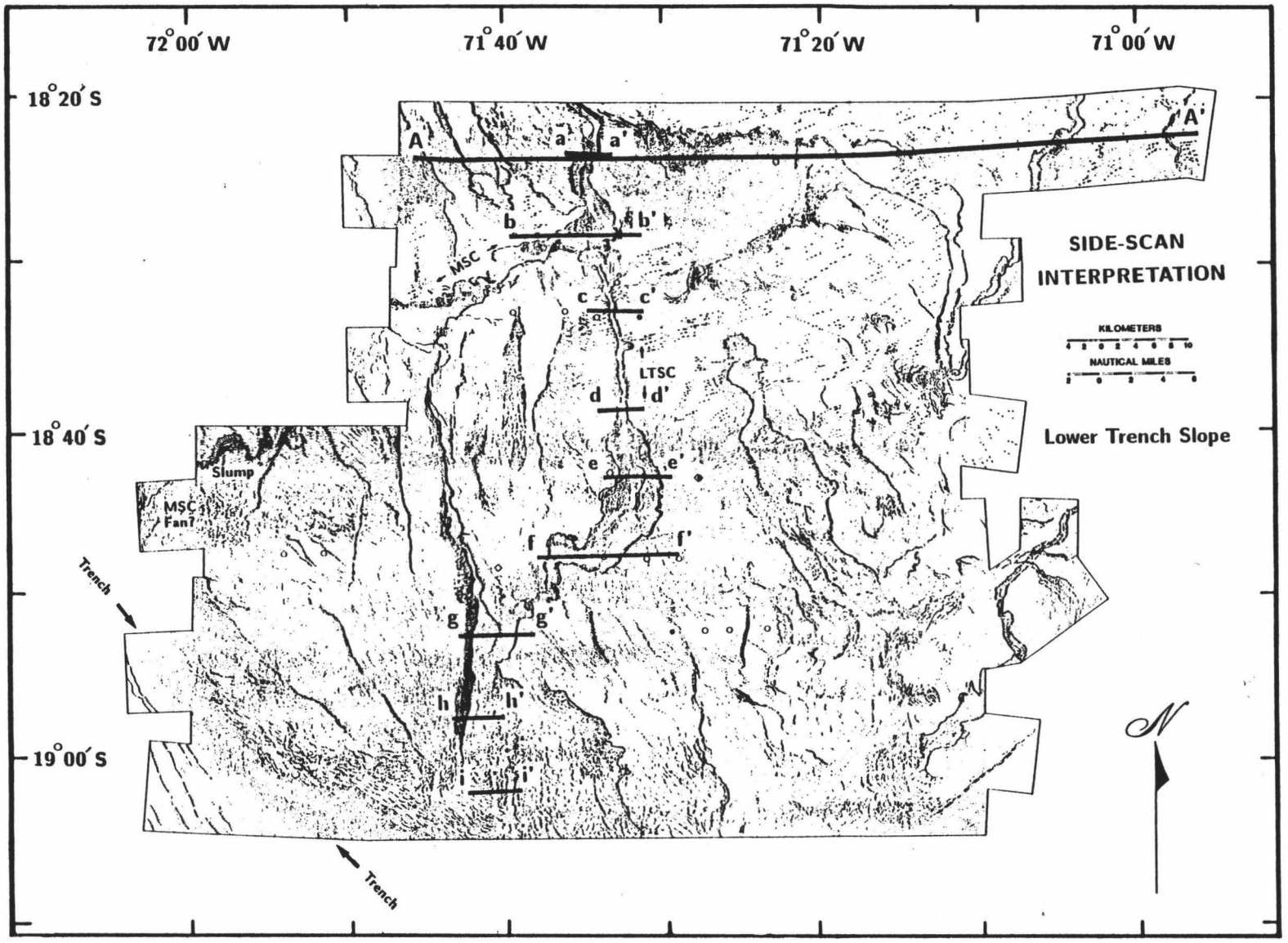
72°00´W
71°40´W
71°20´W
71°00´W
18°20´S
18°40´S
19°00´S
A
A'
a
a'
b
b'
MSC
c
c'
LTSC
d
d'
e
e'
f
f'
g
g'
h
h'
i
i'
Slump
MSC Fan?
Trench
Trench
SIDE-SCAN
INTERPRETATION
KILOMETERS
NAUTICAL MILES
Lower Trench Slope
N

Figure 8. Side-scan images (a) and interpretation (b) of the area where MSC breaches the structural high, turns to the southwest, and the LTSC drainage basin forms. Labels on the side-scan images are discussed in the text.

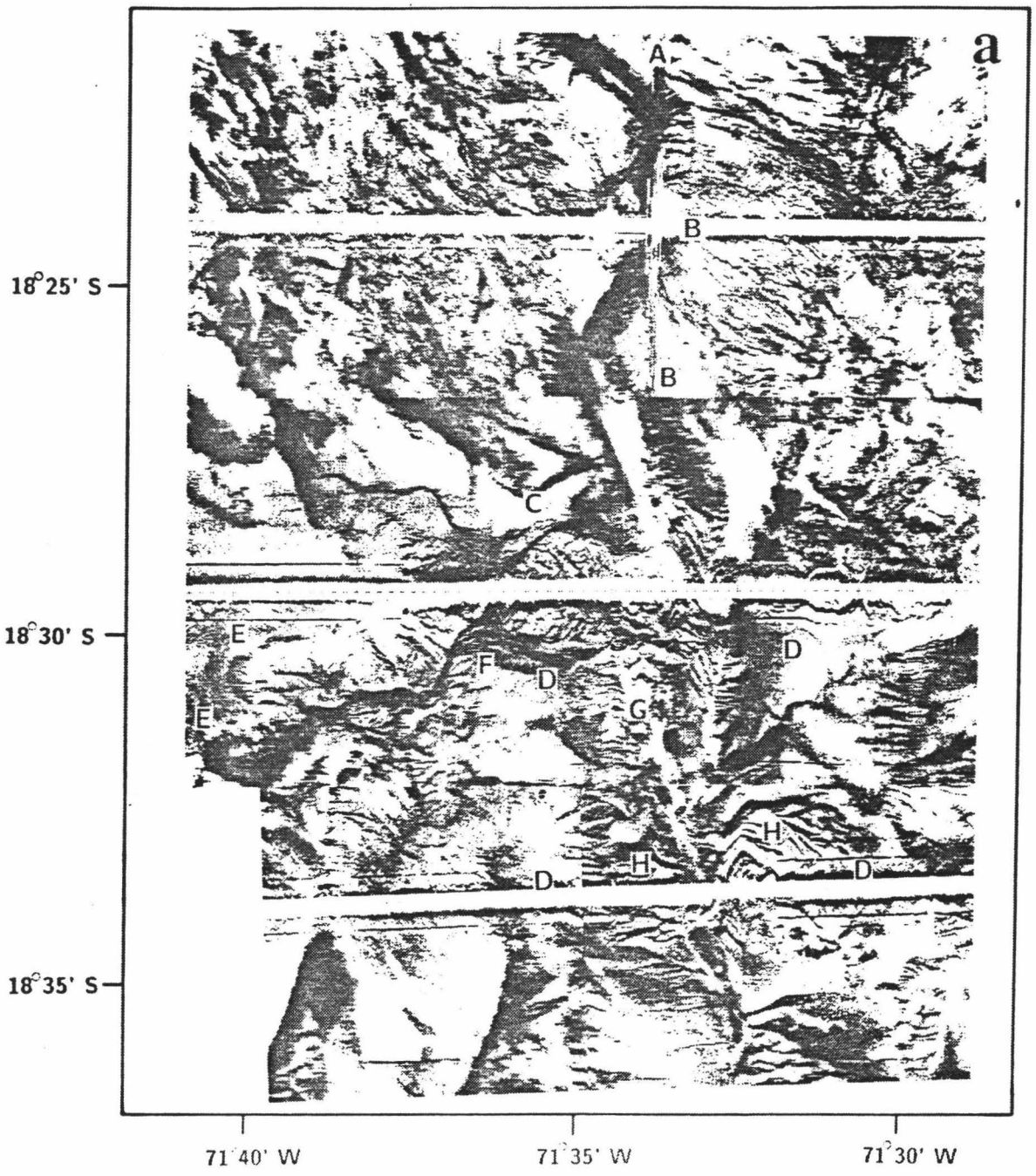
a
A
B
B
C
E
F
D
G
E
D
H
H
D
D
18°25' S
18°30' S
18°35' S
71°40' W
71°35' W
71°30' W

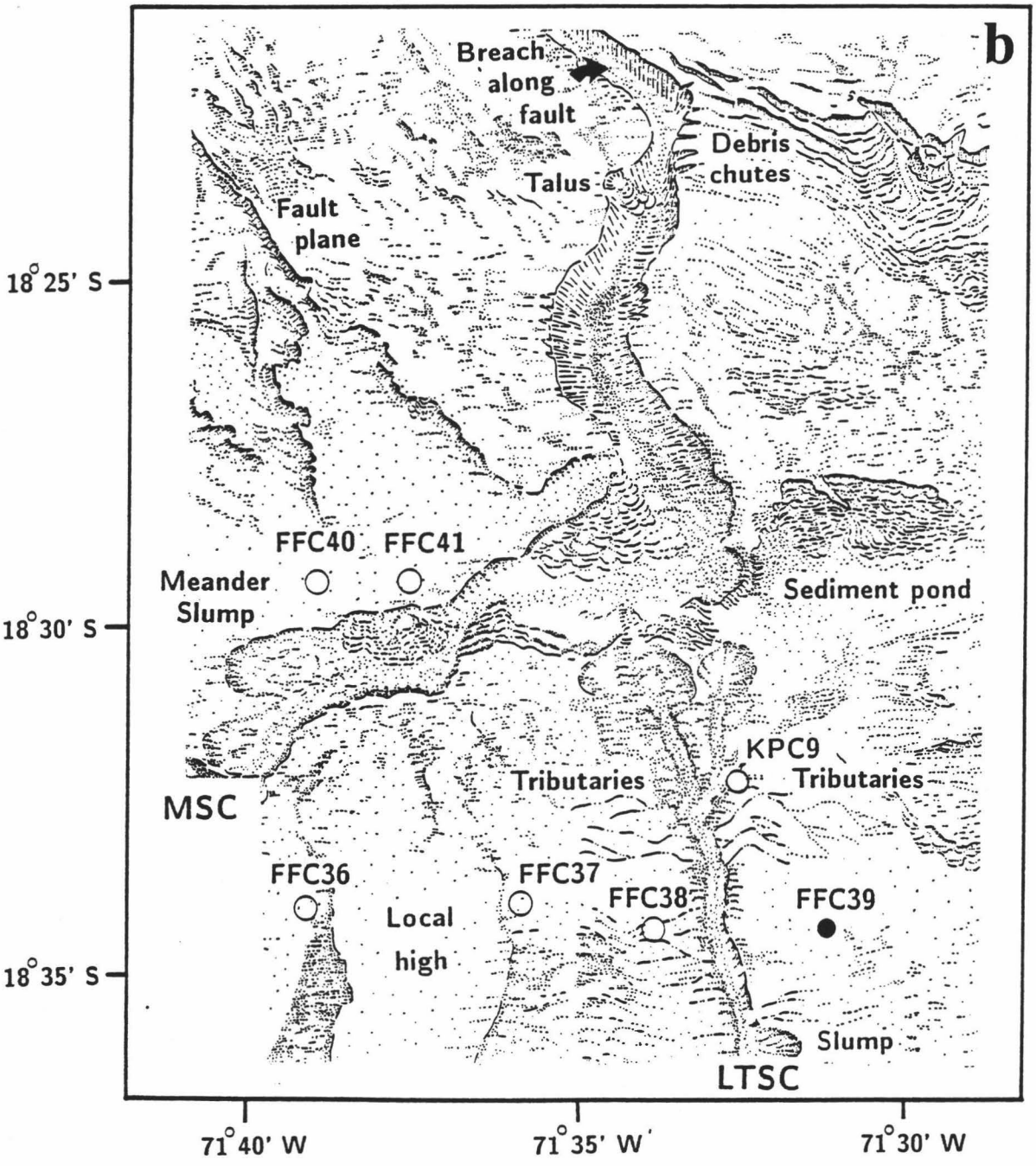
b
Breach along fault
Debris chutes
Talus
Fault plane
18° 25' S
FFC40
FFC41
Meander Slump
Sediment pond
18° 30' S
KPC9
Tributaries
Tributaries
MSC
FFC36
FFC37
FFC38
FFC39
Local high
18° 35' S
Slump
LTSC
71° 40' W
71° 35' W
71° 30' W

Figure 9. Single-channel seismic profile A-A'. Block rotation and landward tilting of reflectors are visible both east and west of the MSC breach. Vertical axis is 2-way travel time.

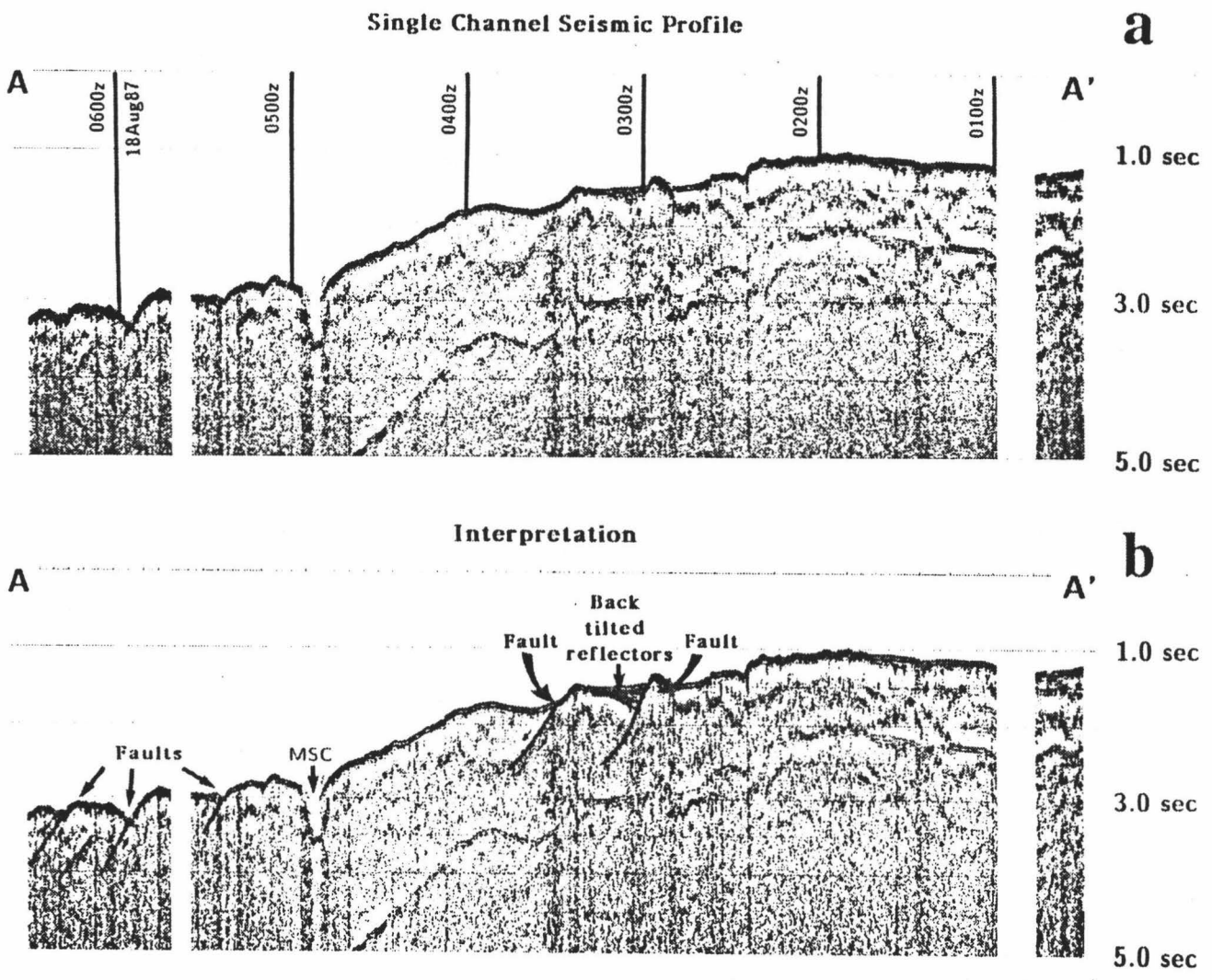
Single Channel Seismic Profile
a
A
A'
0600z
18Aug87
0500z
0400z
0300z
0200z
0100z
1.0 sec
3.0 sec
5.0 sec
Interpretation
b
A
A'
Back
tilted
reflectors
Fault
Fault
Faults
MSC
1.0 sec
3.0 sec
5.0 sec

was termed by Scholl and others (1980) as "subduction erosion." Subduction erosion has been noted along the Peru margin between 11^{o} and 12^{o} S in previous studies (Hussong and others, 1976; Hussong and Wipperman, 1981).

A short distance from the breach in the structural high, MSC departs one fault plane to intersect another farther downslope (Figure 8a, B). The relief of MSC decreases from a maximum of over 700 m at the breach, to less than 200 m at the change in trend of MSC to the SW, and eventually increasing again to around 400 m near the mouth of MSC at the trench (Figure 6b and Figure 10). A small talus accumulation rests on the canyon floor from a failed portion of the western bank (Figures 8a, 8b). Debris chutes cut the eastern bank, disrupting the steep canyon walls. After coursing southward for approximately 5.5 km, MSC jogs sharply to the southwest (Figure 8a, C). A 3.5 kHz profile across this bend (Figure 11) shows levees flanking both banks. Canyon relief varies from 180 to 280 m, whereas levee relief differs by 20 m from west (60 m) to east (40 m). An acoustically stratified sediment pond lies outside the eastern bank. The reflectors probably represent overbank deposits; the fine-fraction of episodic turbidites is ramped over the bank as the channel turns to the southwest. Immediately south of this change in course, a dendritic drainage basin is forming (Figure 8a, D).

As MSC continues to the southwest, slumping becomes more prevalent along the canyon walls. Two of the slumps face upchannel (Figure 8a, E), while others farther downslope face perpendicular to the channel (Figure 7). The slumps probably result from cut-bank erosion; basal sediments are eroded by turbidity currents, leaving a perched, unstable layer of semi-coherent sediment. Eventually, the shear strength of the perched layer is exceeded by its mass, and the sidewall slumps into the channel. Slumping of this sort is ubiquitous throughout the upper reaches of the canyon in the Arequipa Basin. A similar mechanism for channel-wall failure has been proposed for the Valencia Valley in the northwestern Mediterranean (O'Connell and others, 1985). On

Figure 10. 3.5 kHz profiles of MSC and LTSC across the lower trench slope. Location of profiles shown in Figure 7. Profiles show the degradation in relief of MSC and LTSC as they traverse the lower trench slope. All profiles oriented such that east is to the right and west is to the left. Figure labels correspond as follows: a-a' MSC breaches the structural high. The difference in relief between the east and west banks is caused by block rotation. b-b' MSC changes course to the southwest. A sediment pond has formed behind the eastern levee. c-c' LTSC forms between two confining blocks. Undulating topography to the east is caused by tributaries coalescing with the main LTSC channel. d-d' Narrow upper section of LTSC trending in a southward direction. e-e' LTSC begins to widen in response to a decrease in gradient. f-f' LTSC meanders to the west as the confining seaward block loses relief. g-g' LTSC follows the edge of a rotated block. h-h' LTSC barely visible as it continues to trend in a south-southeast direction to the trench. i-i' LTSC has lost all definition prior to terminating at the toe of the lower trench slope.

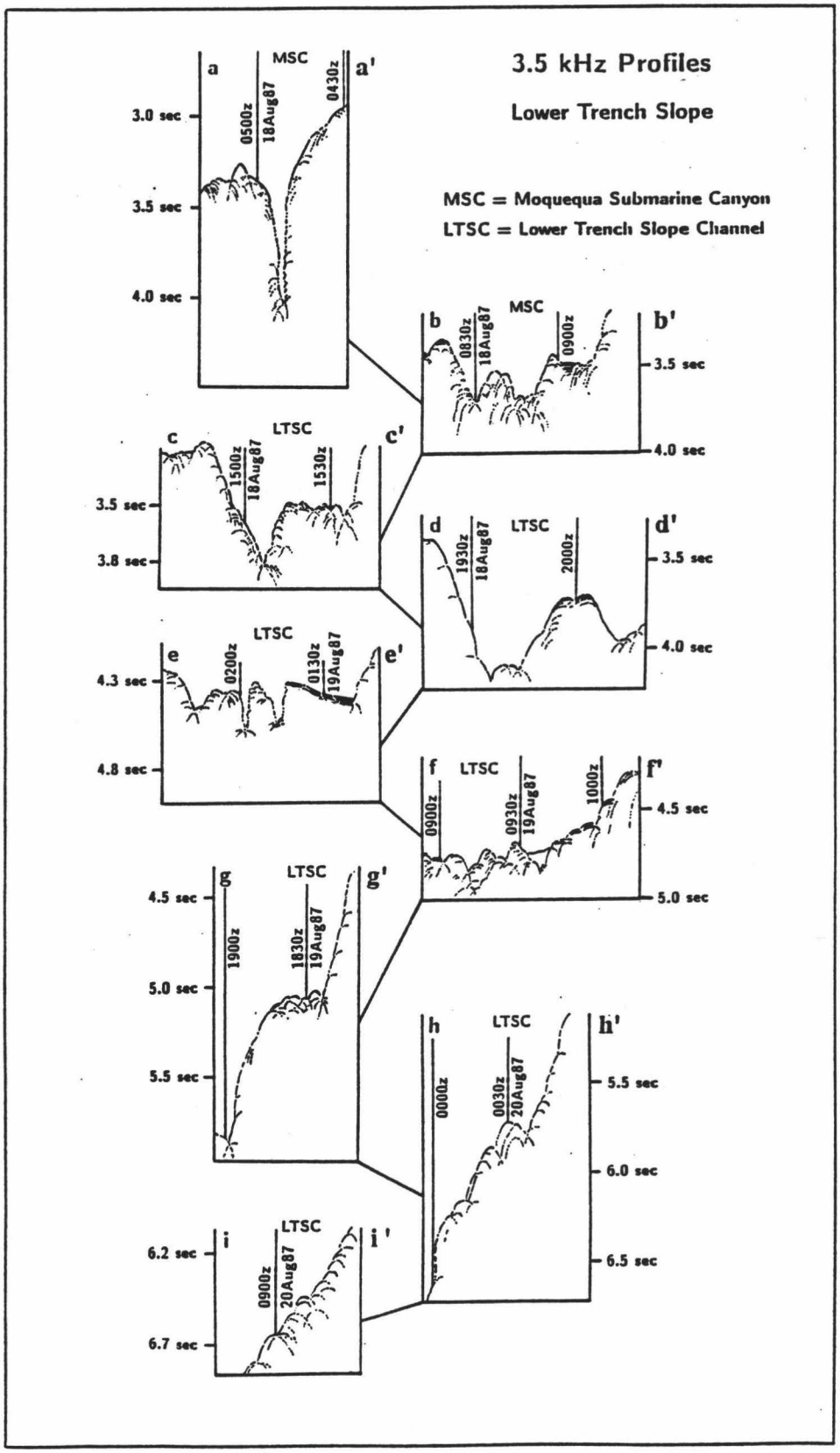
3.5 kHz Profiles
Lower Trench Slope
MSC = Moquequa Submarine Canyon
LTSC = Lower Trench Slope Channel
a
MSC
a'
0500z
18Aug87
0430z
3.0 sec
3.5 sec
4.0 sec
b
MSC
b'
0830z
18Aug87
0900z
3.5 sec
4.0 sec
c
LTSC
c'
1500z
18Aug87
1530z
3.5 sec
3.8 sec
d
LTSC
d'
1930z
18Aug87
2000z
3.5 sec
4.0 sec
e
LTSC
e'
0200z
0130z
19Aug87
4.3 sec
4.8 sec
f
LTSC
f'
0900z
0930z
19Aug87
1000z
4.5 sec
5.0 sec
g
LTSC
g'
1900z
1830z
19Aug87
4.5 sec
5.0 sec
5.5 sec
h
LTSC
h'
0000z
0030z
20Aug87
5.5 sec
6.0 sec
6.5 sec
i
LTSC
i'
0900z
20Aug87
6.2 sec
6.7 sec

Figure 11. 3.5 kHz profile across the change in course of MSC to the southwest (profile location shown on Figure 7, b-b'). Levees flank each bank, a sediment pond has formed outside the eastern levee, and acoustically stratified overbank deposits are visible outside the western levee. The high in the canyon axis is a slump deposit.

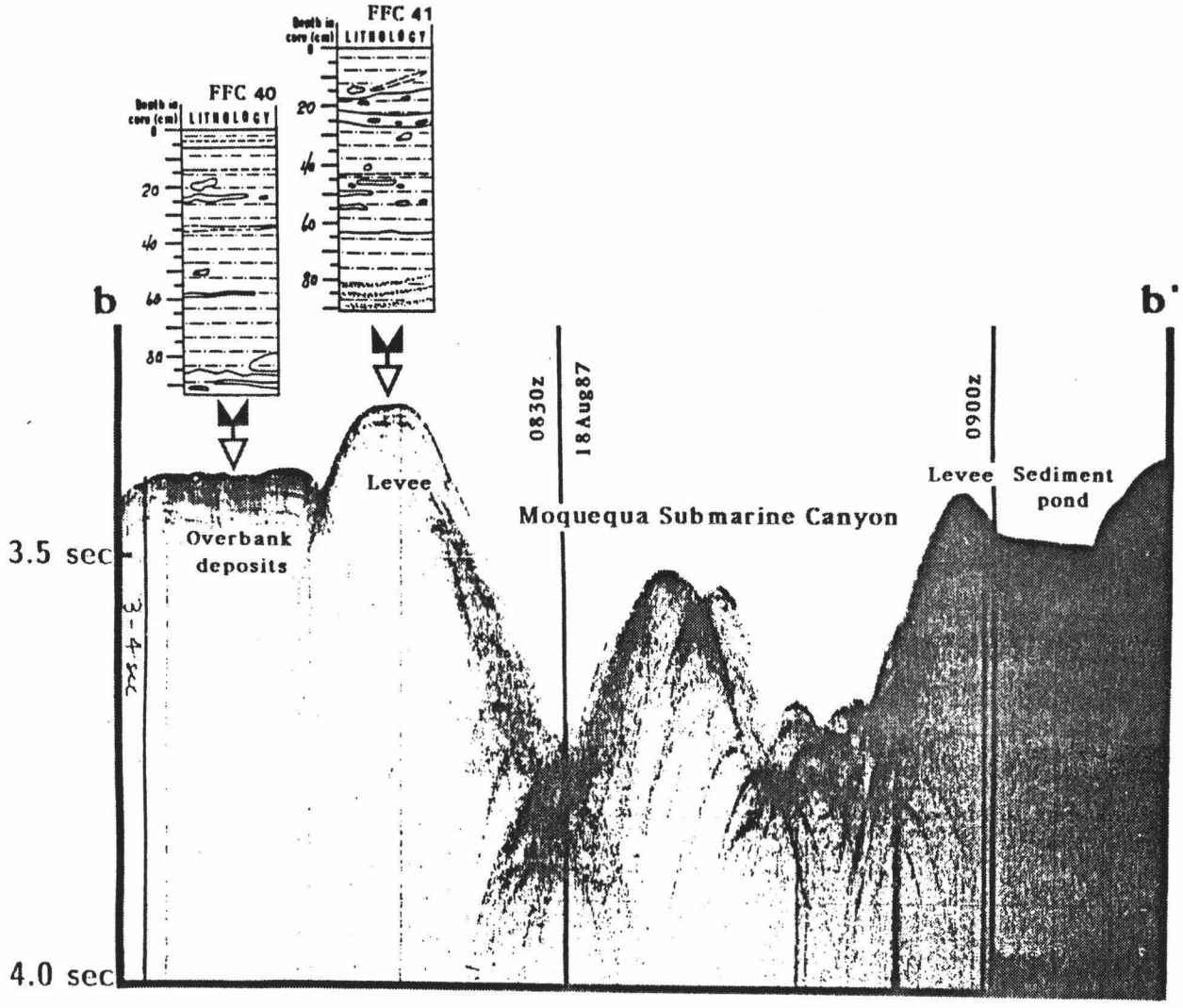
FFC 41
LITHOLOGY
FFC 40
LITHOLOGY
b
b'
0830z
18Aug87
0900z
Levee
Levee
Sediment
pond
Moquequa Submarine Canyon
Overbank
deposits
3.5 sec
3-4 sec
4.0 sec

the insides of bends, O'Connell and others (1985) describe disturbed bedding and chaotic deposits resulting from slumped material breaking into "fields" of contour-parallel blocks (crenulations). Similar crenulations on inner bends are visible along portions of MSC (Figure 8a, F).

The levee and overbank deposits flanking the western bank of MSC where it turns to the southwest (Figure 11) originate from turbidite spillover. Two free-fall cores from this setting show varying degrees of influence from overbank flows. FFC41 sampled a levee and contains a few sandy layers towards its base. Sediment approximately 2 km behind the levee was sampled by FFC40 and shows only a variation in color. Apparently, any sand-size sediment that might be in the system rarely spills over the canyon walls and the levees are composed primarily of silt and clay. MSC appears to terminate in the far western edge of the mosaic (Figure 7, "MSC Fan?"). Any fan directly attributable to MSC is probably beyond the western limitations of the survey. A distinct "meander bend" occurs upslope from the trench (Figure 6b; Figure 7, "Slump"). Its origin probably represents slope failure from oversteepening rather than cut-bank erosion because the slump opens downchannel.

The drainage basin to the south of MSC is marked by the head of a southward trending channel. Because this channel traverses the lower trench slope, I will refer to it as Lower Trench Slope Channel (LTSC). The lobate head of LTSC (Figure 8a, G) can be attributed to a combination of slumping from slope oversteepening (exceeding the angle of repose) and sediment spill-over from MSC as it turns to the southwest. Slumps of similar morphology occur along the Celtic Sea margin (Belderson and Stride, 1969) and are present in both the Arequipa Basin and along other portions of the lower trench slope. A ridge of less than 100 m relief separates the two drainage systems (Figures 6b and 8b). Eventually, this ridge may be completely breached or eroded and LTSC will successfully pirate MSC's bedload. Tributaries feed into LTSC from both the east and

west (Figure 8a, H), giving it a distinct dendritic drainage pattern. Based on regional bathymetry (Figure 6b), single-channel seismics, and side-scan images, this channel has formed within a local depression between two blocks. The confining seaward block may result from horst-like uplift or, alternatively, the depression could have formed along the down-dropped edge of a rotating block. A small slump is visible downslope from the head of LTSC (Figure 8b). The origin for this slump is probably cut-bank erosion and may be a precursor to additional meandering in the upper portions of LTSC as the gradient decreases in the local depression between the two confining blocks.

LTSC maintains its southward trend for approximately 30 km, whereupon it meanders to the west (Figure 12a, A) and finally to a "normal" southwest trend parallel to the regional slope (Figure 12a, B). LTSC also widens, increasing from 0.5 km near the head to over 4 km width near the meander bend. The widening of the channel may be in response both to a decrease in valley gradient, from more than 2.5^{o} to approximately 1^{o}, and to lower relief on the seaward, confining block. The mottled white to grey tones of the side-scan images adjacent to LTSC suggest uneven, disrupted, hummocky topography creating small shadow zones. Based on the reflectivity patterns in the side-scan images (Figure 12a) matched with the 3.5 kHz profiles across LTSC (Figure 10, Figure 13), only a narrow section of the channel is apparently active. In the side-scan images, the "active" channel thalweg exhibits diffuse reflectivity bordered by strongly reflective channel walls (Figure 12a, to the west of "Hummocky topography"). The "inactive" portions (Figure 12a, "Hummocky topography") appear as mottled white to gray tones in the side-scan images and could be overbank flows, temporary channels, or slumps. The low relief of the channel walls (115-140 m) permits sediment coarser than the normal slope deposits of silt and clay to intermittently disperse onto the adjacent slope. This coarser (= rougher) texture is evident in the images as the high reflectivity adjacent to the channel (Appendix B). A line of free-fall cores across the meander bend

Figure 12. Side-scan images (a) and interpretation (b) of the area where LTSC widens and meanders to the west. Labels on the side-scan images are discussed in the text.

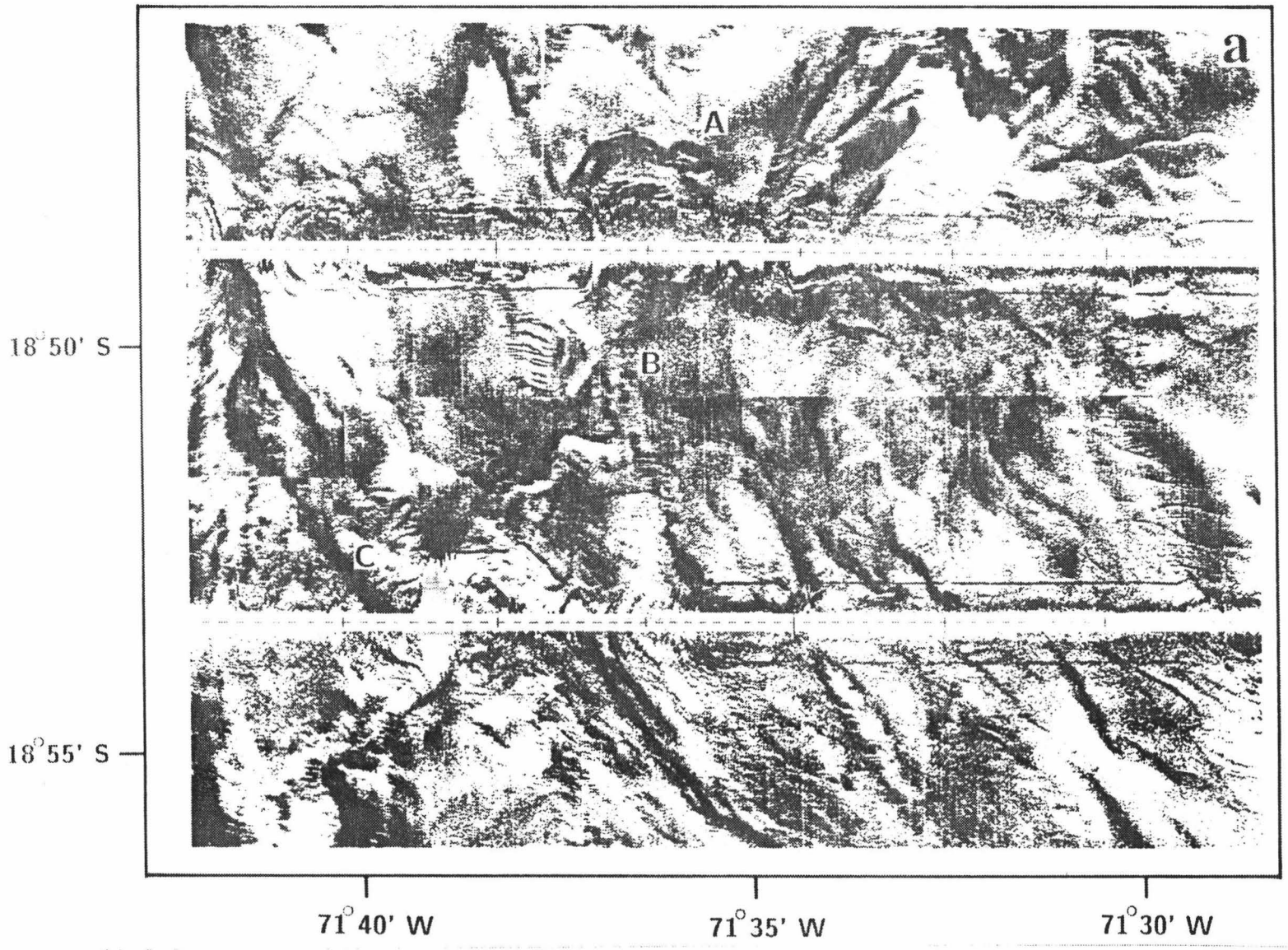
a
A
B
C
18°50' S
18°55' S
71°40' W
71°35' W
71°30' W

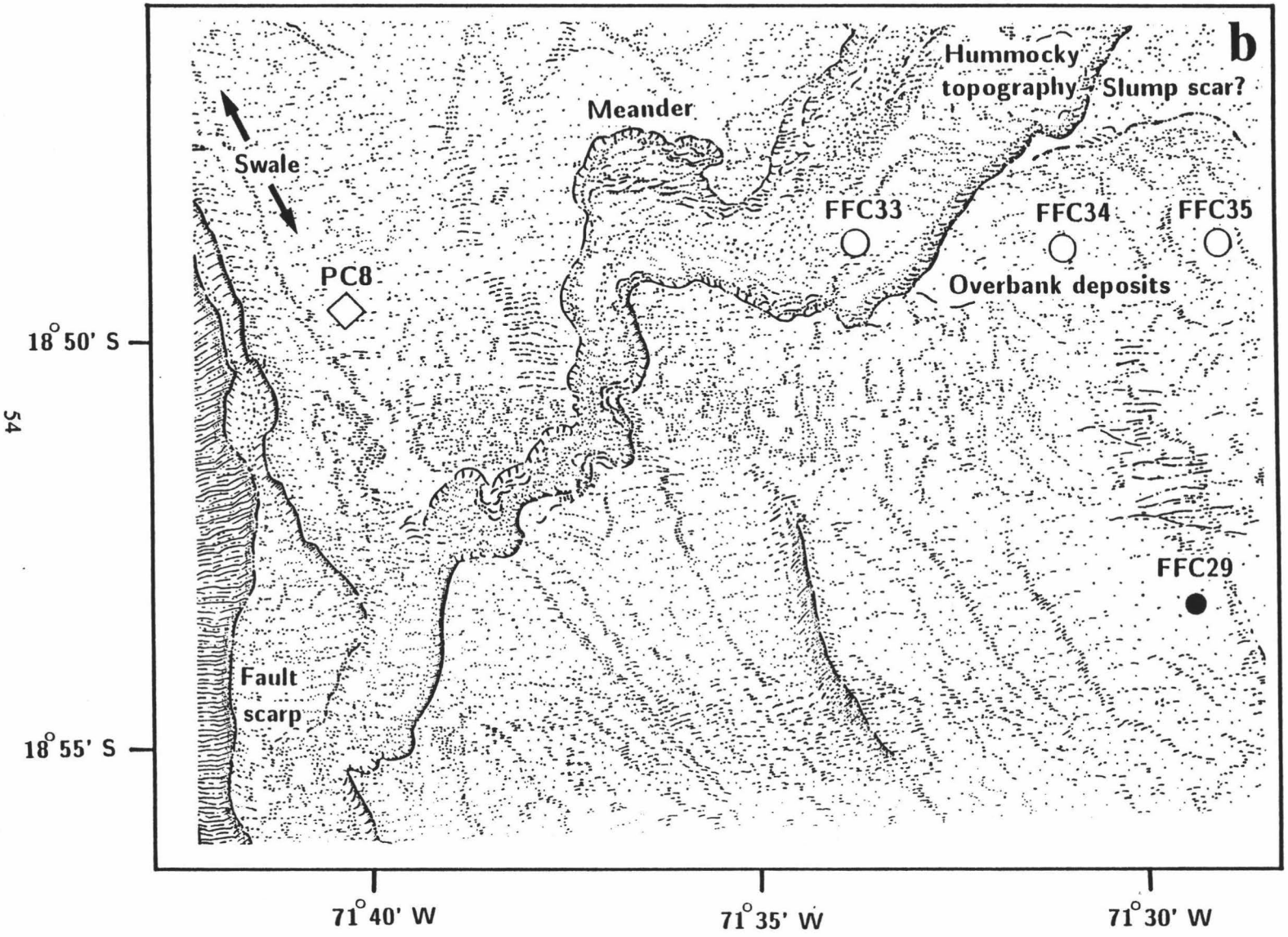
b
Hummocky topography
Slump scar?
Meander
Swale
FFC33
FFC34
FFC35
PC8
Overbank deposits
FFC29
Fault scarp
18° 50' S
18° 55' S
71° 40' W
71° 35' W
71° 30' W

Figure 13. 3.5 kHz profile across the LTSC meander (profile location shown on Figure 7, f-f'). Acoustically transparent sediment, either from a debris flow or a slump, fills one of the channels.

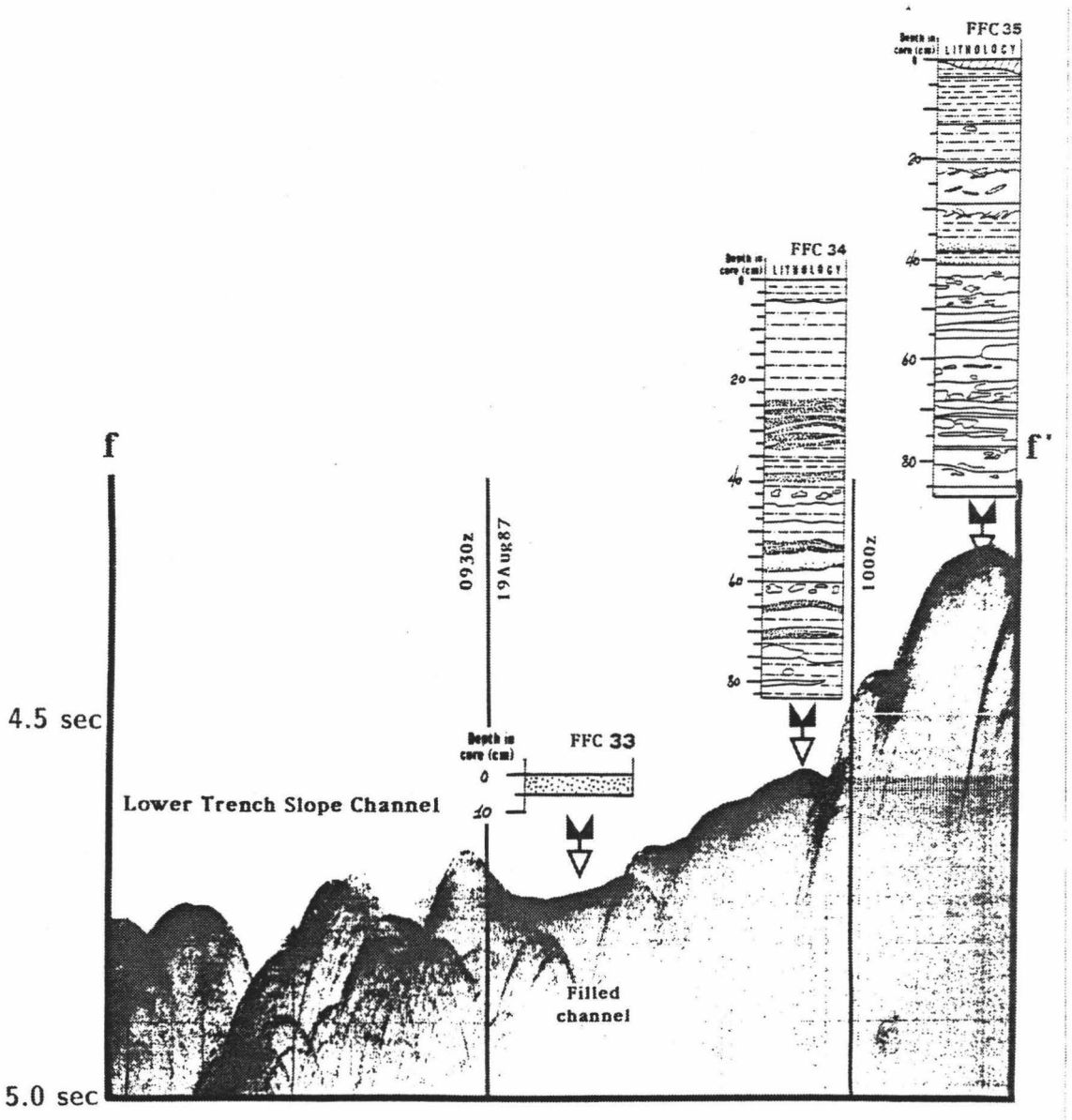
f
f'
FFC 35
FFC 34
FFC 33
LITHOLOGY
0930z
19Aug87
1000z
4.5 sec
5.0 sec
Lower Trench Slope Channel
Filled
channel

(Figure 13) reveals the sediment dispersal pattern. Flanking the meander bend, an old channel, sampled by FFC33, has been filled with predominately sand-size grains. Farther outside the meander, cross-bedded layers of sand appear in FFC34 and color variations in FFC35. The fill in the abandoned channel may be due to either a debris flow or slow infilling by turbidity currents; given the lack of internal acoustic reflectors and coarseness of the fill, a debris flow origin seems more likely.

After flowing approximately 15 km on its southwest trend, LTSC intersects a ridge (Figure 12a, C). This ridge appears to be the high edge of a rotated block. LTSC loses its definition after this point, especially in the 3.5 kHz profiles (Figure 10). It is faintly visible in the side-scan images, coursing adjacent to the ridge until it disappears in the slope deposits located at the toe of the lower trench slope.

Other canyons visible in the mosaic have a southwest trend, parallel to the regional slope (Figures 14, 15, and 16). The regional gradient in this area is about 0.5^{o}. The channel labeled A in Figure 14 exhibits relief of 25 m and a width of 400 m. It meanders to the SW until it intersects a pair of fault scarps (Figure 15a, A), to the west of which a fan has formed over a terraced slope (Figure 15a, B). These scarps parallel the Arica Bight coastline (Figure 7) and are shown by single-channel seismics (Figure 9) to be of listric origin. A small fan or remnant of a large-scale slump is visible to the south (Figure 7; Figure 16a, A). The northern boundary of this deposit is marked by a small channel which meanders to the west. The morphology of the channels feeding this accumulation of sediment seems to be indicative of large-scale slumping. Apparently, these channels follow the slump scarps and, due to a decrease in gradient, begin to meander and lose definition as the toe of the slump is approached. Similar channel morphologies bordering major slumps have been observed in the Iquique Basin portion of the MW87-09 survey. The presence of large-scale slope failure in this area is confirmed by the landward deflection of bathymetric contours (Figure 1).

Figure 14. Side-scan image (a) and interpretation (b) of the study area's northeast section. Channels and sediment waves are clearly visible in this shallow portion of the survey area. Labels on the side-scan image are discussed in the text.

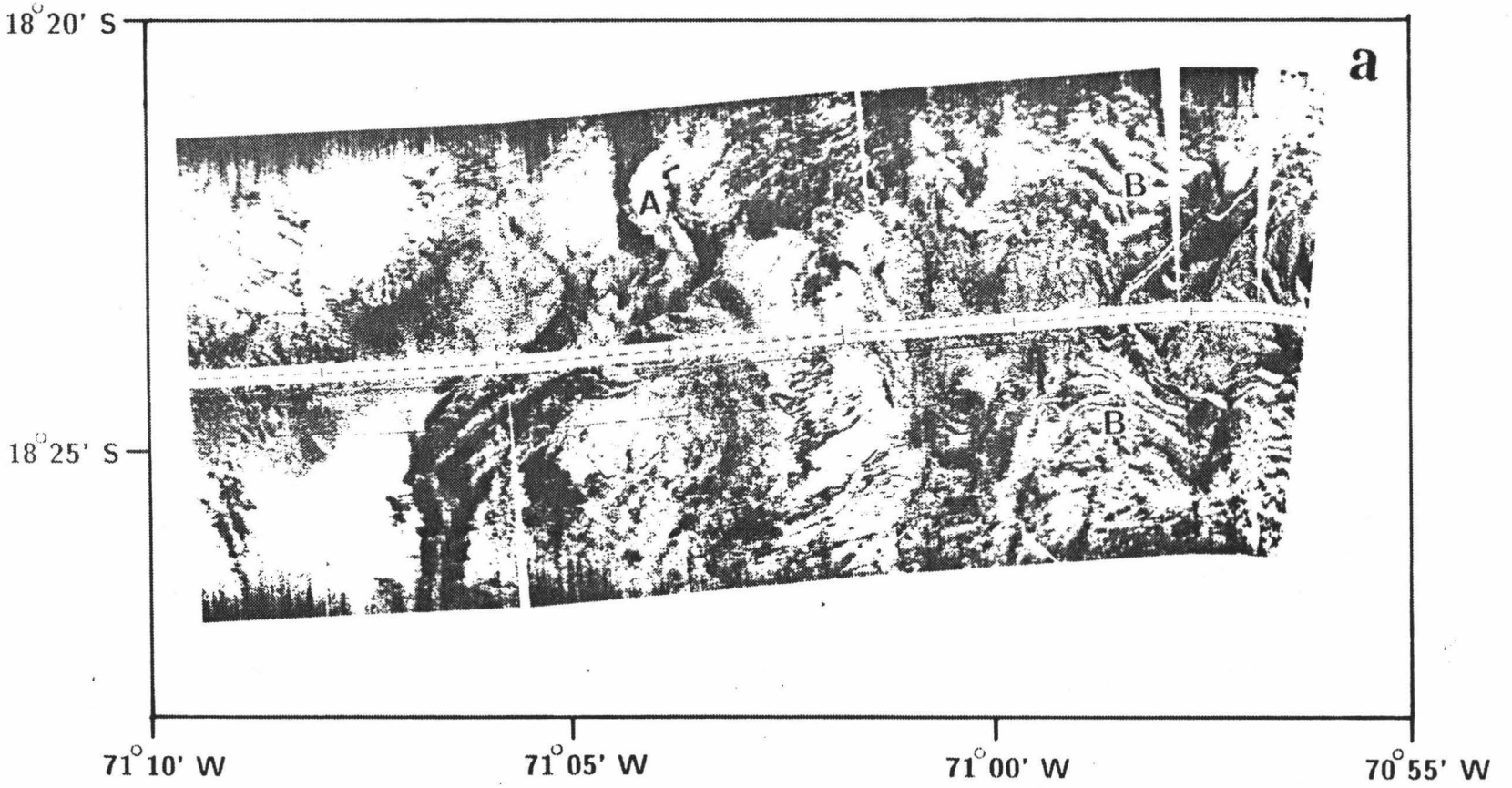
18° 20' S
18° 25' S
71° 10' W
71° 05' W
71° 00' W
70° 55' W
a
A
B
B

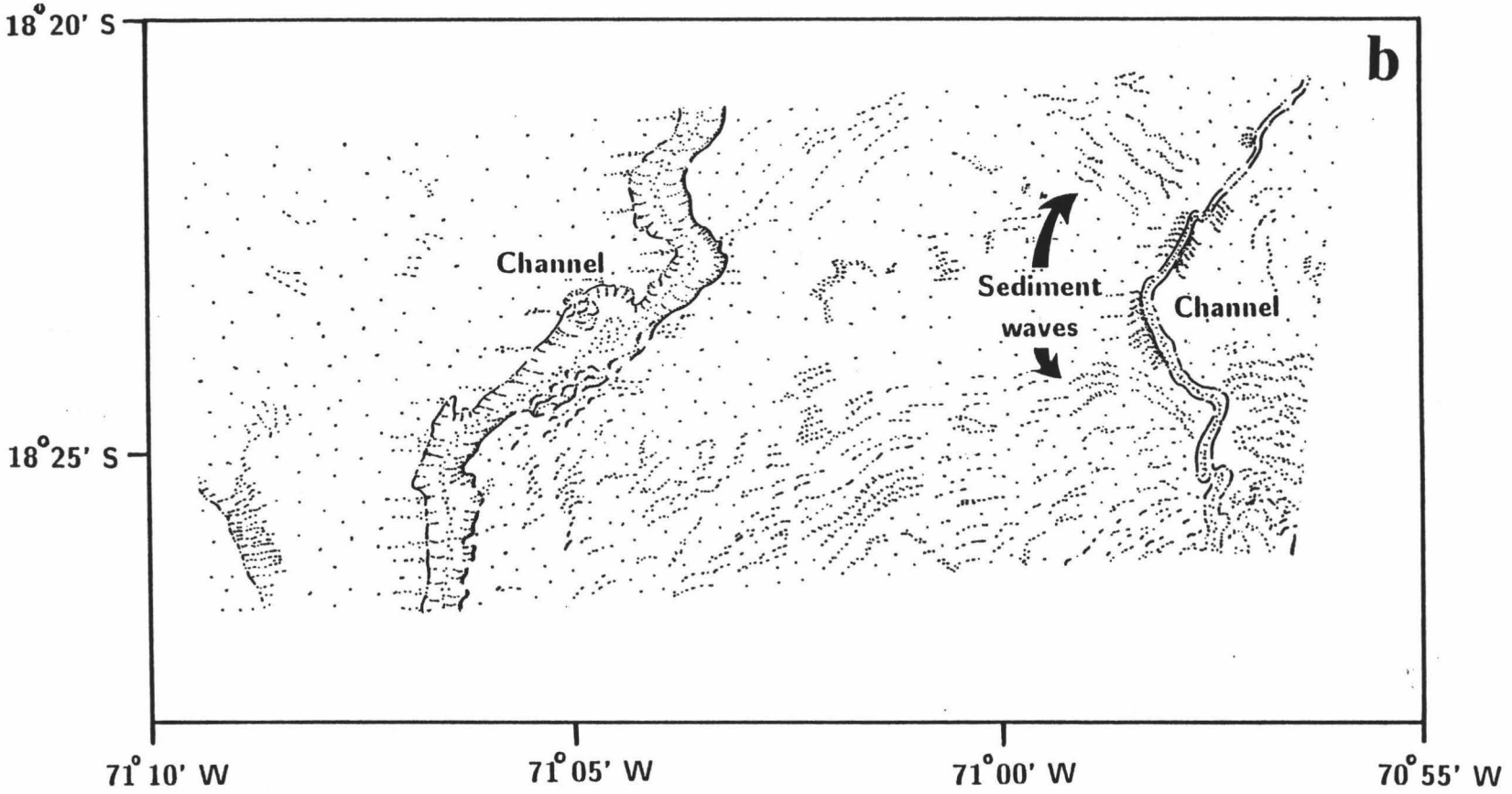
b
Channel
Sediment
waves
Channel
18° 20' S
18° 25' S
71° 10' W
71° 05' W
71° 00' W
70° 55' W

Figure 15. Side-scan images (a) and interpretation (b) of the area where Channel A (shown in Figure 14) intersects a pair of fault scarps. Labels on the side-scan image are discussed in the text.

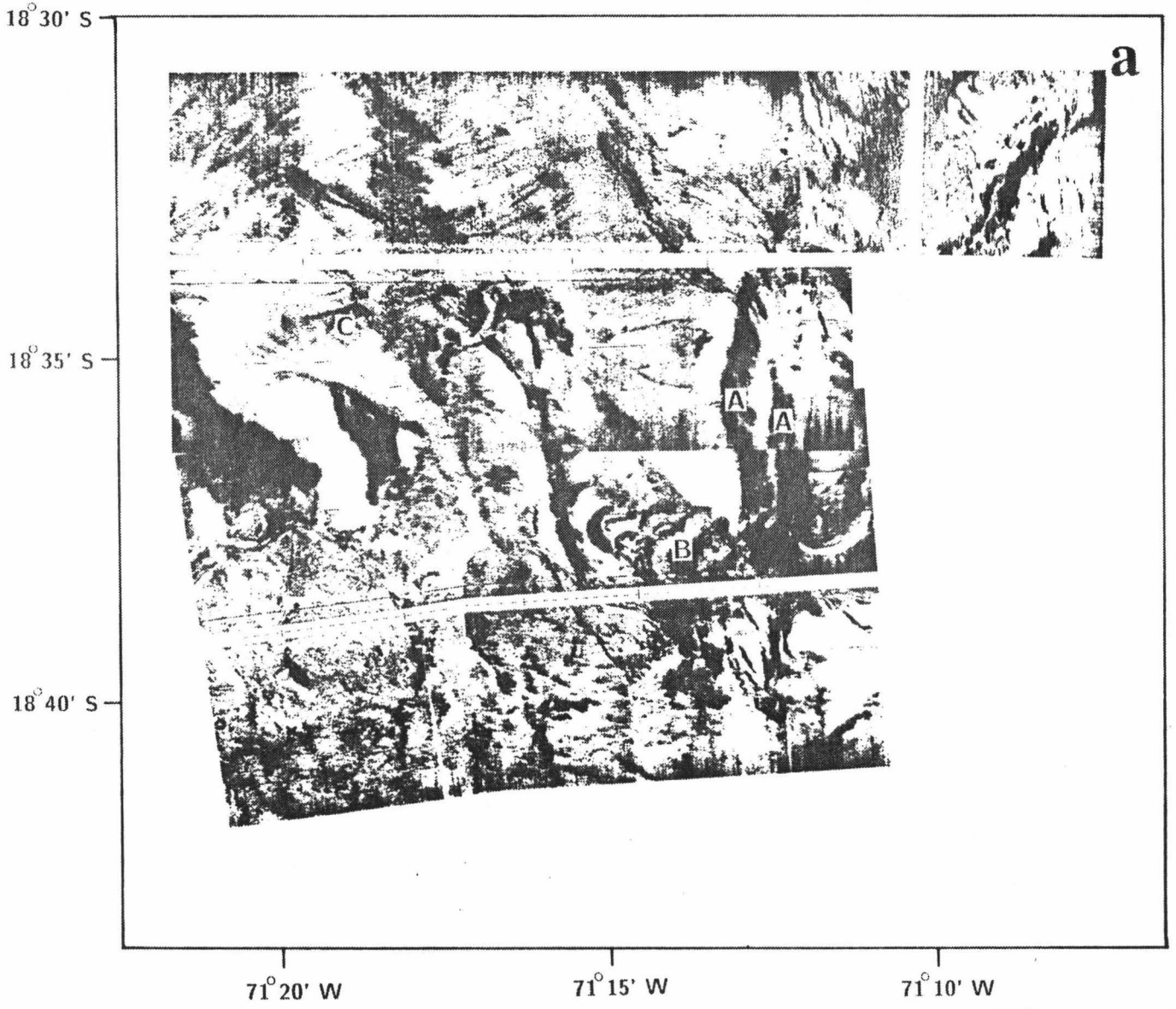
a
18° 30' S
18° 35' S
18° 40' S
71° 20' W
71° 15' W
71° 10' W
A
A'
B
C

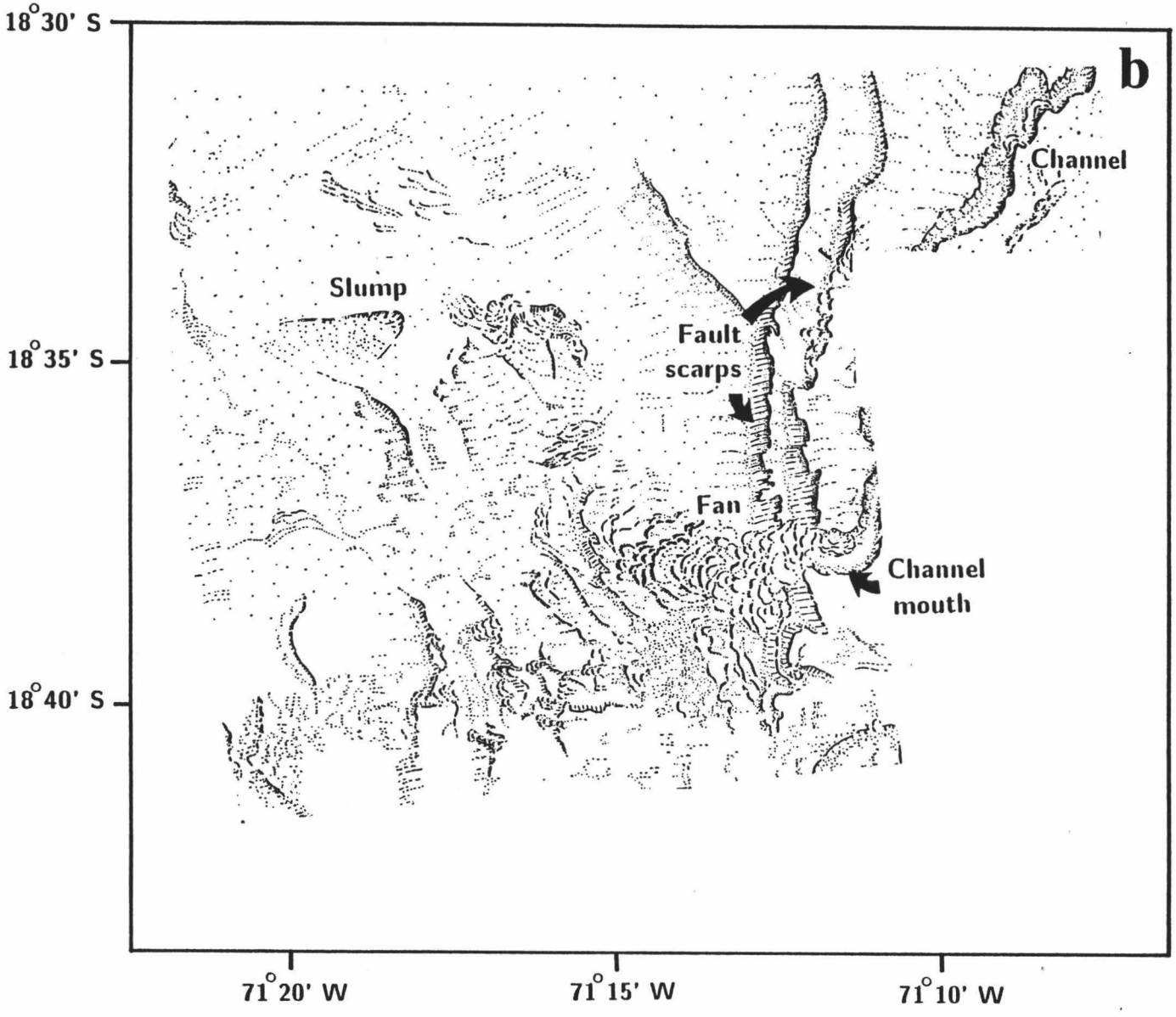
b
Channel
Slump
Fault
scarps
Fan
Channel
mouth
18°30' S
18°35' S
18°40' S
71°20' W
71°15' W
71°10' W

Figure 16. Side-scan images (a) and interpretation (b) of the area where a slope channel terminates into a small submarine fan or the remnant of a slumped mass. The channel appears to follow the slump scarp. Labels on the side-scan images are discussed in the text.

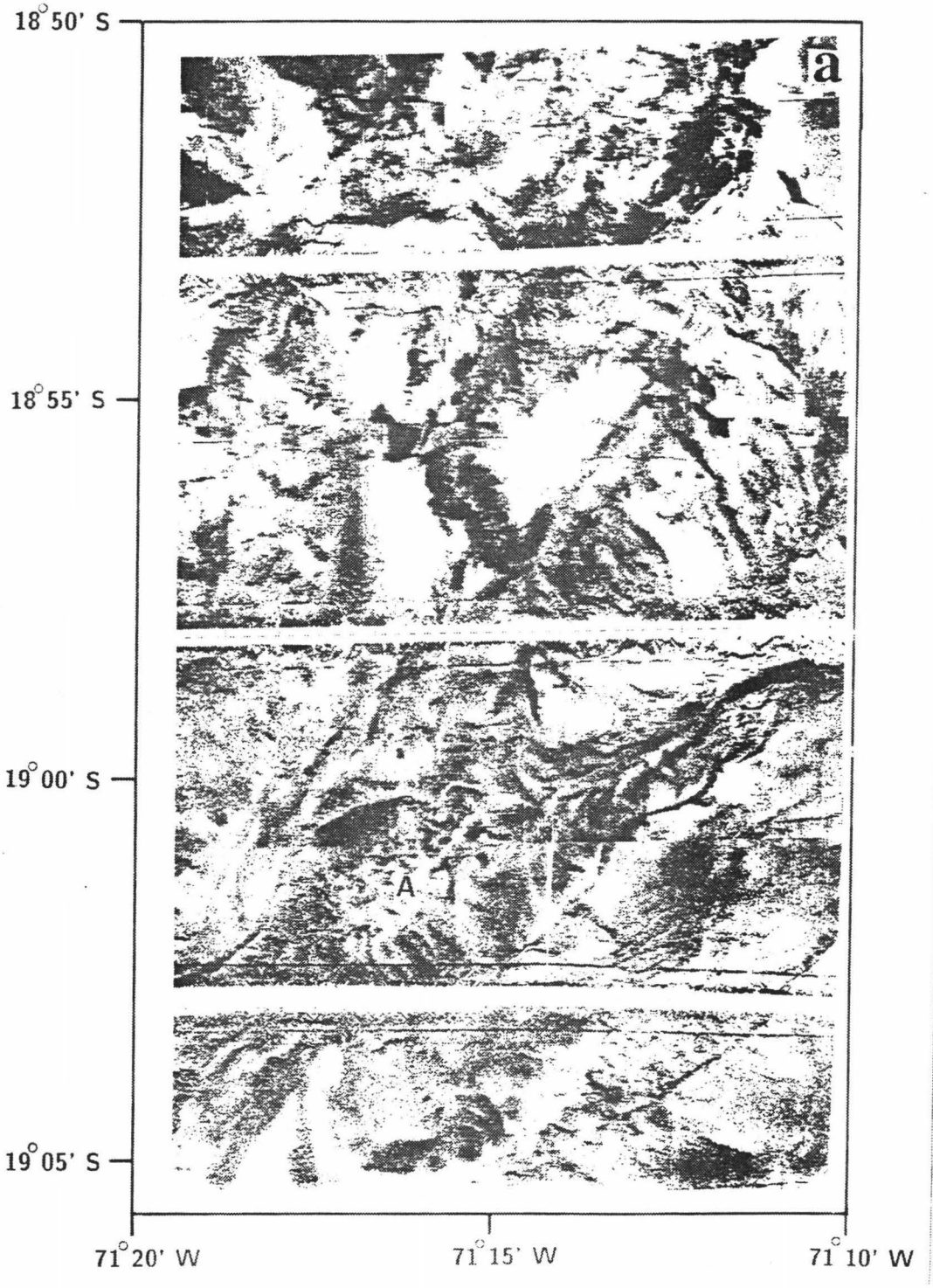
18° 50' S
18° 55' S
19° 00' S
19° 05' S
71° 20' W
71° 15' W
71° 10' W
a
A

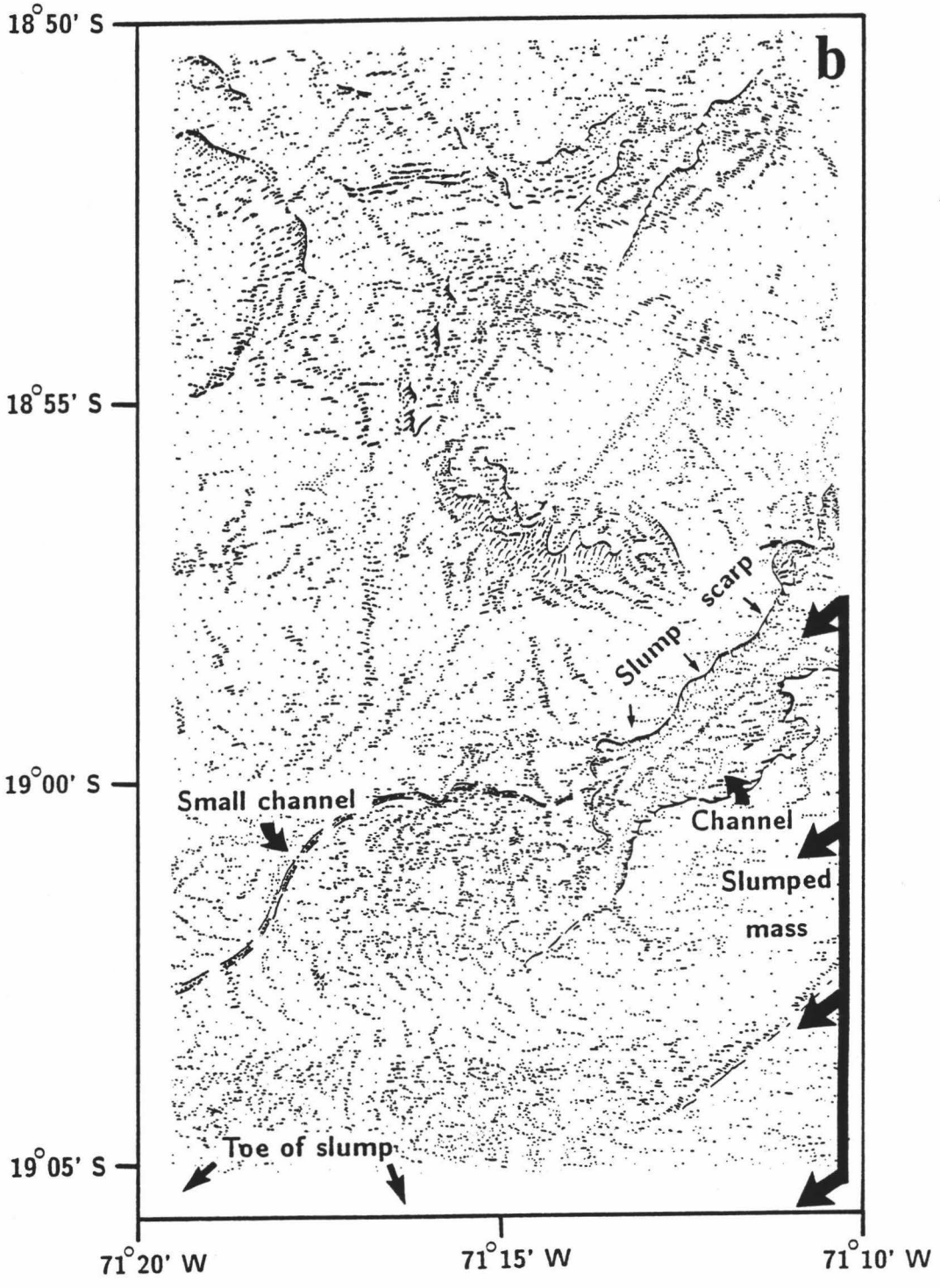
b
18°50' S
18°55' S
19°00' S
19°05' S
71°20' W
71°15' W
71°10' W
Slump scarp
Slump
Small channel
Channel
Slumped mass
Toe of slump

Sediment waves, ubiquitous in the eastern half of the Arequipa Basin, appear in the shallower portions (<1000 m) of this survey area (Figure 14a, B). Karl and Carlson (1982) attribute internal waves generated during a low-stand in the Pleistocene as being responsible for large sand waves in Navarinsky Canyon head in the Bering Sea. The waves in this survey area appear to be more recent features, possibly formed by turbidity, tidal or geostrophic currents sweeping over the shelf edge.

Gravitational effects on sediment stability are clearly shown in the side-scan images throughout the survey area (Appendix B, Figure 7). Sediment creep and unconfined sediment flow, in response to both local oversteepening and current flow over shallower portions of the basin, predominate in the northeast sector of the survey area. Slumping occurs on gradients as low as 3^{o}, but becomes more prevalent when slopes exceed 5^{o}. Within the submarine channels, slumping is prevalent around meander-like bends from cut-bank erosion, and towards the trench as the slope increases (Figure 7, "Slump").

CHAPTER 5

SEDIMENT PROPERTIES

The sediment properties measured on core tops include grain size, mineralogy, carbonate content, and microconstituents. Shear strengths, measured at various intervals, were averaged over a 1 m core interval. As one of the objectives of this thesis is to define sediment properties with which to distinguish thalweg, levee, and overbank deposits from slope deposits, all observations are compared to distance from the nearest canyon or channel. With the suite of cores selected for this study, observations of sediment properties with respect to water depth are biased because samples from the shallow portions of the Arequipa Basin were chosen for their proximity to canyons or channels. Hence, shallow water samples distal from channels in the Arequipa Basin are underrepresented (compare the samples listed in Tables 3-6 with the cores shown in Figure 6a).

Grain-Size Analysis

The grain-size distribution of core tops selected for this study is shown in Table 4. Percentages of sand, silt, and clay, in addition to mean grain-size in mm, were plotted as scattergrams against distance from the thalweg of the nearest channel (Figures 17a-17d).

Because the energy of this setting is presumed to be high, samples located in or near channel thalwegs are expected to contain high percentages of sand; the grain-size distribution outside the channel is less predictable. These analyses show that the sand fraction decreases rapidly away from channels, as expected if the channels are acting as bypassing conduits (Figure 17a). Silt abundance varies widely close to the channels, decreasing slightly with distance (Figure 17b). As expected, the clay fraction is lowest near the channels, then rises to values between 40 % and 50 % at distances greater than

Figure 17. Grain size distribution in core tops from the Moquequa Submarine Canyon system, Peru-Chile margin. All quantities are plotted against distance from the nearest channel thalweg.

GRAIN SIZE ANALYSIS

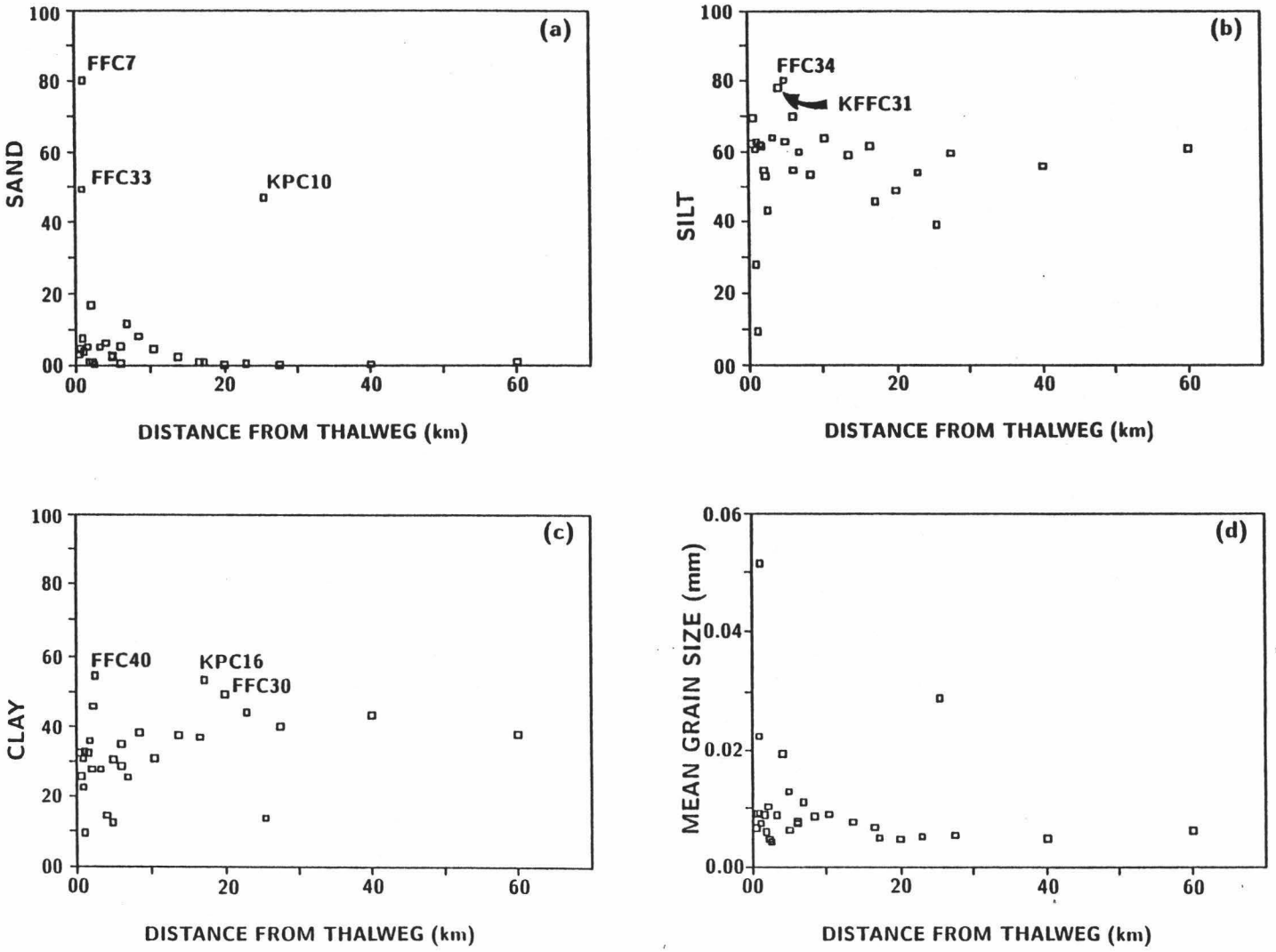

10 km away from the channels (Figure 17c). Mean grain-size grossly mimics the distribution of sand (Figures 17a and 17d). Mean grain-size ranges from clay (approximately 0.005 mm) up to coarse silt (0.052 mm) within 2 km of the thalweg, but stablize at about 0.007 mm at distances greater than 7 km away from the thalweg.

More interesting than the general trends of these samples are the outliers. FFC7, FFC33, and KPC10 all contain high percentages of sand (Figure 17a). FFC7 comes from a levee deposit flanking a tributary channel in the Arequipa Basin and FFC33 comes from a filled channel along the lower trench slope. The coarseness of KPC10 probably reflects the influence of a submarine fan located upslope from the core (note the deflection of contours in Figures 6a and 6b downslope towards KPC10); bypassing of sand to the distal portions of fans has been observed on the Amazon, the Mississippi, and the Navy fans (Damuth and others, 1988; Normark and others, 1986; Normark and Piper, 1985). Samples KFFC31, KFFC32, KFFC34, and KPC11 show very low percentages of sand and, surprisingly, come from the main channel of Moquequa Canyon in the Arequipa Basin (Figure 6a; Figure 18). The low percentage of sand in these samples suggests this throughway has been inactive for a period of time and either 1) blanketed with fine-grained, late-stage, dilute turbidity currents or suspension flows as suggested for the Mississippi and Amazon Fans (Bouma and others, 1986; Damuth and others, 1988), or 2) partially filled by a slumped portion of the channel wall. 3.5 kHz records indicate channel-wall collapse (Figure 18). Grain-size data show that the sediments from this block are approximately the same size as those sampled from the basin floor. Hence, although this block of sea floor has foundered into the channel, its sediments are not influenced by the dynamics of transport occurring in the channel; the samples represent repositioned, but otherwise undisturbed basin sediments. Samples from both KFFC31 and FFC34 contain high percentages of silt (Figure 17b). Given their location relative to the canyon, they may have been influenced by unconfined

Figure 18. 3.5 kHz profile across the main MSC channel in the Arequipa Basin. Profile location is shown in Figure 6a along latitude 17^{o} 59' S, beginning at longitude 71^{o} 38' W (see the line of free-fall cores labeled KFFC31, KFFC32, KFFC33, KFFC34, and KPC11). A section of the wall has slumped into the channel; sedimentological analyses suggest the block slumped as a relatively homogeneous unit and has not been influenced by the transport dynamics occuring within the channel.

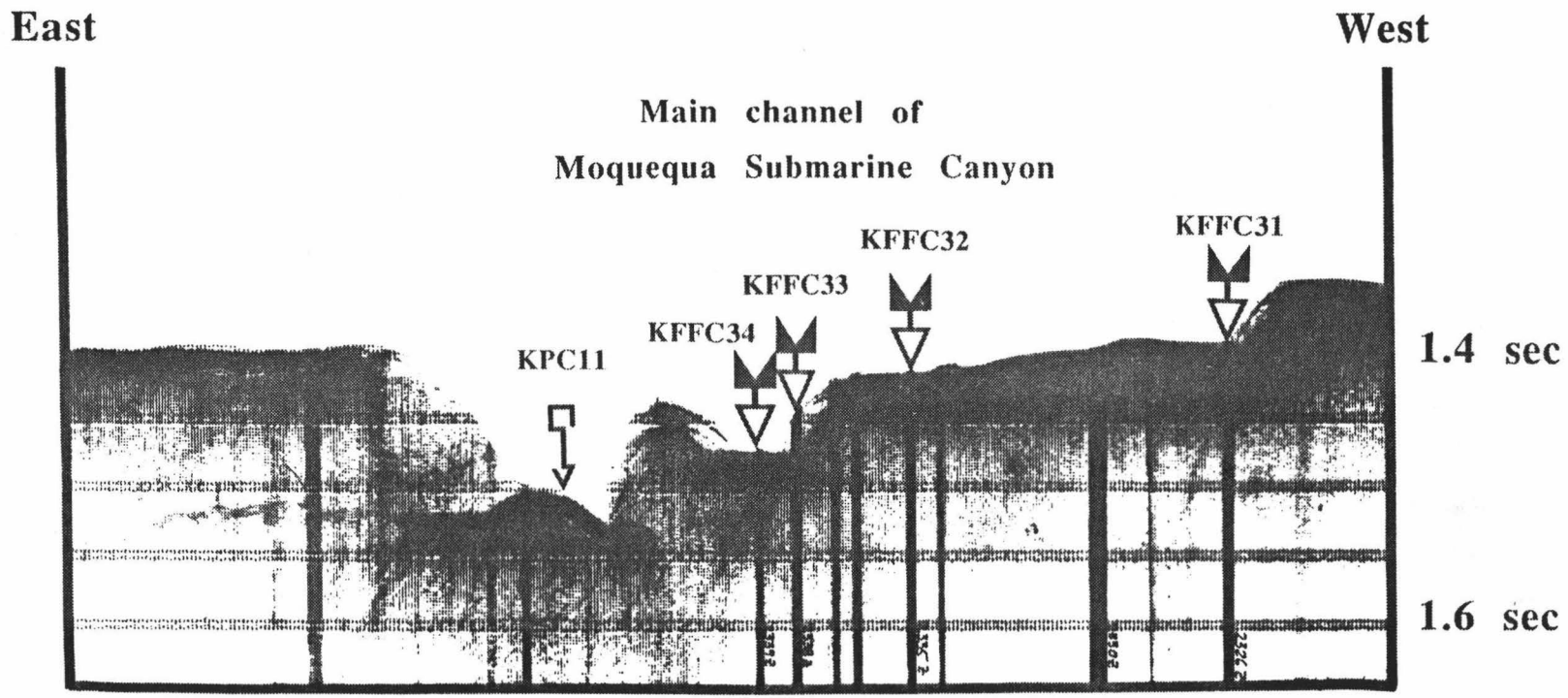
East
West
Main channel of
Moquequa Submarine Canyon
KFFC31
KFFC32
KFFC33
KFFC34
KPC11
1.4 sec
1.6 sec

turbidity currents or overbank flows. The samples with the most clay, KPC16, FFC30, and FFC40 (Figure 17c), are all buffered from the direct influence of canyon sedimentation (Figure 6b). FFC40 lies approximately 2 km behind a levee (Figure 11) whereas FFC30 and KPC16 were obtained well south of LTSC.

Mineralogy

Semi-quantitative analysis of 5 mineral assemblages (quartz (Q), feldspar (F), calcite (Ca), total clay (Clay), and clinoptilolite (Clin)) identified from X-ray diffractograms produced the relative abundances shown in Table 5. These relative abundances were derived with the assumption that these five minerals are the sample's sole constituents. The ratios of F/Q, Clay/Q, Clay/F, and Clay/F+Q are also shown in Table 5. Clinoptilolite occurs in negligible quantities, hence its ratios are ignored in this discussion. Calcite and carbonate content are discussed in a subsequent section.

The ratio which varies the most is F/Q (Figure 19a). Its distribution in scattergrams mimics that of the sand fraction from grain-size analyses; samples with high sand content tend to have higher F/Q ratios. Near the canyon, ratios vary from over 11:1 to less than 1:1 (Figure 19a). As distance increases away from the canyon, the F/Q ratio stabilizes at about 1:1. High ratios occur in regions which may have experienced recent turbidite or debris-flow activity and hence have been swept clean of fine-grained hemipelagic detritus. FFC 33 and FFC 7 have the highest ratios, are the coarsest samples, and are both located near a channel. Based on smear slide analysis, FFC 7 contains approximately 15 % feldspar grains and volcanic glass compared to about 7 % quartz grains. KPC10, a coarse sample obtained downslope from a submarine fan (Figure 6b), shows only a moderate F/Q ratio, possibly due to abrasion of the feldspar grains during transport or to the greater maturity of the deposit. Other samples obtained on this cruise with high F/Q ratios, but not discussed in this paper, come from a

Figure 19. Mineral ratios in core tops from the Moquequa Submarine Canyon system, Peru-Chile margin. All ratios are plotted against distance away from the nearest channel thalweg.

Mineral Analysis

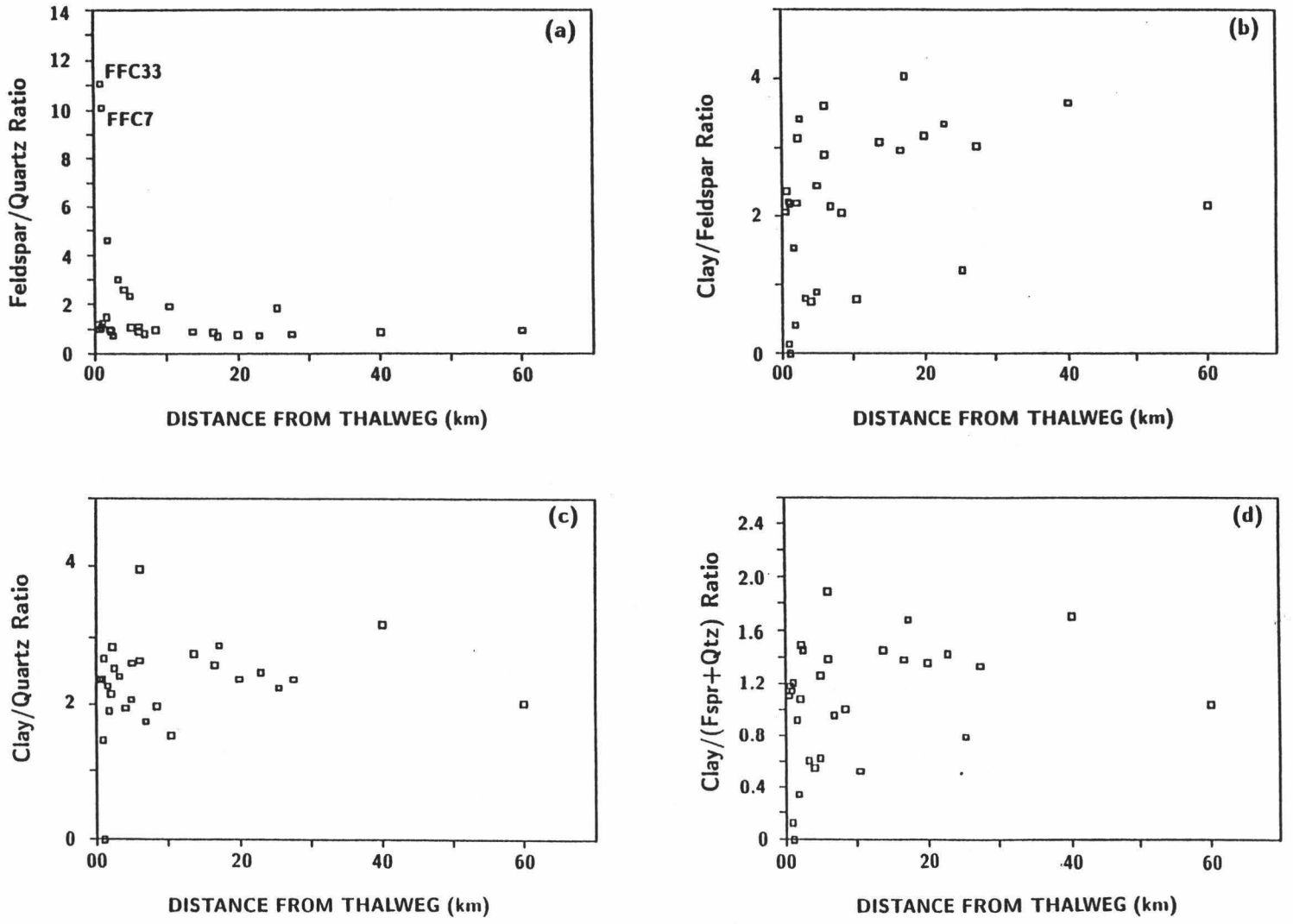

submarine fan within the Arequipa Basin (of which KPC10 is a distal sample) and the structural high bounding the basin. It seems reasonable that the high-feldspar sediment filling the channel adjacent to the meander of LTSC, as represented by FFC33, was either eroded from the structural high or was transported from shallower depths.

To help determine the origin of the sediment filling the channel sampled by FFC33, an oil mount of the sand fraction was analyzed. The sand fraction contains moderate amounts (10 % to 15 %) of andesitic amphibole and plagioclase, suggesting a volcanic source that was fairly evolved. Tosdal and others (1981) note that extensive andesitic volcanism in the Cordillera Occidental continues even to the present day. Accordingly, it seems probable that the fill material had a volcanic-arc origin and, based the absence of acoustic reflectors in 3.5 kHz profiles, was transported in the form of a debris flow or a slump. Analysis of the sand fraction also produced an assemblage of calcareous, benthic foraminifera. Included in this assemblage are *Bulimina exilis*, *Bolivina humilis*, and *Bolivina advena formaninata.* Resig (1981) notes the high dominance of a few *Bolivina* species in the middle- to upper-bathyl regions off the Peru margin. Based on the foraminiferal assemblage in FFC33, the origin of the fill is probably from the upper-bathyl region, perhaps from around 100-150 m water depth (Resig, pers. comm.). The mode of transport as a debris flow for the fill material is supported by the foraminiferal assemblage outside the channel, as represented by FFC35 (Figure 6b; Figure 13). The faunal assemblage of FFC35 is dominated by benthic agglutinate species including *Rhabdammina* sp., *Reophax* sp., and *Saccammina* sp.. These fragile, agglutinate forms suggest a quiet environment, as does the lithology of FFC35 (Figure 13, Table 1). Resig (1981) notes that benthic assemblages consisting predominantly of agglutinate species are generally confined to depths greater than 4100 m in the Peru-Chile Trench. A slump origin for the fill material in the channel sampled by FFC33 is inconsistent with the stable environment suggested by FFC35. Given the

mineralogical information from an oil mount of FFC33's sand-fraction, the faunal assemblages in FFC33 and FFC35, and the 3.5 kHz records, the sediment filling the LTSC channel shown in Figure 13 probably originated in shallow water and was transported to its present position in the form of a debris flow. This debris flow was possibly ramped over from MSC to LTSC at the point where MSC changes course to the southwest.

The samples obtained across the main channel of MSC in the Arequipa Basin, KFFC31, KFFC32, KFFC34, and KPC11, exhibit low F/Q ratios. The abundance of feldspar grains and volcanic glass visible in the smear slides is approximately the same as the amount of quartz (about 10 %). If high feldspar content is associated with coarse sediment proximal to channels or shallow water transport of volcanic ash deposits, then these low F/Q ratios support either inactivity or bypassing or a combination of both in this MSC channel. Scatter plots of the total clay ratios provide minimal information; CLAY/F, CLAY/Q, and CLAY/F+Q ratios show low correlations to increasing distance from the canyon (Figures 19b, 19c, and 19d).

Carbonate Content

Carbonate content shows a slight positive correlation with distance from the channels (Figure 20). Most core tops from the lower slope exhibit between 1 % and 8 % carbonate (Table 3). Two samples exhibit high amounts of carbonate; FFC5 and FFC33 contain approximately 14.5 % and 13.5 % carbonate, respectively. Smear-slide analysis of FFC5 reveals that about 20 % of the sample is composed of small calcite grains, shell fragments, and clasts of micrite; foraminifera and coccoliths make up only about 2 % of the carbonate. The sand-fraction oil mount of FFC33 is composed of approximately 10 % micrite clasts with a few foraminifera. Two cores seaward of the trench (KFFC26 and KFFC27) have low carbonate content and are hemipelagic silts containing shallow-

Figure 20. Carbonate content in core tops from the Moquequa Submarine Canyon system, Peru-Chile margin. All quantities plotted against distance away from the nearest channel thalweg.

Carbonate Content in Core Tops

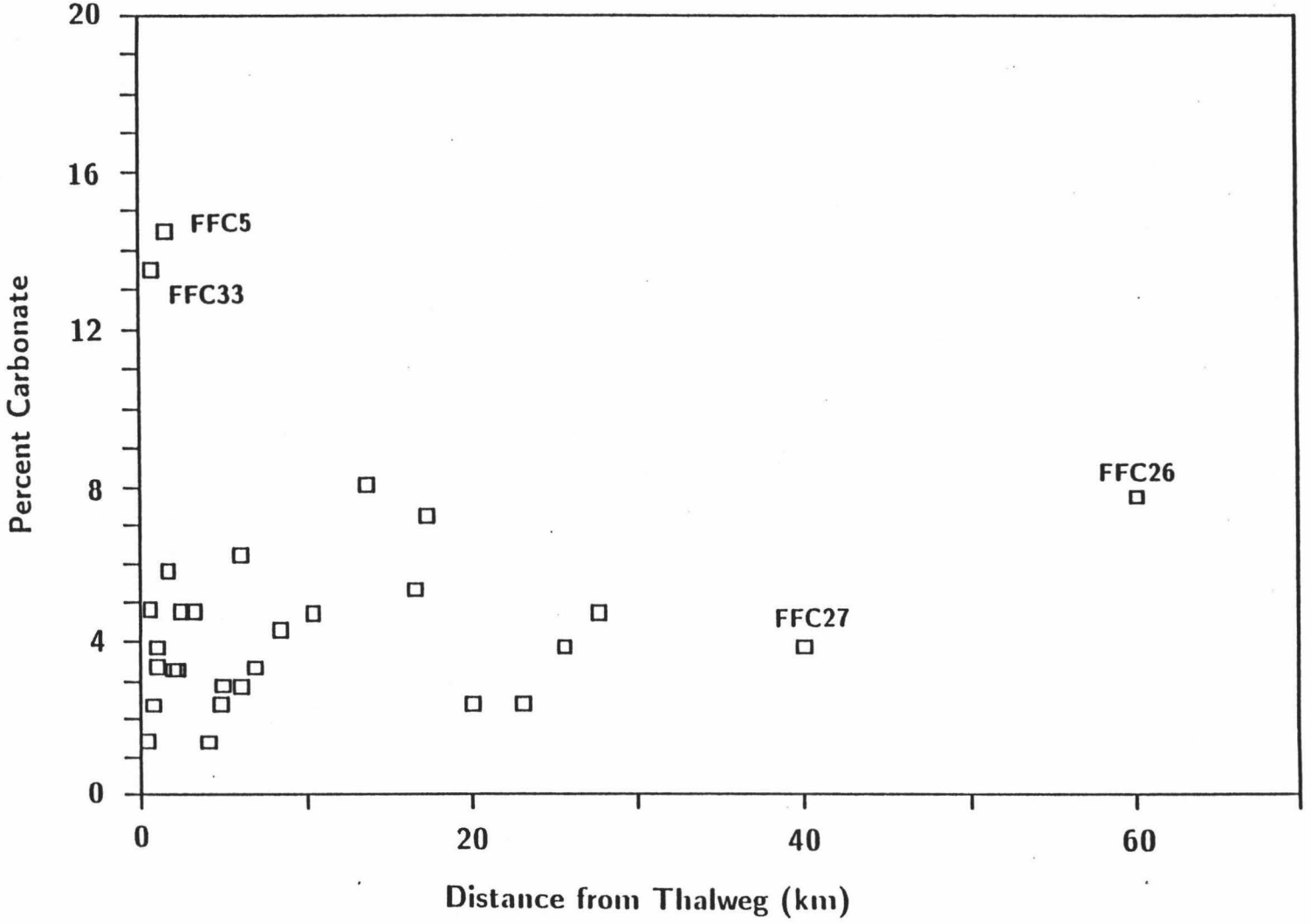

water benthic foraminifera. Farther seaward of the trench, Miocene and Eocene foramiferal oozes were sampled from faulted blocks. The sediment represented by KFFC26 and KFFC27 was probably transported and redeposited rapidly from shallow water to its present depth of about 6600 m, well below the CCD (Coulbourn, 1977).

Shear Strengths

Shear strength of water-saturated muddy sediment is affected most by water content (porosity) and the degree of disturbance (Allen, 1985); an increase in either of these factors decreases the shear strength. As shown by the grain-size analyses, sand is primarily retained within the confines of the channel banks; silts and clays compose the levees bordering the channels, and clays dominate the slope deposits. Hence, its not surprising that a strong trend is absent in the average shear strengths for cores collected outside the channel walls (Figure 21). Most of the cores exhibit strengths between 0.6 and 1.2 kg/cm^2. The lone channel sample, FFC33, consists of highly disturbed, unconsolidated sand-size detritus ; accordingly, it has neglible shear strength. FFC5, collected adjacent to a channel in the Arequipa Basin, shows the highest shear strength. Its core top also contains the most carbonate material (14.5 %). Mayer (1979) notes the strong correlation between saturated bulk density (the inverse of porosity) and carbonate content. It seems logical that FFC5, with its high carbonate content, should have the lowest porosity and therefore the highest shear strength. The core exhibiting the lowest average shear strength is PC8, collected from a swale on the lower trench slope. The low strength of this sediment may reflect an absence of compaction from overburden within this clay-rich depression or may be simply a function of the disturbance accompanying the coring process. A small increase in shear strengths is apparent within 4 km of the channels. This increase could result from compaction or exposure of more consolidated sediments by currents coursing through the channels, or from the mixture

Figure 21. Shear strengths, averaged over a 1 m interval, of cores collected from the Moquequa Submarine Canyon system, Peru-Chile margin. All quantities plotted against distance away from the nearest channel thalweg.

Shear Strength Analysis

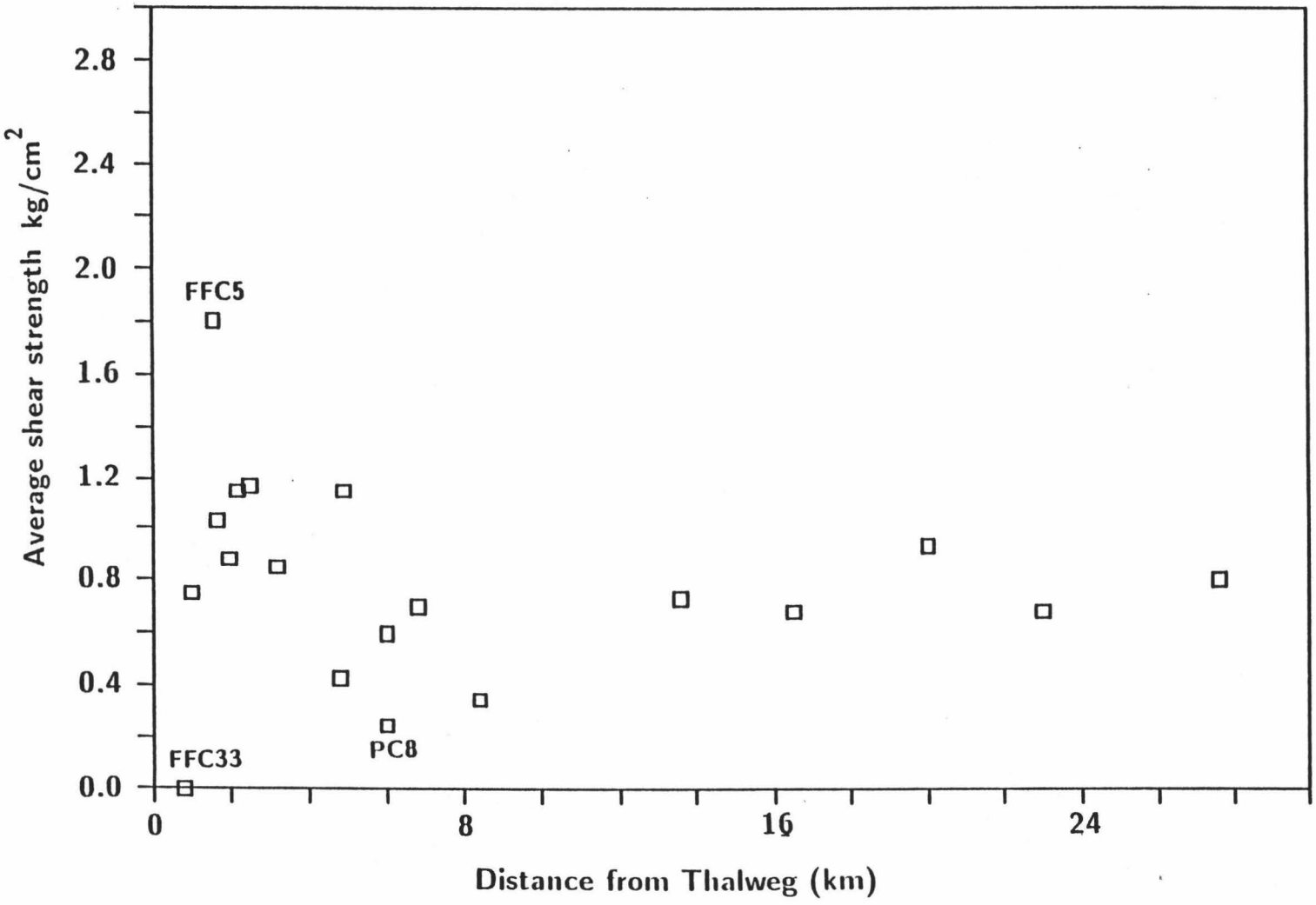

of silts and clays creating more particle interlocking. The significance of these measurements is that they provide a benchmark for understanding the strength at which active continental margin sediments behave as homogeneous units when undergoing cut-bank erosion.

CHAPTER 6

CLUSTER ANALYSIS

Trends or patterns in sedimentological data are often difficult to distinguish by qualitative examination alone; general inferences can be made, but without quantitative support they may lack substance. Cluster analysis is the name given to an assortment of techniques designed to perform classification by assigning observations to groups so each group is more-or-less homogeneous and distinct from other groups (Davis, 1986). Q-mode and R-mode cluster analyses were applied to the grain-size distributions (Table 4). A correlation coefficient was applied as the measure of similarity and the weighted pair group average method (Davis, 1973) was used to construct the dendrograms shown in Figure 22. The objective of the cluster analysis was to identify and understand any underlying patterns between core location and core content.

Grain-size Analysis

From the grain-size data, four clusters and one outlier are identified at a correlation level of 0.60 (Figure 22b). Each cluster corresponds to a broadly regional geographic province influenced to varying degrees by the canyon system.

Samples in Cluster A are influenced the most by the submarine canyon. These samples contain high percentages of sand and occur over a wide range of water depths. FFC7 and FFC33 are levee and filled-channel samples, repectively. KPC10 represents the downslope transport of coarse sediment from a submarine fan.

Samples in Cluster B contain less sand and more silt than Cluster A samples. They also have less clay than all other core tops. The grouping of KFFC31 with FFC34 is somewhat puzzling. FFC34 comes from an area of overbank deposition, as suggested by the numerous cross-bedded sand layers within the core. KFFC31, on the other hand, is over 5 km away from the nearest channel. A smear slide from the core top of KFFC31

Figure 22. R-mode (a) and Q-mode (b) dendrograms produced by cluster analysis of core top grain size distributions from the Moquequa Submarine Canyon system, Peru-Chile margin.

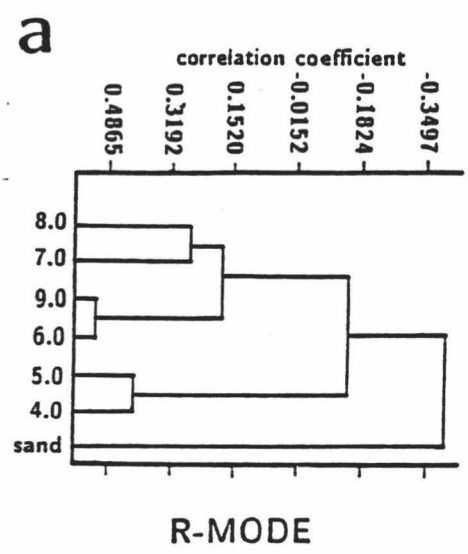

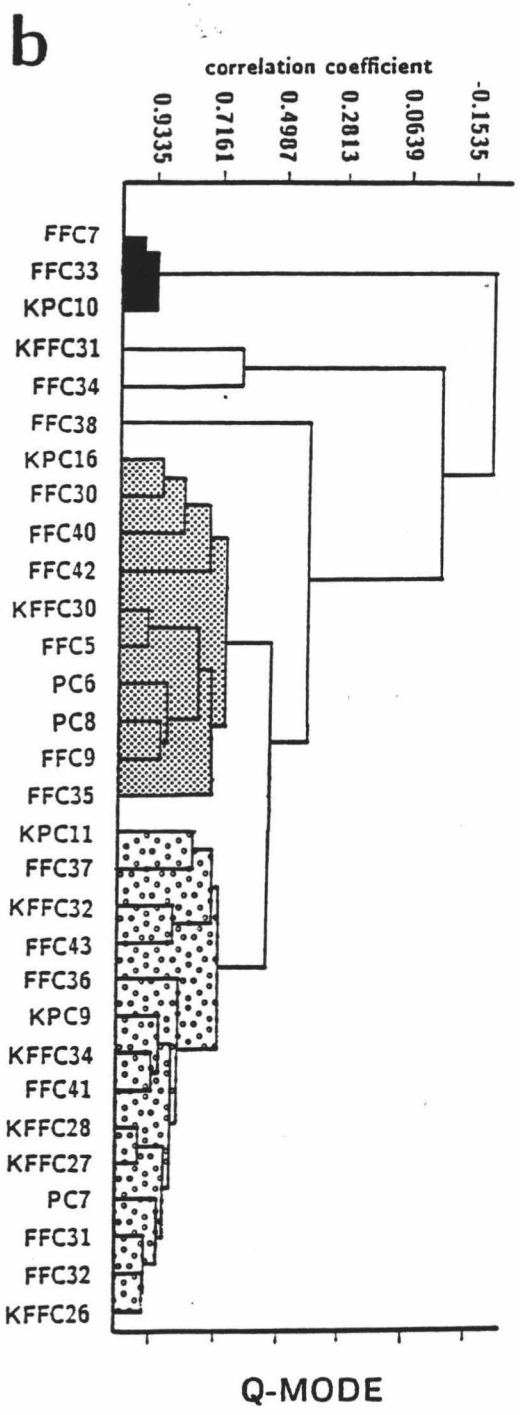

Cluster Analysis on Grain Size

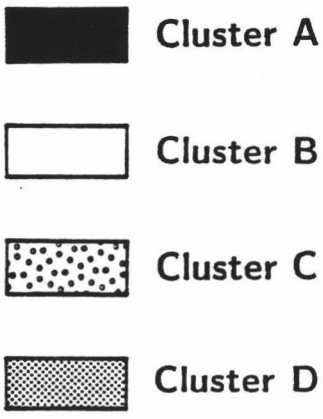

contains over 15 % diatoms, radiolaria, and sponge spicules; the excess biogenic component may account for the high percentage of silt. The diatoms may be part of a localized productivity bloom or they may have been transported from shallower depths by an unconfined turbidity current.

Cluster C and Cluster D samples are the least influenced by sediment carried down the channels and are located outside the channel boundaries (Figures 6a, 6b, and 22b). The difference in grain size between these two groups is not great, but in general Cluster C is coarser. Some of the finer-grained samples group with Cluster C because of the high correlation between the 6.0 to 7.0 and the 9.0 to 10.0 phi-size intervals (Figure 22a). If the coarseness of core tops is related to the transportation and deposition of shelf sediment, and canyon channels are the avenues of this transportation, then the line of free-fall cores across the main channel of MSC (KFFC32, KFFC34, and KPC11) marks sites unaffected by these processes. All of these samples group in Cluster D. Coulbourn (1980) noted that KPC11 contains pebble-sized fragments of displaced shallow-water bivalves, but the core was totally remolded during the process of retrieval so that a core-top sample may not reflect the most recently deposited hemipelagic ooze. Coulbourn (1977) also described the top from KFFC34 as being a diatom strew. Smear-slide analysis confirms the abundance of diatoms (approximately 15 %), in addition to the presence of numerous sponge spicules (approximately 7 %). Adjacent core KFFC32 is nearly devoid of biogenic remains. Based on the grain-size data, smear-slide counts, and 3.5 kHz profiles, this section of MSC is partially filled with a relatively undisturbed slump block from the flanking channel wall.

Other notable cores in Cluster D include FFC41, obtained from a levee, and KPC9, obtained from the head of LTSC. The fine grain-size of FFC41 implies that most sand and coarser sediment is contained within the canyon and accumulations outside the banks consist of silt- to clay-size sediment. The grain-size distribution in

KPC9 suggests that the slumping occurring at the head of LTSC is not exposing coarse sediment and that the overspill of sand from MSC has a restricted lateral distribution.

FFC38 is the outlier in this group (Figure 22b). Located near the head of LTSC, FFC38 contains mostly silt (59 %) and sand (16.9 %). The coarseness of this core top suggests either spillover from MSC (as opposed to hemipelagic rain) or exposure of older, more consolidated sediments from slumping. Given the proximity to MSC and the fine grain-size of KPC9, spillover from a turbidite event in MSC seems more likely.

CHAPTER 7

DISCUSSION

Historically, descriptions of submarine canyon systems have focused on the facies patterns in the fans, with some studies emphasizing the morphology and the erosional or depositional agents responsible for channel development. In a similar fashion, the preceeding sections have described in considerable detail the morphology of the Moquequa Submarine Canyon system. Within this section, three important observations made from the data at hand will be emphasized: 1) submarine canyons are good indicators of structural controls influencing convergent margins, 2) canyons and channels along the Arica Bight margin are very effective in bypassing coarse sediment across the continental slope, and 3) Farre and others' (1983) model for the development of canyon systems is, in general, supported across this region.

Canyons as Tectonic Recorders

The degree to which canyons follow structural trends is debatable. Some researchers believe canyon growth is entirely dependent on retrograde slope failure, while others prefer to believe tectonics are the dominant factor influencing canyon trends. The importance of fault control on canyons has been argued for in the central Aleutians (Gates and Gibson, 1956; LaForge and Engdahl, 1979) and along the upper slope of the central Peruvian margin (Bartlett, 1987; Hussong and others, 1988). This thesis supports the tectonic-control argument, yet it recognizes the importance of slope failure in modifying the path a canyon follows and proposes that scarps bounding major slumps in this region are pathways for canyon development.

The inception of MSC probably occurred during the late Miocene; Tosdal and others (1984) note that canyon incision has dominated the landform development of the entire Pacific slope of the Central Andes since the late Miocene. Transgressions and

regressions throughout the Pliocene and Pleistocene have undoubtedly affected the depositional and erosional capabilities of the system. Side-scan images clearly show that, at present, structural characteristics of this convergent margin are manifested in the trends of the submarine canyons. Rotated blocks, an undulating structural high, faulting, oversteepened slopes, and gravity all play roles in the path MSC and its tributaries eventually follow. Channels coursing oblique to the regional slope must have some factor other than gravity influencing their course; in this area, faulting appears to be the predominant control.

The southward trend of MSC across the Arequipa Basin has not been resolved to be directly fault related, but its breach across the structural high is most certainly fault controlled. The trend of MSC across the structural high parallels fault scarps visible in the side-scan images (compare Figures 8a and 9). Structural controls are also apparent in the southward trend of LTSC; it courses through a local depression formed between two blocks. Another example of structurally controlled trends is the low sinuosity, slope-parallel channels in the eastern section of the survey area (Figure 16a and 16b, "Slump scarp"). These channels appear to follow the scarps bordering a large slump.

The purpose of this thesis is to analyze the relative importance of structural controls, as opposed to gravity, on the trends of canyons for this particular margin. Although much of the structure of this margin is gravity induced, its importance in determining the trend of the canyons is secondary to the structure of the margin. In localized areas, such pure gravitational controls as slope oversteepening and unconfined turbidity flows continue to play a role in the development of channel morphology. For example, the head of LTSC is formed primarily by local slope failure, as are the meander-like bends bordering most channels in this area. The large slump in the eastern portion of the survey area, which probably resulted from slope oversteepening, is another example of gravity at work.

The superior areal resolution offered by side-scan data over seismic lines permits the use of channel trends and channel morphologies as first-order identifiers of structural fabrics affecting convergent margins. A quick means to identify structural features is useful for organizing a sampling program to verify initial hypotheses made about the margin or for revising a pre-determined survey pattern to better meet the cruise objectives. Obviously, these first-order observations must be further supported by other data (seismic, coring), but as an initial means of interpreting a margin's tectonic history, canyons may be quite diagnostic recorders.

Canyons as Bypassing Mechanisms

The combination of side-scan imaging and 3.5 kHz profiling permits the collection of very precisely located samples with respect to seafloor morphologic units, in this case channel thalweg, levee, overbank, and basin deposits. Our understanding of the specific events responsible for keeping canyon thalwegs in this area free of fine-grained sediment is poor, although the standard erosional agents of turbidity currents and density flows probably apply. The frequency of these events is also poorly understood. What we can address with this particular suite of cores is the effectiveness of a canyon system for bypassing coarse sediment across a trench slope environment. This bypassing efficiency can in turn place some constraints on the size of the turbidite events flowing down the channels while enhancing our understanding of the facies associated with submarine canyons.

Sedimentological data in and adjacent to this canyon system suggest most coarse-grained sediment is transported within its banks; very little sand is deposited in levee and overbank environments. In turn, the thalwegs appear to contain very little fine-grained sediment. Free-fall cores dropped in canyon thalwegs did not return (e.g. Figure 6a, FFC 6, FFC 10, KFFC33), presumably because core penetration was

insufficient to trigger the release mechanism. The lone channel sample, FFC33, was only 5 cm in length. Core penetration was probably prevented by coarse (i.e. sand-size and larger) thalweg deposits. Additional evidence supporting a coarse-grained canyon floor hypothesis comes from dredging results and 3.5 kHz profiling. Dredges from the MSC thalweg near the structural high contained large blocks of mudstones, apparently eroded from the adjacent walls, whereas 3.5 kHz records fail to show any sediment ponding within the active channel axis.

The bypassing of sand in canyons differs from the processes on most modern fan systems, which in general are actively aggrading features (Bouma and others, 1986; Maldonado and others, 1985; Damuth and others, 1988). The only places where sediment is able to ramp over the canyon banks are at abrupt changes in channel course, along channel-wall slumps, and where the relief of the banks is sufficiently low. In general, it appears that bank relief under 140 m in this area permits the spillover of sand and silt, which in turn implies a limit to the thickness of the turbidity current head travelling down the channels.

The channels across the structural high and the lower trench slope are primarily erosional features; based on the 3.5 kHz profiles, dredge hauls, and coring experience, the channel thalwegs appear to be free of fine-grained sediment. Given a sedimentation rate of 3.6 mm per year along the margin at 15^{o} S (Kim and Burnett, preprint), the events sweeping the thalwegs "clean" must be fairly frequent, perhaps on the order of decades. Whether or not these events are similar to the high-frequency, low-volume turbidites suggested for channel development on the Amazon Fan (Damuth and others, 1988) is unclear. The exceptional precision of this data set relates only to the surface layer of sediment. Subsequently, only general inferences can be made about canyon facies because of the limited number and stratigraphic penetration of the free-fall cores. The persistence of the general facies observations discussed in the above sections is

unknown; they can only be tested by acquiring cores with deeper stratigraphic resolution and samples from other canyon systems in active margin settings.

MSC in relation to the Farre and others' model

Farre and others' (1983) model for the development of submarine canyons is based on observations of canyon systems that cross the U.S. Middle Atlantic continental slope. It emphasizes the importance of the shelfbreak for classifying whether a canyon is young or mature. Youthful canyons occur on the slope; their initiation and continued erosional development occurs by retrogressive slope failure. Canyons enter maturity upon breaching the shelfbreak; their erosional development is more influenced by the downslope movement of turbidity currents originating at shallow depths than by slope failure.

In many respects, LTSC and MSC adhere to the model for canyon maturity propounded by Farre and his associates. The morphology of LTSC is dominated by slope failure features (e.g. the lobate, dendritic head, the slumped sidewalls) and can therefore be classified as youthful; MSC apparently breaches the shelfbreak (assuming the Moquequa River as a source) and appears to develop primarily from turbidity currents (e.g. the cut-bank slumps), thus categorizing it as mature. These two drainage systems differ from the canyon systems studied by Farre and others (1983) through the influence of this margin's structure. LTSC does not exhibit a pinnate drainage network with tributaries meeting at knife-edged spurs as noted by Farre and others (1983) along the Mid-Atlantic slope. Instead, LTSC has a dendritic drainage network resulting from its location within a local structural depression. This drainage network probably results from a combination of slope failure and turbidite spillover from MSC. According to the Farre and others (1983) model, a decrease in the canyon gradient is expected upon reaching maturity; such a simple pattern is not evident in the gradients of MSC and

LTSC. MSC maintains a channel gradient across the lower trench slope of less than 0.5^{o} up to the point where it changes course to the southwest; along this southwest trend the gradient increases to 1.75^{o}. LTSC, on the other hand, exhibits gradients of 1.5^{o} near its head, 0.8^{o} near the meander bend, and more than 2^{o} downslope from the meander. If a low channel gradient suggests downcutting by turbidity currents, then the high gradient along the southwest portion of MSC suggests this section of the canyon formed by slope failure and may be continuing to erode on a northeast trend.

CHAPTER 8

CONCLUSIONS

The combination of side-scan imaging and bottom sampling permit a simplified, tentative interpretation for the origin and history of the submarine canyon system off the Arica Bight. Without good stratigraphic control through drilling, however, the timing of certain events is speculative.

1. During the late Miocene to early Pliocene, sea level dropped to a position at or below its present level, allowing rivers to incise deep canyons into the Cordillera de la Costa. Inception of Moquequa Canyon probably occurred at this time. Continued uplift of the structural high or basin subsidence or both caused the axis of maximum sedimentation to migrate eastward.

2. Channels in the Arequipa Basin were deflected by the uplifted portions of the basin. The channels followed the deepest portion of the basin along southward trends, helping to fill the basin until sediment began spilling over the top. Moquequa Submarine Canyon may have crossed the undulating structural high at this time along a local saddle, but downcutting was probably minimal at this stage.

3. Listric faulting and block rotation disrupted and dissected the structural high, permitting MSC to breach the structural high along a fault plane. Sediment emptying from the basin across the lower trench slope dispersed on a southward trend.

4. Headward erosion by slumping of a southwest-trending channel eventually pirated the sediment being passed through the structural high. This southwest portion of Moquequa Submarine Canyon continues to act as an effective bypassing mechanism for the transportation of sediment across the lower trench slope. Very little sand is distributed outside the canyon, with the exception of where MSC changes course to the southwest.

5. Due to a combination of block rotation, sediment spillover, and local slumping, LTSC formed and remained active within a local depression. LTSC is not as effective as MSC for transporting sediment across the lower trench slope because of lower channel gradient and lower channel-wall relief; sand and silt are periodically dispersed outside its banks. An occasional slump upslope from LTSC or large-scale debris flow breaching the ridge separating MSC and LTSC may plug channels with sand-size detritus. After coursing to the south for approximately 35 km, LTSC meanders to the west in response to a decrease in relief of the confining seaward block. LTSC eventually follows the regional slope on a southwest trend until it abuts a local high and is deflected to the south-southeast. An upraised edge of a rotated block forms the local high. The channel follows this ridge along a south-southeast trend until it loses definition in the toe of the lower trench slope.

This simple history is subject to complications arising from such changes as the location of channels composing MSC, the rotation of blocks across the structural high, slumping of continental slope areas, and the flucuation of sea level along this margin. The trend and sedimentology of canyon systems reflect the interaction between tectonic and gravitational forces. Through time, structural controls on canyons are continually changing, altering canyon courses in defiance of pure gravitational controls. With the gathering of new data by side-scan and swath mapping techniques across the continental slopes of forearc regions, the importance of canyons for interpretating paleo- and present-day tectonics affecting active margins should become more apparent. In addition, high precision data sets, acquired with the help of side-scan images, from other canyon systems should augment the preliminary canyon facies findings discussed in this thesis.

APPENDIX A

SIDE-SCAN PROCESSING PROCEDURES

1. Navigation correction.

An initial template of side-scan images was constructed to correct the shipboard navigation. A standard set of processing parameters was applied to the data at this stage, with the emphasis on navigation correction, not image quality. The template was constructed by first laying down side-scan images on tracks with GPS navigation, as these tracks were considered the most accurate. Template construction progressed outwards from these tracks by matching features on the adjacent side-scan images. This side-scan feature matching gives an indication of how much the Transit satellite-based navigation is in error. The navigation file was edited accordingly so that the position of ship tracks corresponded to the features shown in the side-scan images.

At this initial processing stage, the images were globally corrected for gain steps along each track, assuming a starboard gain shift of 3dB and a port gain shift of 1dB. Angle varying gain corrections (resulting from the array beam pattern) and contrast mapping corrections were applied on a track to track basis. Additional image processing techniques applied to the data are described below.

2. Gain-step corrections.

In general, the 3dB and 1dB gain step corrections for the starboard and port sides was valid; most gain jumps were eliminated by applying these intensity corrections to the data. Spurious gain shifts along tracks may be caused by a series of gain changes within a short time interval (either increasing or decreasing the gain) or by changing the gain in increments of 2 as opposed to single gain changes. These spurious gain jumps were corrected on an individual basis by an iterative process of changing the correction factor (signal intensity) within the "GAIN" file. A GAIN file consists of intensity changes at a corresponding time and is produced from a "SWITCH" file. A SWITCH file

is simply a record of all gain changes made during the course of the cruise. A systematic pattern to these spurious gain jumps was not observed.

3. **Angle-varying gain correction.**

Angle varying gain (AVG) problems arise due to the array beam pattern; AVG corrections eliminate streaking (white or dark stripes) along the ship track. At the time of processing, the best method for correcting this streaking was to construct an "AVG" file from a representative portion of a particular track and to apply that AVG file to the entire track. Each track therefore has its own AVG file constructed from a portion of that same track. If a single AVG file was insufficient for correcting the data, then the track was partitioned and a second or third AVG file was constructed and the track was processed again. Most tracks were corrected using a single AVG file.

4. **Contrast correction.**

Contrast mapping is the application of a function so that gray levels plotted on the Raytheon thermal printer are distributed equally among the data. Assuming a Gaussian distribution, approximately 95 % of the data values should lie between +/-2 standard deviations. Accordingly, most of the gray levels plotted by the Raytheon should be dispersed over this area. High- and low- end data values are compressed into a very few gray tones. Assuming that these values are a relatively minor portion of the data set, not much information is lost by applying this scheme. In general, one contrast map ("CMAP" file) was constructed per track. As in the case of AVG corrections, this procedure did not work equally well on all tracks; additional CMAP files were constructed for certain tracks.

5. **Overview**

Given the data correction procedures at the time of processing, the side-scan images look reasonably well. All gain changes were corrected to a satisfactory level, although image resolution on some tracks across the trench (deep water) are still not

good; a "cloudiness" permeates some of the images. This cloudiness results in part from problems associated with the angle varying gain corrections and the contrast mapping. New processing techniques, such as roll-along angle-varying gain correction and roll-along contrast mapping, are capable of substantially improving the image resolution.

APPENDIX B

SIDE-SCAN IMAGES OF LOWER TRENCH SLOPE, PERU-CHILE MARGIN

The side-scan images collected from offshore the Arica Bight of southern Peru and northern Chile are shown as plates in this appendix. When assembled, the images form the side-scan mosaic of the lower trench slope, the area discussed in this thesis. A diagram of how the plates may be assembled is shown below.

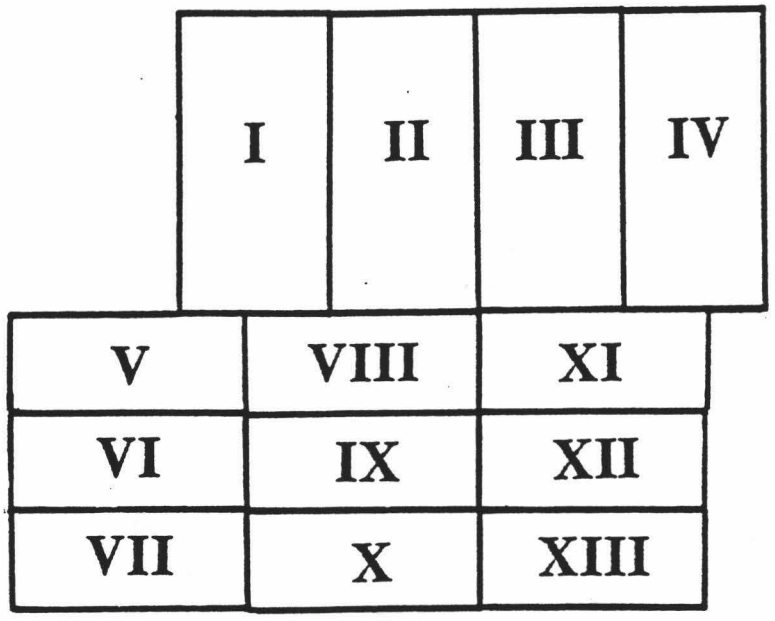

PLATE I

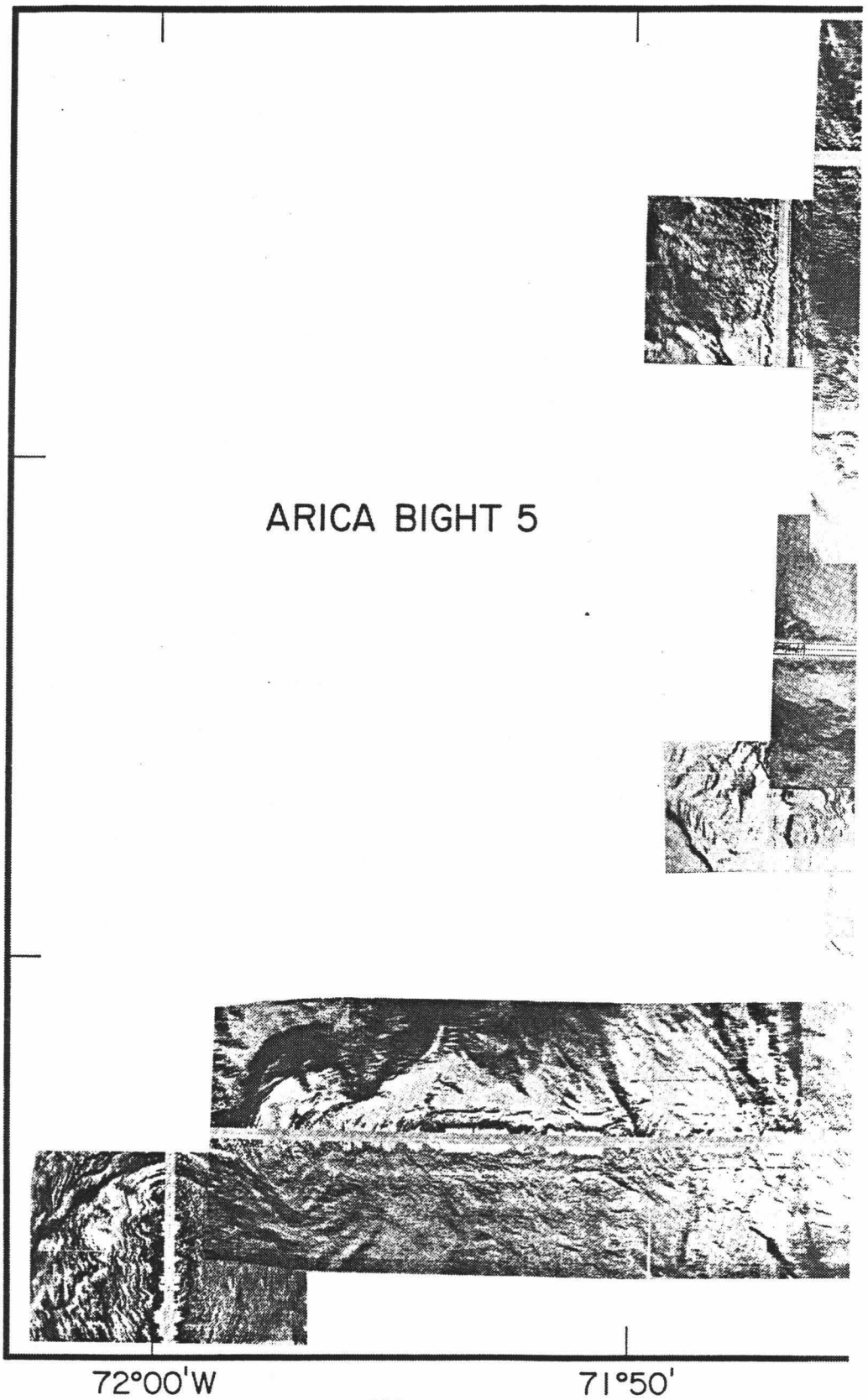

PLATE II

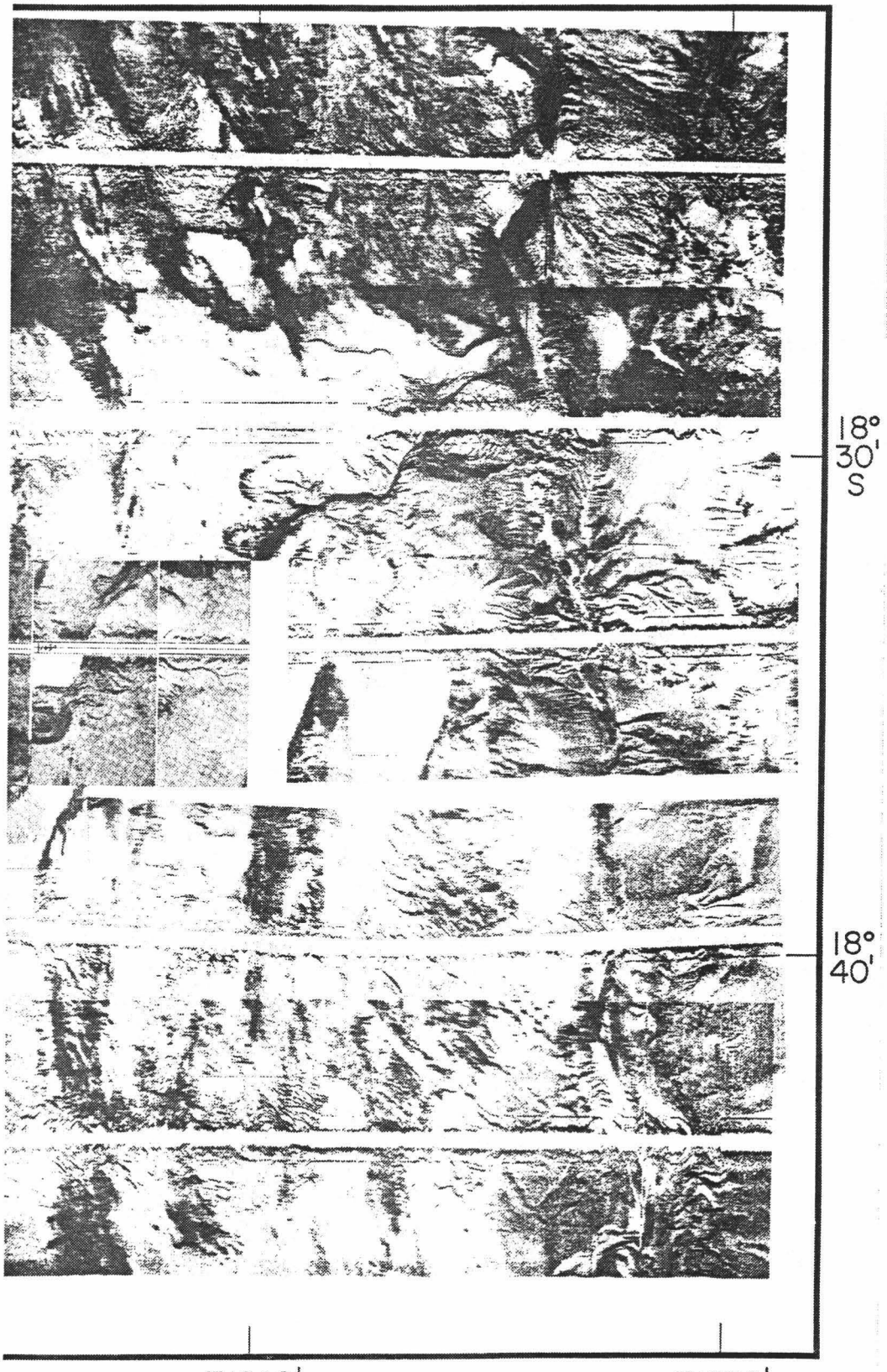

PLATE III

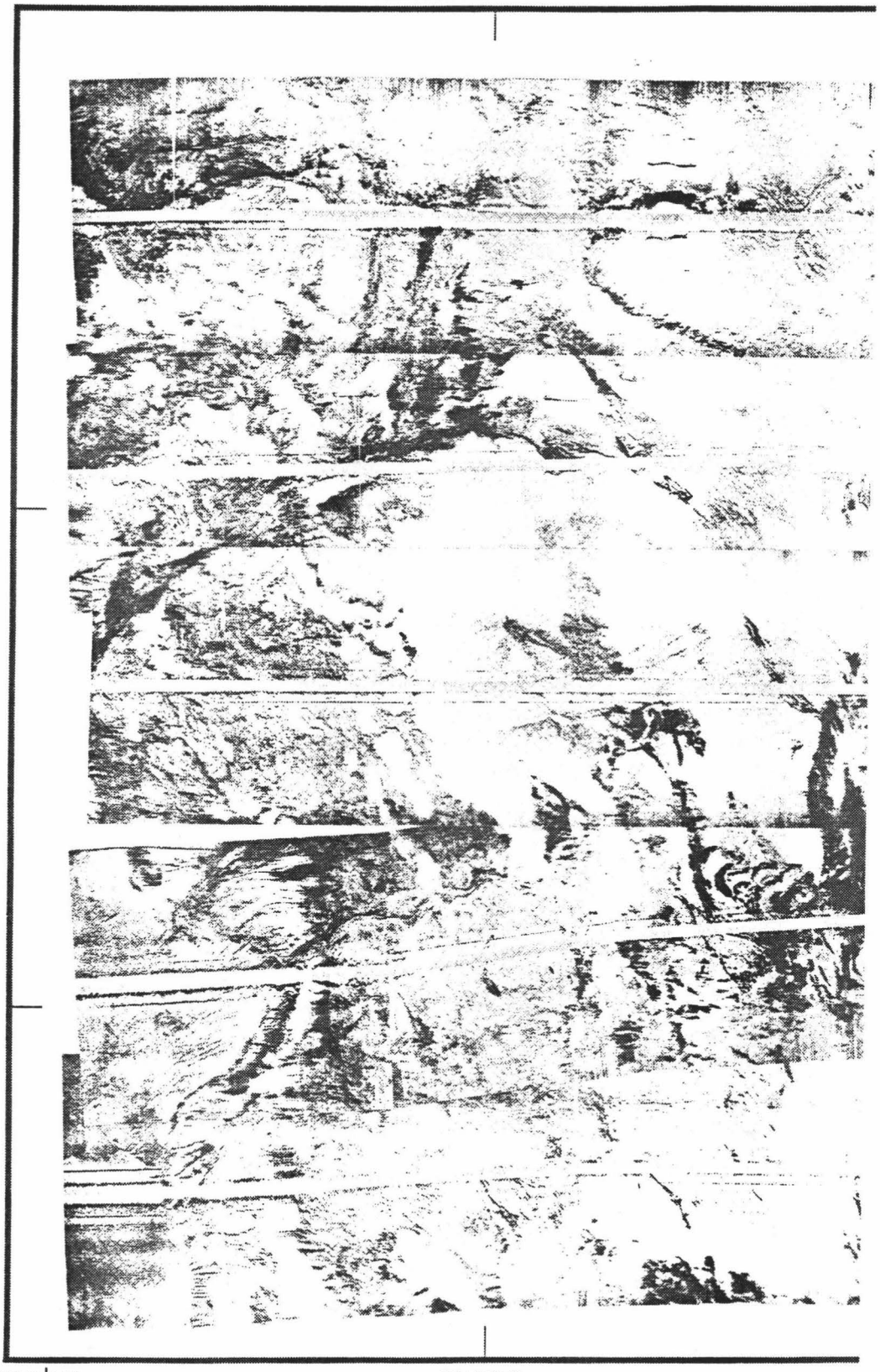

71°30'W 71°20

PLATE IV

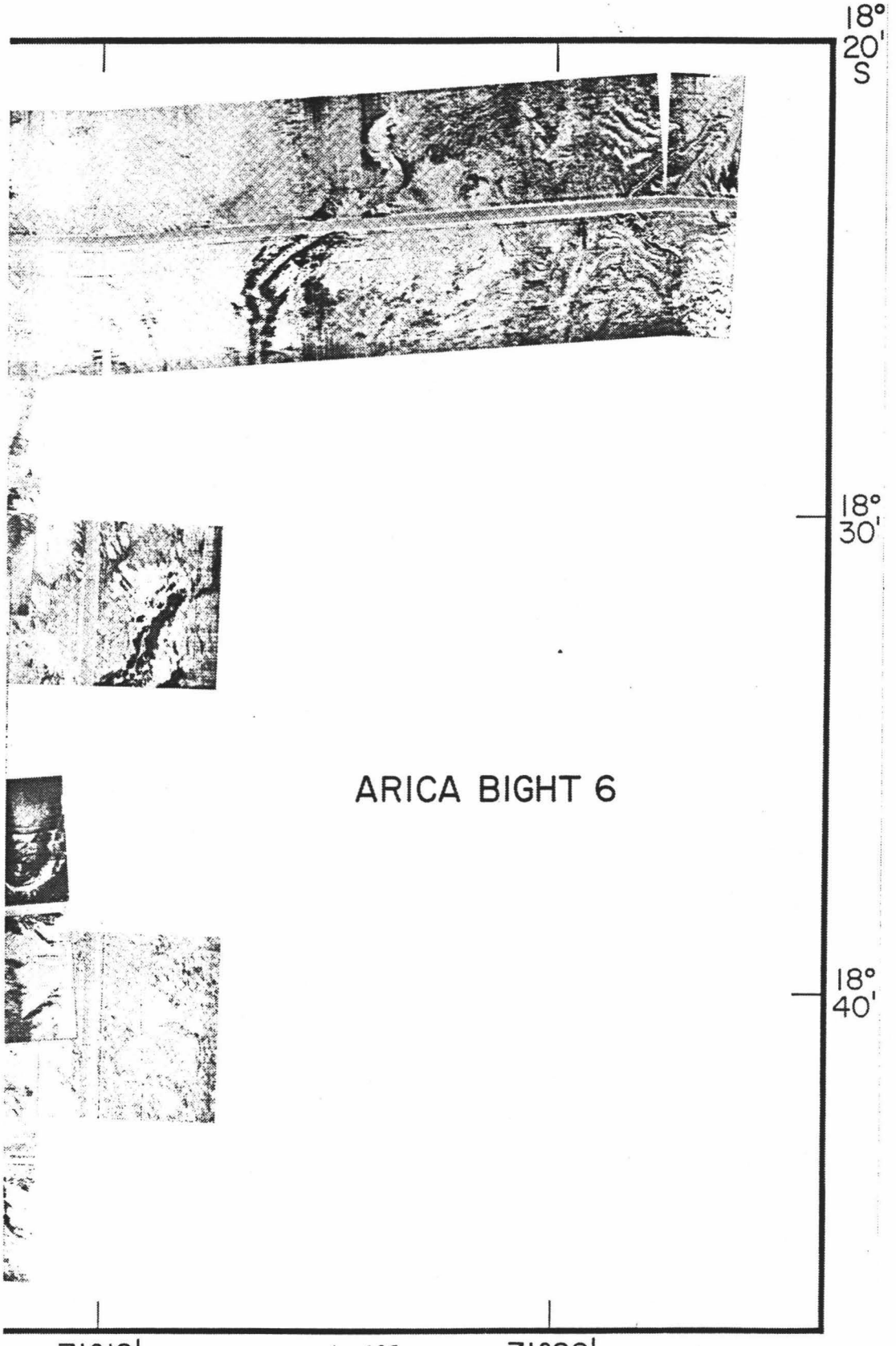

PLATE V

18° 50' S

ARICA BIGHT 7

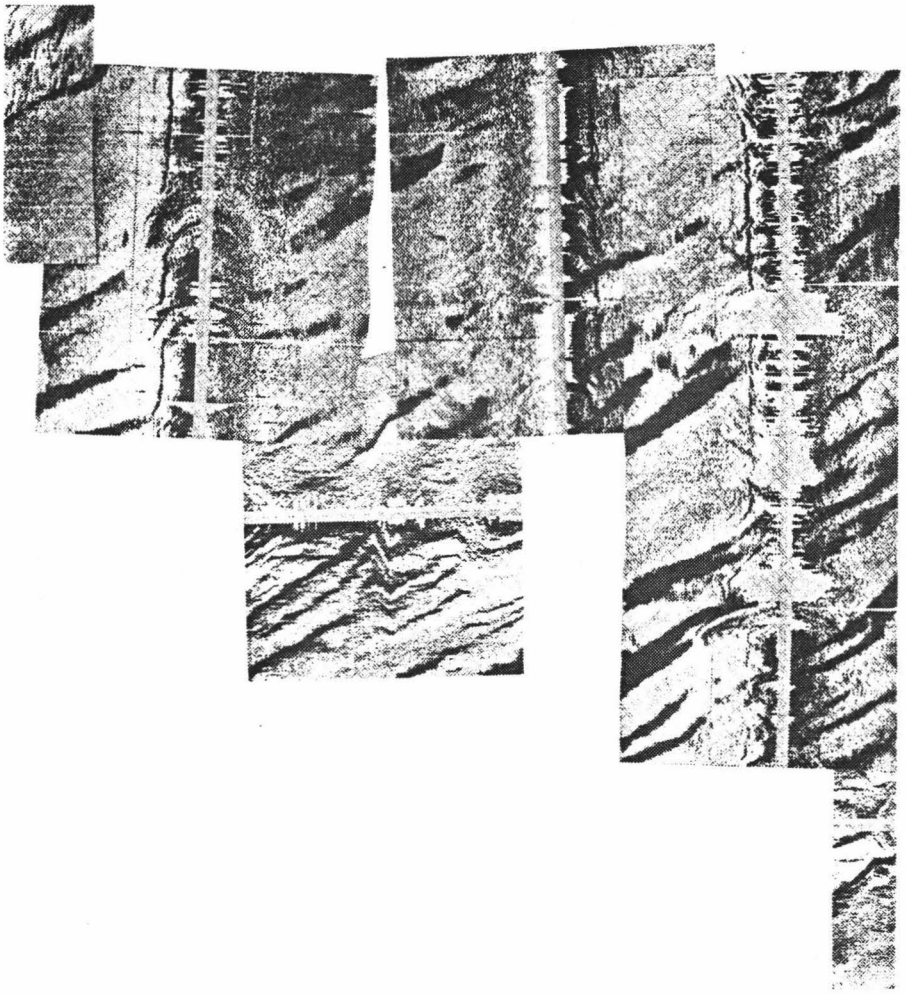

PLATE VII

18° 50' S

PLATE VIII

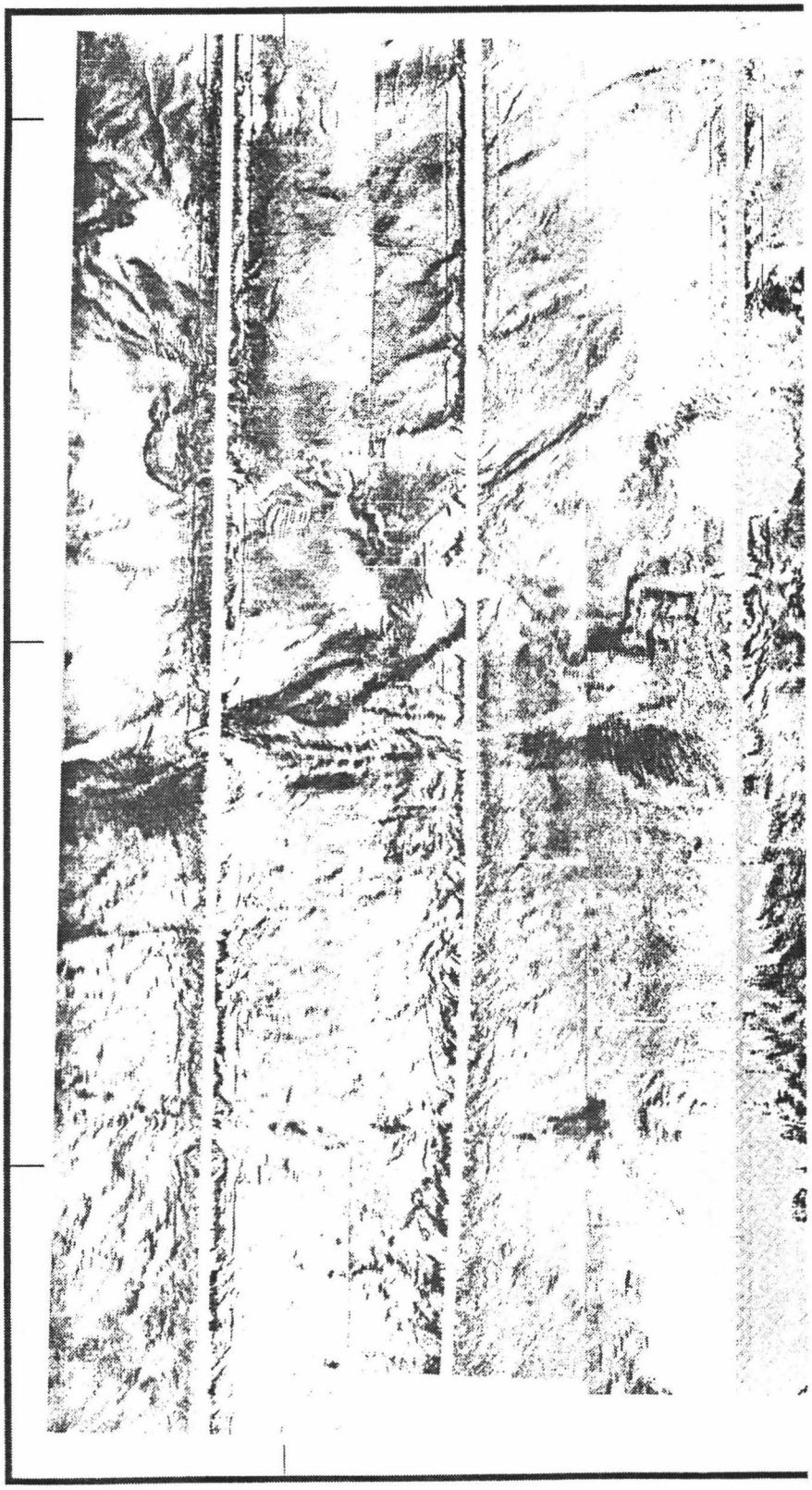

PLATE IX

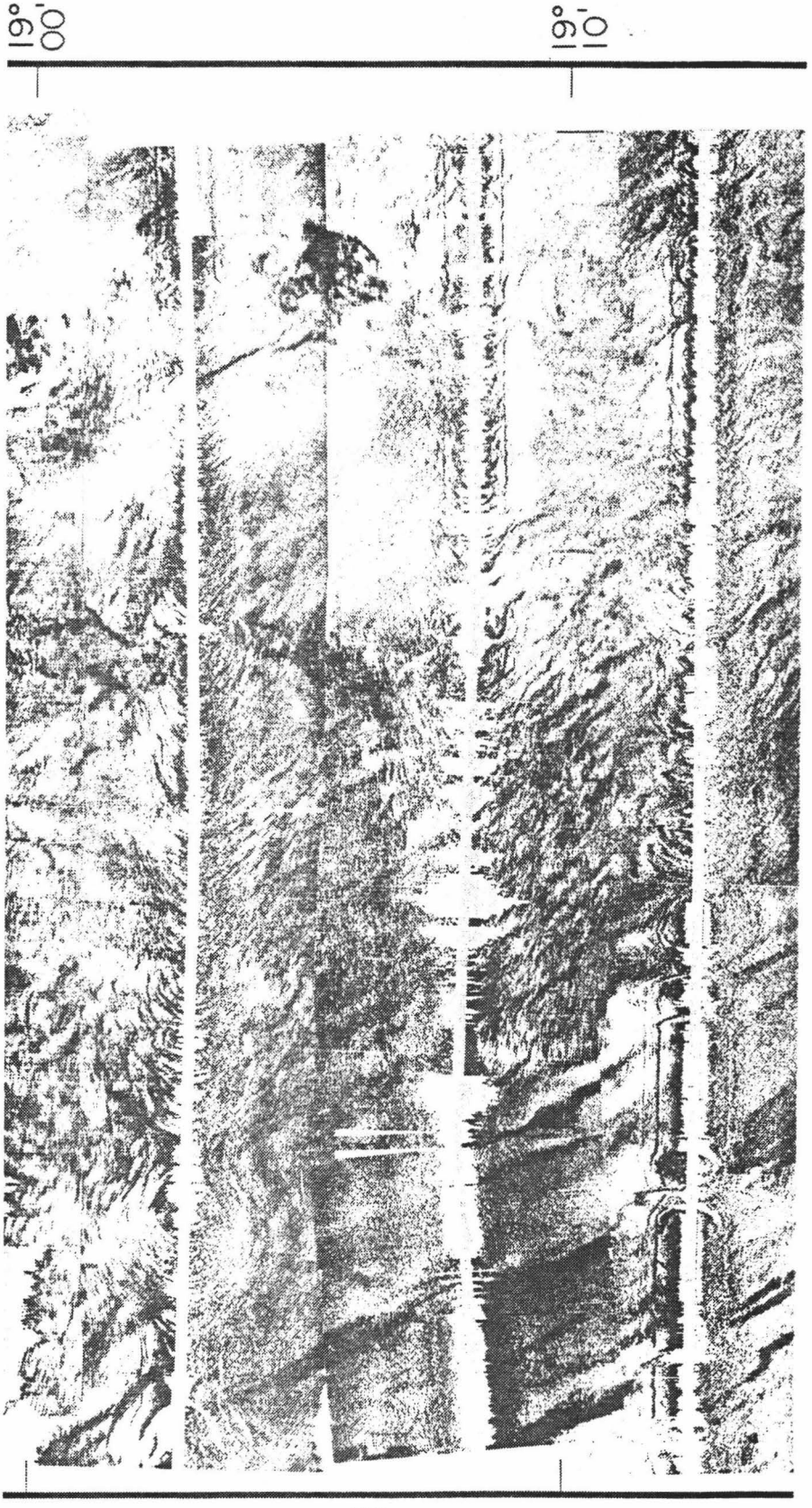

PLATE X

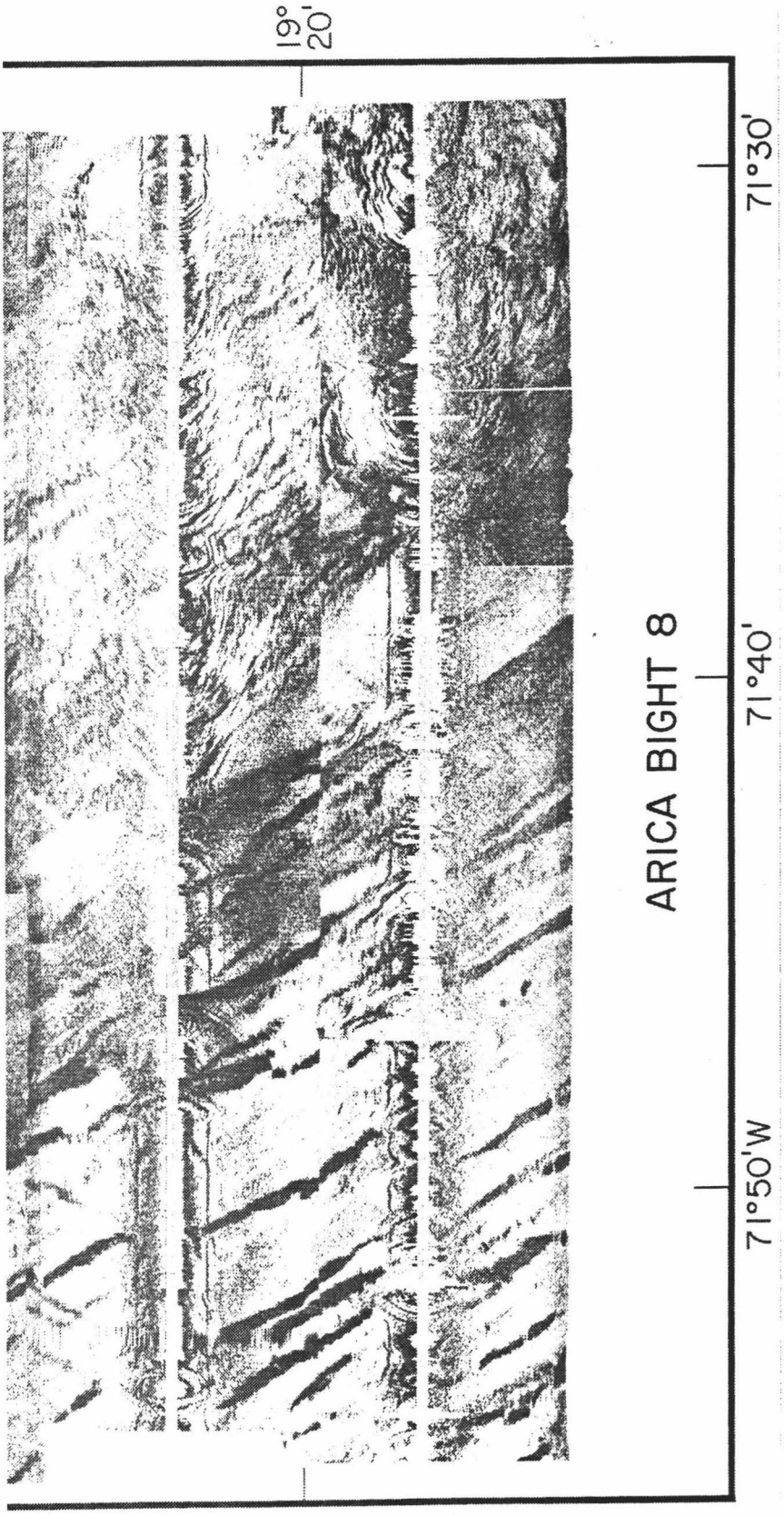

PLATE XI

PLATE XII

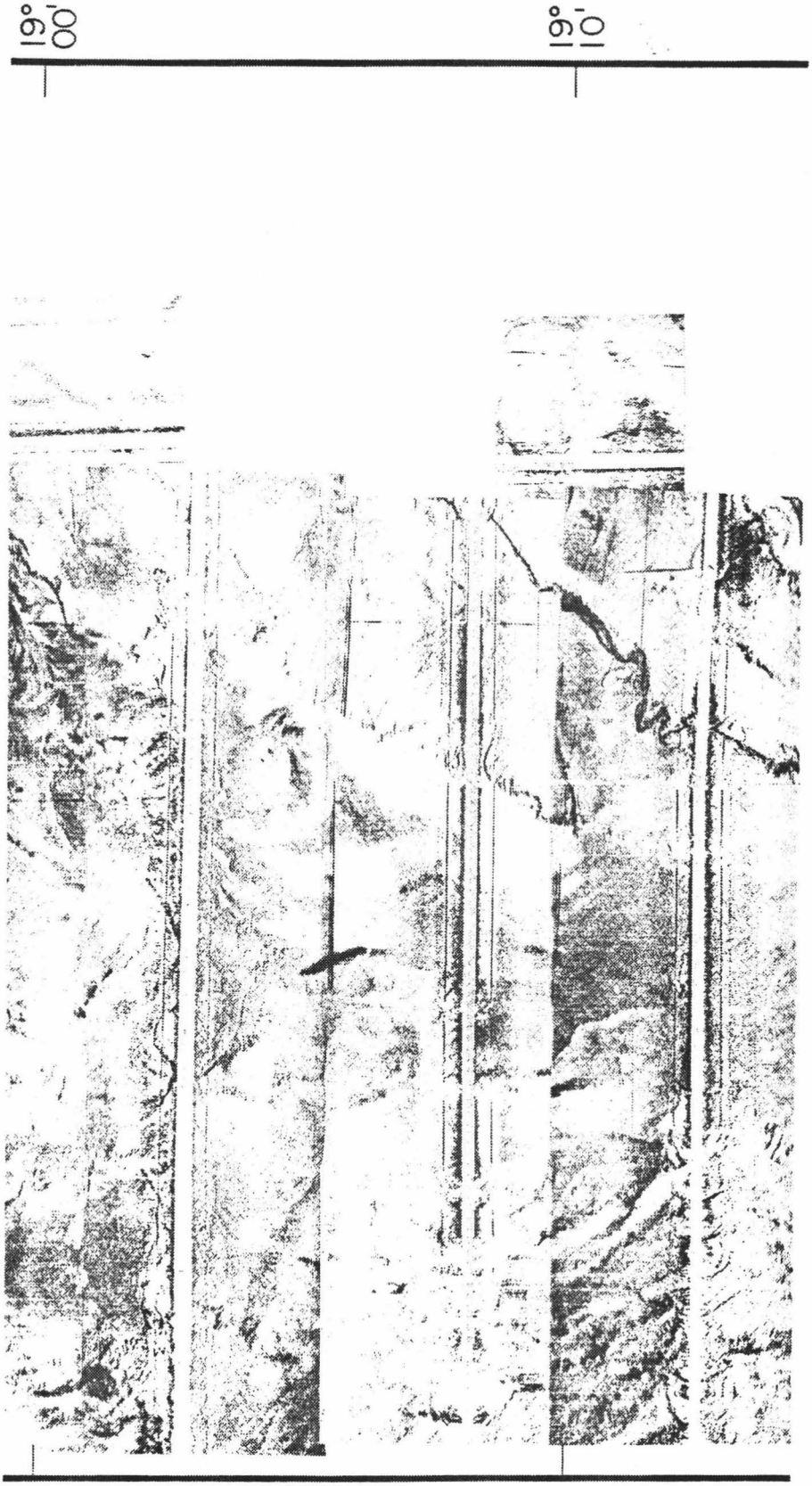

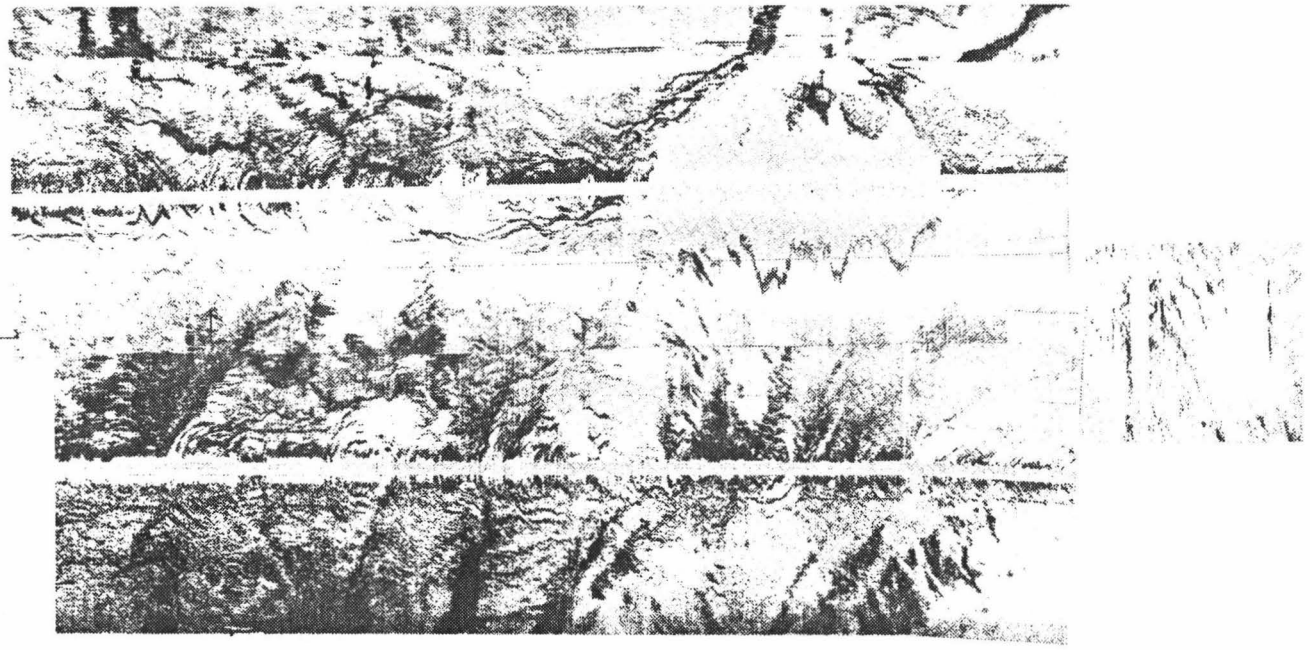

ARICA BIGHT 9

114

19°
20'

71°30'W

71°20'

71°10'

PLATE XIII

APPENDIX C

PIPETTE ANALYSIS

The following is an outline of the procedures employed in the grain-size analysis of ocean sediments collected from the Peru-Chile margin. As a "cookbook" approach to pipetting in the HIG lab did not exist prior to the writing of this thesis, this outline should provide the basic information for analyzing grain sizes by this method. Included in this appendix are the laboratory procedures followed for the preparation and separation of sediments, a list of equipment, a sample data sheet, and the FORTRAN code for a program designed to analyze the grain-size results.

Laboratory Procedures

1. Obtain a representative sample.

Weigh a 250 ml beaker and record on a data sheet (see attached *DATA SHEET*). Place the sample in the beaker and dry in an oven for 3 to 4 days. After this drying period, remove the beaker from the oven and place in a dessicator. Allow approximately 2 hours for both to equilibrate with the room temperature. Weigh beaker and sample, and record on data sheet.

2. Remove organic material and disaggregate sample.

Organic material may by removed with hydrogen peroxide; either a warm 10 % H_2O_2 solution or a cold 30 % H_2O_2 solution. Add small amounts of distilled water to sample until frothing ceases. I found that a mixture of 10 ml 30 % H_2O_2 and 10 ml distilled water removes all organic material without excessive frothing. Place sample in oven and dry for 4 days. Remove sample and allow it to equilibrate to room

temperature in a dessicator. Weigh sample and beaker, and record on data sheet; the weight lost is the amount of organic material removed.

Disaggregation may be facilitated by adding 20 ml of a dispersant solution. I suggest creating a stock solution of 50 g sodium hexametaphosphate, "Calgon", per liter of distilled water. If the sample contains a substantial amount of clay, letting it sit overnight in the Calgon bath may be helpful.

Washing with a solution of acetone and distilled water, to remove soluble salts contained in the pore water, is recommended by some researchers. Bruce Tsutsui of the HIG core lab (pers. comm.) determined that samples not washed with acetone exhibited an absolute weight difference equal to a size difference of approximately 1/10 phi. I feel the magnitude of this size discrepency is sufficiently small so that elimination of the acetone washing step will not significantly alter the results.

3. Separate the less than 62 micron (4 phi) fraction of the sample.

Place a 62 micron (230 mesh) sieve over a 1000 ml graduated cylinder; depending on the diameter of the sieve, you may have to use a funnel. Place the sample in the sieve and wash with distilled water. After the water level in the cylinder reaches the 600 ml mark, let the silt settle out and use the partially clear water for further wet-sieving. Always finish sieving with clean distilled water. If dispersant has not been added, do not exceed 900 ml of water and mud total.

4. Measure the sand fraction.

Transfer the residual sediment in the sieve to an evaporating basin or beaker (use wash bottle). Dry this sand fraction for 3-4 days, remove it from the oven and allow it to equilibrate with room temperature in a dessicator, then weigh it to the nearest 0.001 g and record the weight on the data sheet. Depending on the amount of sand and the

objectives of the project, dry sieving to recover any additional silt or clay may be required prior to pipette analysis.

5. Disaggregate the sample.

If dispersant was not added during disaggregation step or if the sample contains a high percentage of clay, add 20 ml of Calgon solution at this point. Based on a stock solution of 50 g sodium hexametaphosphate to 1 liter distilled water, each 20 ml of solution is equivalent to adding 1 g of pure Calgon. You will have to subtract the amount of dispersant added before calculating any size fractions, so you should record the amount on the data sheet. Top the cylinder to 1000 ml with distilled water. Thoroughly stir the column using a brass stirring rod.

6. Prepare phi-interval beakers for pipetting.

Label and weigh 50 ml beakers, and record on data sheet. The number of beakers per sample should equal the number of phi sizes being examined. Arrange the beakers in front of the cylinder.

7. Check for clay flocculation.

Cover the cylinder with a watchglass and allow it to stand overnight. This step checks for clay flocculation prior to performing the pipette analysis. Fill a beaker with tap water and insert a thermometer to determine temperature. The depth of sample withdrawl is dependent on the water temperature.

If flocculation has occurred (recognized by curdling and rapid settling of clumps of particles, or by a distinct transition between a thick, soupy layer at the bottom of the cylinder and an overlying clear liquid), try adding more dispersant or creating a new

suspension with a smaller sample. Using a mechanical stirrer for 5 minutes may assist dispersion. Remember, do not exceed 1000 ml in the cylinder.

NOTE: You should allow 12 hours to complete the following steps of the analysis, depending on the number of samples being analyzed. The number of samples run per day depends on the skill of the researcher. Four samples may be a workable number with which to start; increased expertise in pipetting may permit an increased number of samples to be run.

8. Determine the depth of withdrawl.

Record the water temperature and apply the sampling depth corrections shown on the *TEMPERATURE CORRECTION SHEET*; Lewis, 1984). Select a 20 ml pipette and have a large beaker of distilled water ready for rinsing the pipette. Mark the depths of sample withdrawl on the pipette with an insoluble ink pen.

9. Begin the first withdrawl.

Start a timepiece 1 minute before initial withdrawal (e.g. 11:59). Immediately begin stirring the first cylinder. Start with short, quick strokes at the bottom and work up the column with long, vigorous strokes. At precisely time zero (12:00), remove the stirrer. Lower the pipette to 20 cm. At precisely 20 seconds, extract a 20 ml sample. Empty it into the appropriate 50 ml beaker and rinse the pipette into the same beaker with 20 ml of distilled water.

This first withdrawal is particularly critical since it represents everything finer than 4 phi.

NOTE: Folk (1974) suggests the following procedure for making withdrawals: fifteen seconds before the time of withdrawal, grasp the rubber tube of the pipette with the left hand and convey it to the mouth. With the right hand, insert the glass part of the pipette to the proper depth, and steady it by resting the right hand on the rim of the cylinder. With your left hand grasp the pipette at the place where the rubber tube is attached to the glass, so you will be able to get an exact volume in the pipette by using your left index finger to clamp the rubber tube shut against the end of the glass tube. When the time arrives, begin sucking very rapidly and draw the suspension up about an inch above the volumetric mark, and clamp with the left finger. Then let the suspension drain by slowly unclamping the finger, until the liquid surface hits the volumetric mark. If you are off by no more than 3 mm either way, it is sufficiently accurate. Remove the pipette, expel the suspension into a weighed 50 ml beaker, suck up 20 ml of distilled water to rinse out the pipette, and expel the rinse water into the same beaker.

The HIG lab is equipped with rubber pipette bulbs which eliminate most of these steps. Some of the sampling intervals shown on the *TIME SCHEDULE SHEET* (Lewis, 1984) are spaced 1 minute apart. These sampling intervals can be attained if the distilled water used for rinsing is forcefully expelled from the pipette by applying pressure to the bulb, as opposed to allowing the water to drain freely.

10. Continuing with sample withdrawls.

Subsequent withdrawals occur at the times listed on the *TIME SCHEDULE SHEET* (Lewis, 1984). If a phi interval is missed, an alternative time may be derived for that interval from the attached phi diameter versus time of withdrawl graph. Alternatively, the missed interval may be obtained by restirring the column after all other withdrawals have been completed. You should avoid restirring if at all possible.

When all withdrawals are completed, dry the beakers in an oven. If additional analyses of the clays are to follow, do not heat above 65^{o} C. Dave Obrien of HIG (pers. comm.) has found the optimum time for drying sediments to be 4 days. To compensate for the excess water associated with pipetting, 5 days for drying is recommended.

11. Calculating coarse- and fine-fractions.

When the samples are dry, remove the beakers from the oven and leave them to equilibrate with the room temperature in a desiccator for at least 2 hours. Weigh them to the nearest 0.001 g and record on the data sheet.

Note: Folk (1974, p.35) discusses the hazards associated with weighing samples in an absolute dry state (i.e. baking clean beakers, equilibriating in a desiccator, maintaining a desiccating chemical in the scales). The key is to remain consistent with whatever weighing procedures you choose to follow.

To calculate the cumulative weight percentages:

a) Subtract the 50 ml beaker weights (**B**) from the total sample weight (**TSW=B+S+D**), where **S** is the sample weight and **D** is the weight of dispersant present in each 50 ml beaker. To determine the weight of dispersant in each beaker, divide the weight of the dispersant in the entire column of water by 50. Subtract this amount (**D**) from the total weight to give the sediment weight (**S**).

$$S = TSW-B-D$$

b) Multiply S by 50 in the <4 phi beaker to give the total weight of the fine-fraction (FF).

$$FF = (S \times 50)$$

This value added to the weight of the sand-fraction (SF) determined by sieving in step #4 provides the total sample weight (TSW) minus the organic matter, which can be checked against the weight of organics removed in the hydrogen peroxide step (#2).

$$\text{Organics} = TSW - SF - FF$$

c) Each pipette sample represents the amount of sediment in the column finer than a certain grain size. To obtain weight percentages for each size interval, multiply each sample weight (S) by 50, subtract this number from the next largest size interval, divide by the TSW and multiply by 100.

$$\text{Weight \% (size interval)} = [(S_{t1} - S_{t2} \times 50)/TSW] \times 100$$

$$\text{where } S_{t1} > S_{t2} \text{ in size and weight}$$

NOTE: The principle behind these computations is if the sediment within the cylinder is assumed to be uniformly distributed by stirring and exactly 20 ml is drawn off at stated time, then the amount of mud in each withdrawal is equal to 1/50 of the total amount of mud remaining suspended. In other words, each pipette sample represents the amount of mud finer than the given phi diameter -- all material coarser than the given diameter will have settled past the depth of withdrawal.

The FORTRAN code for a program (PIPE.FOR) compatible with IBM PCs is included in this appendix. The program is designed to calculate weight percents for each phi size interval and print histograms showing the grain-size distribution for each sample.

EQUIPMENT

For each sample:

a. 1 x data sheet
b. 1 x 250 ml beaker or basin for disaggregation
c. 1 x 1000 ml graduated cylinder
d. 8 x or 9 x 50 ml beakers (one for each phi-size measured)
e. 1 x watch glass for cylinder

General materials:

a. 0.062 mm (230 mesh) sieve
b. large evaporating basin or 2 x 650 ml beakers
c. wash bottle with distilled water
d. large funnel (if 4-phi sieve does not fit over 1000 ml cylinder mouth
e. solution of dispersant (e.g. 50 g "Calgon"/liter distilled H_2O)
f. brass stirring rod
g. thermometer
h. 20 ml pipette with extraction depths marked from the lower tip of the pipette; a few additional marks at 0.5 cm intervals around those depths may also be useful.
i. timepiece with hours, minutes, and seconds
j. oven
k. dessicator cabinet
l. dessicant crystals

PIPETTE DATA SHEET

Sample I.D._____
Sample # _____ Date _____
Temperature _____ Operator _____
Type of Dispersant _____ Comments:
Amount of Dispersant _____
Weight of beaker _____
Weight of beaker + sed _____
Weight of beaker + sed after H2O2 _____

Diameter ϕ	Depth of Withdrawal (cm)	Time of Withdrawal (hr:min:sec)	Evaporating Dish #
4.0	20	00:00:20	
4.5	20	00:02:00	
5.0	20	00:04:00	
5.5	20	00:08:00	
6.0	20	00:15:00	
7.0	10	00:30:00	
8.0	10	02:00:00	
9.0	10	08:00:00	
10.0	10	32:00:00	

Sand Fraction _____

ED=Evaporating Dish S=Sample D=Dispersant gm

4.0 ϕ

ED+S+D= _____ gm
minus ED _____
S+D _____
minus D _____
S _____
multiply x50 to give total sample weight in 1000 ml
S_t = _____

4.5 ϕ

ED+S+D= _____ gm
minus ED _____
S+D _____
minus D _____
S _____
multiply x50 to give total sample weight in 1000 ml
S_t = _____

5.0 ϕ

ED+S+D= _____ gm
minus ED _____
S+D _____
minus D _____
S _____
multiply x50 to give total sample weight in 1000 ml
S_t = _____

5.5 ϕ

ED+S+D= _____ gm
minus ED _____
S+D _____
minus D _____
S _____
multiply x50 to give total sample weight in 1000 ml
S_t = _____

6.0 ϕ

ED+S+D= _____ gm
minus ED _____
S+D _____
minus D _____
S _____
multiply x50 to give total sample weight in 1000 ml
S_t = _____

7.0 ϕ

ED+S+D= _____ gm
minus ED _____
S+D _____
minus D _____
S _____
multiply x50 to give total sample weight in 1000 ml
S_t = _____

8.0 ϕ	9.0 ϕ	10.0 ϕ
ED+S+D= _____ gm	ED+S+D= _____ gm	ED+S+D= _____ gm
minus ED _____	minus ED _____	minus ED _____
S+D _____	S+D _____	S+D _____
minus D _____	minus D _____	minus D _____
S _____	S _____	S _____
multiply x50 to give total sample weight in 1000 ml	multiply x50 to give total sample weight in 1000 ml	multiply x50 to give total sample weight in 1000 ml
S_t = _____	S_t = _____	S_t = _____

```
c*********************************************************************
c PIPE.FOR                                                            *
c Program created by Doug D. Bergersen in April, 1988.                *
c Plotting routine revised from Stewart and Gedlinske, 1986, Computers *
c                                and Geosciences, v. 12, p. 81-87.    *
c      *      *      *      *      *      *      *      *             *
c This program is designed to compute from raw pipette analyses data  *
c the weight percents for each phi interval, the fine fraction, and   *
c the coarse fraction. It also plots a histogram of the weight percent *
c within each phi interval and a histogram of the cummulative weight  *
c percent within each sample.                                         *
c                                                                     *
c The data file should consist of:                                    *
c       1. Amount of dispersant added (in grams).                     *
c       2. Weight of beaker                                           *
c       3. Weight of beaker + sediment                                *
c       4. Weight of beaker + sediment after H2O2 treatment           *
c       5. Weight of the beaker + sand fraction.                      *
c       6-?. Pairs of phi interval beaker + pipetted sample weights and*
c            beaker weights.                                          *
c NOTE: One line per sample. Each entry should be separated by a space *
c       as the program reads the data with a free format. The program  *
c       is dimensioned to handle data matrices up to 50 X 50.         *
c                                                                     *
c This program is interactive. Most of the questions asked are self-  *
c explanatory. When asked to insert variable names, the first five    *
c entries should always represent the amount of dispersant added (wod),*
c the weight of the sample beaker (wosb), the weight of beaker +      *
c sample (wb+s), weight of beaker + sample after H2O2 treatment       *
c (ws-o), and the weight of beaker + sand fraction (w+sf).            *
c The remaining variable names represent the various phi sizes        *
c measured and should alternate between the phi size label and the    *
c beaker label.                                                       *
c                                                                     *
c NOTE: Only 10 variable names per line, each variable name 4         *
c       characters in length.                                         *
c                                                                     *
c The computer will prompt you for the names of two external files.   *
c One of these files is the data file and should be entered under      *
c UNIT 5. The other file is the output file and should be entered      *
c under UNIT 6.                                                       *
c                                                                     *
c                        ****PRINTING*****                           *
c                                                                     *
c The output from this program exceeds the normal maximum of 80       *
c characters per line specified for most printers. Hence, the user    *
c must tell the output device to print in COMPRESSED MODE prior to     *
c running this program. Two BASIC programs are outlined below. The    *
c only changes the user has to make on these programs is possibly the  *
c function code (function number). The function code informs the       *
c printing device which mode it is supposed to print the output.      *
c Function codes can be found in the printer manual. The programs     *
c are written for a PANOSONIC printer, whereas an OKIDATA printer     *
c requires CHR$(29) for compressed mode and CHR$(30) to release the   *
c compressed mode. Compressed mode prints 16.5 characters per inch    *
c (CPI) -- normal print is 10 CPI.                                    *
c                                                                     *
c BASIC PROGRAMS TO RUN FOR COMPRESSED PRINT                          *
c       10 REM PROGRAM #1 -- COMPRESSED CHARACTERS                    *
c       20 LPRINT CHR$(15)                                            *
c       30 END                                                        *
```

```
c       10 REM PROGRAM #2 -- RELEASE COMPRESSED MODE                    *
c       20 LPRINT CHR$(18)                                              *
c       30 END                                                          *
c-----------------------------------------------------------------------*
c VARIABLE DEFINITIONS                                                  *
c                                                                       *
c       xdata : array containing input data from pipette analysis.      *
c               1st entry = amount of dispersant added (g)              *
c               2nd entry = weight of beaker                            *
c               3rd entry = weight of beaker + sediment                 *
c               4th entry = weight of beaker + sediment after H2O2      *
c               5th entry = weight of sand fraction + beaker            *
c       n : number of samples                                           *
c       m : number of phi intervals measured                            *
c       tw : total weight of sample                                     *
c       oc : organic content                                            *
c       twwo : total weight of sample without organics                  *
c       wd : weight of dispersant in each pipette interval              *
c       ws : weight of sample in each pipette interval                  *
c       pws : percent weight of sample in each pipette interval         *
c       ff : fine fraction                                              *
c       cf : coarse fraction                                            *
c       pcf: percent coarse fraction                                    *
c       var: array containing variable names                            *
c       tag: array containing selected variable names used in plotting  *
c       samp: vector containing sample tags                             *
c       ispot: dummy variable used as a pass in printing subroutine     *
c              (0=normal matrix    1=inverted matrix)                   *
c-----------------------------------------------------------------------*
c DIMENSION BLOCK
c
        dimension xdata(75,50),tw(75),oc(75),twwo(75),wd(75),
     &          ws(75,50),pws(75,50),ff(75),cf(75),var(75),samp(75),
     &          tag(75),pcf(75)
        double precision samp,var,tag
        character*80 title
        nd=75
        md=75
        ispot=0
c-----------------------------------------------------------------------*
c READING IN THE DATA
c
        write(*,*)' Enter title card (up to 80 characters): '
        read(*,1003)title
        write(*,*)' Enter the number of samples: '
        read(*,*)n
        write(*,2019)
        do 5 i=1,n
                read(*,1001)samp(i)
    5   continue
        write(*,*)' Enter the number of phi intervals measured: '
        read(*,*)m
        m2=2*m
        write(*,2020)
        read(*,1002)(var(i),i=1,m2+6)
c
c Reduce the number of variable names to be used in plotting histograms
        k=5
        tag(1)='org'
        tag(2)='pcf '
        do 6 i=1,m
```

```
                k=k+1
   6    continue
c
        write(*,*)' Enter the name of data file: '
        do 10 i=1,n
                read(5,*)(xdata(i,j),j=1,m2+5)
   10   continue
        write(*,*)' Enter the name of output file: '
        write(6,2021)title
        call printm(xdata,n,m2+5,nd,md,var,samp,ispot)
c-----------------------------------------------------------------------*
c BEGIN COMPUTATIONS
c
c Calculate total weight, organic content, and total weight - organics
        do 20 i=1,n
                tw(i)=xdata(i,3)-xdata(i,2)
                oc(i)=xdata(i,3)-xdata(i,4)
                if (oc(i) .lt. 0.0) then
                write(6,*)'OC LESS THAN 0 -- CHECK DATA INPUT'
                endif
                twwo(i)=tw(i)-oc(i)
   20   continue
c
c Calculate weight of dispersant and weight of sediment in each phi size
        do 30 i=1,n
                wd(i)=xdata(i,1)/50.0
                l=0
                do 25 j=1,m
                     ws(i,j)=(xdata(i,j+l+5)-xdata(i,j+l+6)-wd(i))*50.0
                     l=l+1
   25           continue
c
c Calculate percent weight of sample in each phi interval
                do 26 k=1,m-1
                        pws(i,k+2)=(ws(i,k)-ws(i,k+1))/tw(i)*100.0
   26           continue
c
c Calculate coarse fraction, fine fraction, and percent coarse fraction
                cf(i)=xdata(i,5)-xdata(i,2)
                ff(i)=twwo(i)-cf(i)
                pcf(i)=cf(i)/tw(i)*100.0
                pws(i,1)=oc(i)/tw(i)*100.0
                pws(i,2)=pcf(i)
   30   continue
c-----------------------------------------------------------------------*
c BEGIN WRITING RESULTS
c
        write(6,2021)title
        write(6,2000)
        do 32 i=1,n
                write(6,2001)samp(i),(xdata(i,j),j=1,5)
   32   continue
        write(6,2006)
        do 33 i=1,n
                write(6,2005)samp(i),tw(i),oc(i),twwo(i),wd(i),cf(i),ff(i)
   33   continue
        write(6,2007)
        call print2(ws,n,m+2,nd,md,tag,samp,ispot)
        write(6,2008)
        do 50 i=1,n
                write(6,2009)samp(i)
```

```
                do 45 j=1,m+1
                        write(6,2010)tag(j),tag(j+1),pws(i,j)
  45            continue
  50    continue
        write(6,2021)title
        do 60 i=1,n
                write(6,1001)samp(i)
                k=i
                call histo (pws,tag,samp,n,m+2,k,nd,md)
  60    continue
 1001   format(a8)
 1002   format(10(a4,1x))
 1003   format(a)
 2000   format(9x,'AMOUNT OF',2X,'WEIGHT OF',3X,'WEIGHT OF',3X,'WEIGHT S
     &ANS',2x,'SAND FRACTION',/,9x,'DISPERSANT',2X,'BEAKER',3X,'BEAK + S
     &ED',5X,'ORGANICS',5X,'+ BEAKER',/,9x,10('-'),1X,9('-'),1X,11('-'),
     &3X,10('-'),2X,13('-'))
 2001   format(' ',a8,2(f10.3),1x,f10.3,2x,f10.3,4x,f10.3)
 2005   format(' ',a8,6(f7.3))
 2006   format(//,11x,'tw',6x,'oc',5x,'twwo',5x,'wd',5x,'cf',6x,'ff',/,9
     &x,6(7('-'),1x))
 2007   format(//,' WEIGHT OF SAMPLE IN EACH PIPETTE BEAKER')
 2008   format(//,' PERCENT WEIGHT OF SAMPLE IN EACH PHI INTERVAL')
 2009   format(//,a8,/,16X,'% WEIGHT',/,' PHI INTERVAL',2X,'OF SAMP',/,1
     &X,13('-'),1X,8('-'))
 2010   format(1X,a4,'-',a4,1x,f7.3,'%')
 2011   format(/,' PERCENT COURSE FRACTION =',f7.3,'%',/)
 2019   format(//,' Enter an 8 character tag for each sample. Enter the
     &8 character tag followed',/,' by <RETURN>: ')
 2020   format(//,' Enter variable names, 4 cols. per name, 10 names per
     & line, each name',/,' separated by a space. The first 5 variable n
     &ames should represent',/,' weight of dispersant added (wod), weigh
     &t of beaker (wob), weight of',/,' beaker + sediment (wb+s), weight
     &of beaker + sediment without organics',/,' (wbwo), weight of beake
     &r + sand fraction (wbsf). The remaining variable names',/,' repres
     &ent the various phi sizes measured and should alternate between',/
     &,' the phi size being measured and the beaker number containing th
     &at',/,' size fraction. An example is:',//,' WOD  WOB  WB+S WBWO WB
     &SF 4.0  BK1  4.5  BK2  5.0',/,' BK3  5.5  BK4 ect....')
 2021   format(//,a,//)
        stop
        end
c=======================================================================
        SUBROUTINE PRINTM(X,N,M,N1,M1,COL,ROW,ISPOT)
c Prints data matrix with sample tags and variable headings
c=======================================================================
        dimension x(n1,m1),col(m1),row(n1)
        double precision row,col
c-----------------------------------------------------------------------
      DO 100 IB=1,M,10
      IE=IB+9
      IF(IE-M) 2,2,1
    1 IE=M
    2 WRITE(6,3)(I,I=IB,IE)
      IF(ISPOT.EQ.1) GO TO 10
      WRITE(6,200) (COL(I),I=IB,IE)
      GO TO 300
   10 WRITE(6,199) (COL(I),I=IB,IE)
  300 WRITE(6,6)
      DO 101 J=1,N
      WRITE(6,201) ROW(J),(X(J,K),K=IB,IE)
```

```
      WRITE(6,5)
  100 CONTINUE
      RETURN
    3 FORMAT(' ',7X,10I10)
    5 FORMAT(/,1X)
    6 FORMAT(10X,25('----'))
  199 FORMAT(/,8X,10(2X,A8))
  200 FORMAT(/,8X,10(6X,A4))
  201 FORMAT(' ',A8,10F10.3)
      END
C=======================================================================
C
C THIS SUBROUTINE PLOTS A HISTOGRAM OF THE PERCENTAGE OF SEDIMENT
C CONTAINED IN HALF PHI INTERVALS. IT ALSO PLOTS THE CUMULATIVE
C PERCENTAGES FOR HALF PHI INTERVALS.
C-----------------------------------------------------------------------
      SUBROUTINE HISTO(XX,tag,samp,n,m,k,n1,m1)
      double precision tag,samp
      dimension XX(N1,M1),tag(m1),samp(n1)
      dimension diff(75),temp(75)
      INTEGER COUNT,SUM
      CHARACTER GRID*115,LINE(100)*1
      DATA LINE /100*' '/
      DATA GRID /'              |---------|---------|---------|---------
     &|---------|---------|---------|---------|---------|---------|'/
      NUM=1
      write(6,1004)samp(i)
      WRITE(6,1000)GRID
C
c Testing if weight percent should be rounded-up. If so, the difference
c between the actual value and the rounded-down integer value are summed
c and stored in the vector TEMP. The integer value of TEMP is used to
c determine the number of "*" plotted, effectively rounding the weight
c percent up to the next whole number.
      do 10 i=1,m
            diff(i)=0
            temp(i)=0
            diff(i)=xx(k,i)-int(xx(k,i))
            if (diff(i) .ge. 0.5) then
                  temp(i)=xx(k,i)+diff(i)
            else
                  temp(i)=xx(k,i)
            endif
   10   continue
C
c Determine the number of "*" used in plotting histogram
      DO 20 I=1,m-1
           DO 25 COUNT=1,INT(temp(I))
              LINE(COUNT)='*'
   25      CONTINUE
           WRITE(6,1001)tag(i),tag(i+1),LINE,GRID
           DO 30 COUNT=1,INT(temp(I))
              LINE(COUNT)=' '
   30      CONTINUE
   20 CONTINUE
      WRITE(6,1002)GRID
      SUM=0
      DO 35 I=1,m-1
           SUM=SUM+int(temp(i))
           DO 40 COUNT=1,SUM
              LINE(COUNT)='*'
```

```
            WRITE(6,1001)tag(I),tag(i+1),LINE,GRID
            DO 50 COUNT=1,SUM
               LINE(COUNT)=' '
 50         CONTINUE
 35    CONTINUE
1000   FORMAT(//,10X,'PLOT OF PERCENT IN INTERVAL',/,' PHI INTERVAL
    &',10X,'PERCENT IN INTERVAL',/,A)
1001   FORMAT(A4,'-',a4,6x,100A1,/,A)
1002   FORMAT(///////,15X,'CUMULATIVE PLOT  *=1% ',/,' INTERVAL',7X,'PE
    &RCENT',/,A)
1004   format(a8)
       RETURN
       END
c=======================================================================
       SUBROUTINE PRINT2(X,N,M,N1,M1,COL,ROW,ISPOT)
c Prints data matrix with sample tags and variable headings
c=======================================================================
       dimension x(n1,m1),col(m1),row(n1)
       double precision row,col
c-----------------------------------------------------------------------
      DO 100 IB=1,M,10
      IE=IB+9
      IF(IE-M) 2,2,1
    1 IE=M
    2 WRITE(6,3)(I,I=IB,IE-2)
      IF(ISPOT.EQ.1) GO TO 10
      WRITE(6,200) (COL(I),I=IB+2,IE)
      GO TO 300
   10 WRITE(6,199) (COL(I),I=IB+2,IE)
  300 WRITE(6,6)
      DO 101 J=1,N
      WRITE(6,201) ROW(J),(X(J,K),K=IB,IE-2)
  101 CONTINUE
      WRITE(6,5)
  100 CONTINUE
      RETURN
    3 FORMAT(' ',7X,10I10)
    5 FORMAT(/,1X)
    6 FORMAT(10X,25('----'))
  199 FORMAT(/,8X,10(2X,A8))
  200 FORMAT(/,8X,10(6X,A4))
  201 FORMAT(' ',A8,10F10.3)
      END
```

REFERENCES

Allen, J. R. L., 1985, Principles of Physical Sedimentology. George Allen and Unwin Ltd., London, England, 272 pp.

Alonso, B., K. A. Kastens, A. Maldonado, A. Malinverno, C. H. Nelson, S. O'Connell, A. Palanques, and W. B. F. Ryan, 1985, Morphology of the Ebro Fan Valleys from SeaMARC and Sea Beam profiles. Geo-Marine Letters, 5, 141-148.

Aubouin, J., J. Stephan, and V. Renard, 1982, The Middle America Trench as an example of a subduction zone. Tectonophysics, 86, 275-304.

Barnard, W. D., 1978, The Washington continental slope: Quaternary tectonics and sedimentation. Marine Geology, 27, 79-114.

Bartlett, W. A., 1987, Peru Fore-arc Sedimentation: SeaMARC II Side-scan Interpretation of an Active Continental Margin. Master's Thesis, University of Hawaii, 87 pp.

Belderson, R. H., and A. H. Stride, 1969, The shape of submarine canyon heads revealed by Asdic. Deep Sea Res., 16, 103-104.

Belderson, R. H., and N. H. Kenyon, 1976, Long-range sonar views of submarine canyons. Marine Geology, 22, 69-74.

Blackinton, J. G., D. M. Hussong, and J. Kosalos, 1983, First results from a combination of side-scan sonar and seafloor mapping system (SeaMARC II). Offshore Tech. Conf., 4478, 307-311.

Bouma, A. H., and T. H. Nilsen, 1978, Turbidite facies and deep-sea fans - with examples from Kodiak Island, Alaska. Offshore Tech. Conf. Proc., 1, 559-570.

Bouma, A. H., W. R. Normark, and N. E. Barnes, 1985, Submarine Fans and Related Turbidite Systems. Springer-Verlag, New York, N.Y., 351 pp.

Bouma, A. H., J. M. Coleman, A. W. Meyer, and Scientific Party, 1986, Initial Reports of the Deep Sea Drilling Project, 96, U.S. Government Printing Office, Washington, D.C., 824 pp.

Brindley, G. W., and G. Brown, 1980, Crystal Structures of Clay Minerals and Their X-ray Identification. Spottiswoode, London, 495 pp.

Bucher, W. H., 1940, Submarine valleys and related geologic problems of the North Atlantic. Geol. Soc. America Bull., 51, 489-512.

Carlson, P. R., and H. A. Karl, 1984, Discovery of two new large submarine canyons in the Bering Sea. Marine Geology, 56, 159-179.

Coulbourn, W. T., 1977, Tectonics and Sediments of the Peru-Chile Trench and Continental Margin at the Arica Bight. Ph.D. Dissertation, University of Hawaii, 243 pp.

Coulbourn, W. T., 1980, Relationship between the distribution of foraminifera and geologic structures of the Arica Bight, South America. Jour. of Paleontol., 54, 696-718.

Coulbourn, W. T., and R. Moberly, 1977, Structural evidence of the evolution of fore-arc basins off South America. Can. Jour. Earth Sci., 14, 102-116.

Coulbourn, W. T., R. Hesse, J. Azema, and T. Shiki, 1982, A summary of sedimentology of Deep Sea Drilling Project Leg 67 sites: The Middle America trench and slope off Guatemala -- an active margin transect. In: J. Aubouin, and R. von Huene (eds.), Initial Reports of the Deep Sea Drilling Project, 67, U.S. Government Printing Office, Washington, D.C., 759-774.

Daly, R. A., 1936, Origin of submarine canyons. American Jour. Sci., 31, 401-420.

Damuth, J. E., 1980, Quaternary sedimentation processes in the South China basin as revealed by echo-character mapping and piston-core studies. In: D. E. Hayes (ed.), The Tectonic and Geologic Evolution of Southeast Asian Seas and Islands, American Geophysical Union, Washington, D.C., 105-125.

Damuth, J. E., and R. D.Flood, 1983, Morphology, sedimentation processes, and growth pattern of the Amazon Deep-Sea Fan. Geo-Marine Letters, 3, 109-117.

Damuth, J. E., R. D. Flood, R. O. Kowsmann, R. H. Belderson, and M. A. Gorini, 1988, Anatomy and growth pattern of Amazon Deep-Sea Fan as revealed by long-range side-scan sonar (GLORIA) and high-resolution seismic studies. American Assoc. Petrol. Geol. Bull., 72, 885-911.

Davis, J. C., 1973, Statistics and Data Analysis in Geology. John Wiley and Sons, New York, NY, 550 pp.

Davis, J. C., 1986, Statistics and Data Analysis in Geology. John Wiley and Sons, New York, NY, 646 pp.

Farre, J. A., B. A. McGregor, W. B. F. Ryan, and J. M. Robb, 1983, Breaching the shelfbreak: Passage from youthful to mature phase in submarine canyon evolution. In: D. J. Stanley, and G. T. Moore (eds.), The Shelfbreak: Critical Interface on Continental Margins, Soc. Econ. Paleontol. and Mineral. Spec. Pub. 33, 25-39.

Flood, R. D., and J. E. Damuth, 1987, Quantitative characteristics of sinuous distributary channels on the Amazon Deep-Sea Fan. Geol. Soc. America Bull., 98, 728-738.

Folk, R. L., 1974, Petrology of Sedimentary Rocks. Hemphill Publishing Co., Austin, TX, 185 pp.

Garrison, L. E., N. H. Kenyon, and A. H. Bouma, 1982, Channel systems and lobe construction of the eastern Mississippi Fan lobe. Geo-Marine Letters, 2, 31-39.

Gates, O., and W. Gibson, 1956, Interpretation of the configuration of the Aleutian Ridge. Geol. Soc. America Bull., 67, 127-146.

Griffiths, J. C., 1967, Scientific Methods in Analysis of Sediments. McGraw-Hill Book Co., New York, NY, 508 pp.

Handschumacher, D. W., 1976, Post-Eocene plate tectonics of the eastern Pacific. In: G. H. Sutton, M. H. Manghnani, and R. Moberly (eds.), The Geophysics of the Pacific Ocean Basin and Its Margin, American Geophysical Union Mono. 19, 177-202.

Hussong, D. M., and L. K. Wipperman, 1981, Vertical movement and tectonic erosion of the wall of the Peru-Chile trench near 11^{o} 30' S latitude. In: L. D. Kulm, J. Dymond, E. J. Dasch, and D. M. Hussong (eds.), Nazca Plate Crustal Formation and Andean Convergence, Geol. Soc. America Memoir 154, 509-524.

Hussong, D. M., and P. Fryer, 1983, Back-arc seamounts and the SeaMARC II seafloor mapping system. EOS, 64, 627-632.

Hussong, D. M., P. B. Edwards, S. H. Johnson, J. F. Campbell, and G. H. Sutton, 1976, Crustal structure of the Peru-Chile trench: 8^{o}-12^{o} S Latitude. In: G. H. Sutton, M. H. Manghnani, and R. Moberly (eds.), The Geophysics of the Pacific Ocean Basin and its Margin, American Geophysical Union Mono. 19, 71-86.

Hussong, D. M., T. B. Reed IV, and W. A. Bartlett, 1988, SeaMARC II sonar imagery and bathymetry of the Nazca plate and Peru forearc, ODP Leg 112. In: E. Suess, and R. von Huene (eds.), Proc. Ocean Drilling Program, Initial Reports., 112, College Station, TX, 125-130.

James, D. E., 1971, Plate tectonic model for the evolution of the Central Andes. Geol. Soc. America Bull., 82, 3325-3346.

James, D. E., 1981, Role of subducted continental material in the genesis of calc-alkaline volcanics of the central Andes. In: L. D. Kulm, J. Dymond, E. J. Dasch, and D. M. Hussong (eds.), Nazca Plate Crustal Formation and Andean Convergence, Geol. Soc. America Memoir 154, 769-790.

Johnson, D. W., 1939, The Origin of Submarine Canyons, a Critical Review of Hypotheses. Columbia Univ. Press, New York, N.Y., 126 pp.

Johnson, S. H., G. E. Ness, and K. R. Wrolstad, 1975, Shallow structures and seismic velocities of the southern Peru margin. EOS (Abstract), 56, 443.

Jordan, T. E., B. L. Isacks, R. W. Allmendinger, J. A. Brewer, V. A. Ramos, and C. J. Ando, 1983, Andean tectonics related to geometry of subducted Nazca plate. Geol. Soc. America Bull., 94, 341-361.

Karl, H. A., and P. R. Carlson, 1982, Large sand waves in Navarinsky Canyon head, Bering Sea. Geo-Marine Letters, 2, 157-162.

Kastens, K. A., and A. N. Shor, 1986, Evolution of a channel meander on the Mississippi Deep-Sea Fan. Marine Geology, 71, 165-175.

Kim, K. H., and W. C. Burnett, preprint, Accumulation and biological mixing of Peru margin sediments, 46 pp.

Knebel, H. H., S. A. Wood, and E. C. Spiker, 1979, Hudson River: Evidence for extensive migration on the exposed continental shelf during Pleistocene time. Geology, 7, 254-258.

Laforge, R., and E. R. Engdahl, 1979, Tectonic implications of seismicity in the Adak Canyon region, Central Aleutians. Bull. Seismological Soc. America, 69, 1515-1532.

Lewis, D. W., 1984, Practical Sedimentology. Hutchinson Ross Publishing Co., Stroudsburg, PA, 229 pp.

Malahoff, A., R. W. Embley, R. B. Perry, and C. Fefe, 1980, Submarine mass-wasting of sediments on the continental slope and upper rise south of Baltimore Canyon. Earth and Plan. Sci. Letters, 49, 1-7.

Maldonado, A., A. Palanques, B. Alonso, K. A. Kastens, C. H. Nelson, S. O'Connell, and W. B. F. Ryan, 1985, Physiography and deposition on a distal deep-sea system: The Valencia Fan (northwestern Mediterranean). Geo-Marine Letters, 5, 157-164.

Mann, U., and G. Muller, 1979, X-ray mineralogy of Deep Sea Drilling Project Legs 51 through 53, western North Atlantic. In: T. W. Donnelly, and J. Francheteau (eds.), Initial Reports of the Deep Sea Drilling Project, 51, 52, 53 (part 2), U.S. Government Printing Office, Washington, D.C., 721-729.

May, J. A., J. E. Warme, and R. A. Slater, 1983, Role of submarine canyons on shelfbreak erosion and sedimentation: Modern and ancient examples. In: D. J. Stanley, and G. T. Moore (eds.), The Shelfbreak: Critical Interface on Continental Margins, Soc. Econ. Paleontol. and Mineral. Spec. Publ. 33, 315-332.

Mayer, L. A., 1979, Deep sea carbonates: Acoustical, physical, and stratigraphic properties. Jour. of Sed. Petrol., 49, 819-836.

McGregor, B., W. L. Stubblefield, W. B. F. Ryan, and D. C. Twichell, 1982, Wilmington Submarine Canyon: A marine fluvial-like system. Geology, 10, 27-30.

McMillen, K. J., R. H. Enkeball, J. C. Moore, T. H. Shipley, and J. W. Ladd, 1982, Sedimentation in different tectonic environments of the Middle America trench, southern Mexico and Guatemala. In: J. K. Leggett (ed.), Trench-Forearc Geology, Geol. Soc. London Spec. Pub. 10, 107-119.

Megard, F., and H. Philip, 1976, Plio-Quaternary tectono-magmatic zonation and plate tectonics in the central Andes. Earth and Plan. Sci. Letters, 33, 231-238.

Minster, J. B., and T. H. Jordan, 1978, Present-day plate motions. Jour. Geophys. Res., 83, 5331-5353.

Moore, G. W., 1983, Structural dynamics of the shelf-slope boundary at active subduction zones. In: D. J. Stanley, and G. T. Moore (eds.), The Shelfbreak: Critical Interface on Continental Margins, Soc. Econ. Paleontol. and Mineral. Spec. Pub. 33, 97-105.

Morris, W. R., and C. J. Busby-Spera, 1988, Sedimentologic evolution of a submarine canyon in a forearc basin, Upper Cretaceous Rosario Formation, San Carlos, Mexico. American Assoc. Petrol. Geol. Bull., 72, 717-737.

Muller, G., and M. Gastner, 1971, The "Karbonat Bombe," a simple device for the determination of the carbonate content in sediments, soils and other materials. Neues. Jahrb. Mineral. Monatsh., 10, 466-469.

Mutti, E., 1974, Examples of ancient deep-sea fan deposits from circum-Mediterranean geosynclines. In: R. H. Dott, and R. H. Shaver (eds.), Modern and Ancient Geosynclinal Sedimentation, Soc. Econ. Paleontol. and Mineral. Spec. Pub. 19, 92-105.

Normark, W. R., and D. J. W. Piper, 1985, Navy Fan, Pacific Ocean. In: A. H. Bouma, W. R. Normark, and N. E. Barnes (eds.), Submarine Fans and Related Turbidite Systems, Springer-Verlag, New York, NY, 87-94.

Normark, W. R., and Shipboard Scientific Party, 1986, Summary of drilling results for the Mississippi fan and considerations for applications to other turbidite systems. In: A. H. Bouma, J. M. Coleman, and A. W. Meyer (eds.), Initial Reports of the Deep Sea Drilling Project, 96, U.S. Government Printing Office, Washington, D.C., 425-436.

O'Connell, S., B. Alonso, K. A. Kastens, A. Maldonado, A. Malinverno, C. H. Nelson, A. Planques, and W. B. F. Ryan, 1985, Morphology and downslope sediment displacement in a deep-sea valley, the Valencia Valley (northwestern Mediterranean). Geo-Marine Letters, 5, 149-156.

Resig, J. M., 1981, Biogeography of benthic foraminifera of the northern Nazca plate and adjacent continental margin. In: L. D. Kulm, J. Dymond, E. J. Dasch, and D. M. Hussong (eds.), Nazca Plate Crustal Formation and Andean Convergence, Geol. Soc. America Memoir 154, 619-666.

Ricci Lucchi, F., and E. Valmori, 1980, Basin-wide turbidites in a Miocene, over-supplied deep sea plain: A geometrical analysis. Sedimentology, 27, 241-270.

Scholl, D. W., R. von Huene, T. L. Vallier, and D. G. Howell, 1980, Sedimentary masses and concepts about tectonic processes at underthrust ocean margins. Geology, 8, 564-568.

Schumm, S. A., and L. Phillips, 1986, Composite channels of the Canterbury Plain, New Zealand: A Martian analog? Geology, 14, 326-329.

Shackleton, R. M., A. C. Ries, M. P. Coward, and P. R. Cobbold, 1979, Structure, metamorphism and geochronology of the Arequipa Massif of coastal Peru. Geol. Soc. London Jour., 136, 195-214.

Shanmugam, G., and R. J. Moiola, 1988, Submarine fans: Characteristics, models, classification, and reservoir potential. Earth-Science Rev., 24, 383-428.

Shepard, F. P., 1933, Canyons beneath the seas. Scientific Monthly, 37, 31-39.

Shepard, F. P., and R. F. Dill, 1966, Submarine Canyons and Other Sea Valleys. McNally, Chicago, IL, 397 pp.

Shor, A. N., and K. A. Kastens, preprint, Channel fill deposits of the middle Mississippi Fan: One catastrophic debris flow or numerous small-volume turbidites?

Smoot, N. C., 1983, Ogasawara Plateau: Multi-beam sonar bathymetry and possible tectonic implications. Jour. Geol., 91, 591-598.

Spencer, J. W., 1903, Submarine valleys off the American coasts and in the North Atlantic. Geol. Soc. America Bull., 14, 207-226.

Stanley, D. J., S. J. Culver, and W. L. Stubblefield, 1986, Petrologic and foraminiferal evidence for active downslope transport in Wilmington Canyon. Marine Geology, 69, 207-218.

Stetson, H. C., 1936, Geology and paleontology of the Georges Bank canyons. Geol. Soc. America Bull., 47, 339-366.

Stubblefield, W. L., B. A. McGregor, E. B. Forde, D. N. Lambert, and G. F. Merrill, 1982, Reconnaissance in DSRV Alvin of a "fluvial-like" meander system in Wilmington Canyon and slump features in South Wilmington Canyon. Geology, 10, 31-36.

Taylor, B., and N. C. Smoot, 1984, Morphology of Bonin fore-arc submarine canyons. Geology, 12, 724-727.

Tosdal, R. M., E. Farrar, and A. H. Clark, 1981, K-Ar geochronology of the late Cenozoic volcanic rocks of the Cordillera Occidental, southernmost Peru. Jour. of Volc. and Geotherm. Res., 10, 157-173.

Tosdal, R. M., A. H. Clark, and E. Farrar, 1984, Cenozoic polyphase landscape and tectonic evolution of the Cordillera Occidental, southernmost Peru. Geol. Soc. America Bull., 95, 1318-1332.

Veatch, A. C., and P. A. Smith, 1939, Atlantic submarine valleys of the United States and the Congo submarine valley. Geol. Soc. America Spec. Paper 7, 101 pp.

von der Borch, C. C., A. E. Grady, R. Aldam, D. Miller, R. Neumann, A. Rovira, and K. Eickhoff, 1985, A large-scale meandering submarine canyon: Outcrop example from the late Proterozoic Adelaide Geosyncline, South Australia. Sedimentology, 32, 507-518.

von Huene, R., 1972, Structure of the continental margin and tectonism at the eastern Aleutian Trench. Geol. Soc. America Bull., 83, 3613-3626.

Whitaker, J. H. McD., 1974, Ancient submarine canyons and fan valleys. In: R. H. Dott Sr., and R. H. Shaver (eds.), Modern and Ancient Geosynclinal Sedimentation, Soc. Econ. Paleontol. and Mineral. Spec. Pub. 19, 106-125.

Zen, E., 1959, Mineralogy and petrography of marine bottom sediment samples off the coast of Peru and Chile. Jour. Sed. Petrol., 29, 513-539.